

Lawrence Berkeley National Laboratory

Lawrence Berkeley National Laboratory

Title

Sea anemone genome reveals the gene repertoire and genomic organization of the eumetazoan ancestor

Permalink

<https://escholarship.org/uc/item/3b01p9bc>

Authors

Putnam, Nicholas H.
Srivastava, Mansi
Hellsten, Uffe
et al.

Publication Date

2007

Peer reviewed

Sea anemone genome reveals the gene repertoire and genomic organization of the eumetazoan ancestor

Nicholas H. Putnam[1], Mansi Srivastava[2], Uffe Hellsten[1], Bill Dirks[2], Jarrod Chapman[1], Asaf Salamov[1], Astrid Terry[1], Harris Shapiro[1], Erika Lindquist[1], Vladimir V. Kapitonov[3], Jerzy Jurka[3], Grigory Genikhovich[4], Igor Grigoriev[1], JGI Sequencing Team[1], Robert E. Steele[5], John Finnerty[6], Ulrich Technau[4], Mark Q. Martindale[7], Daniel S. Rokhsar[1,2]

[1] Department of Energy Joint Genome Institute, Walnut Creek, CA 94598

[2] Center for Integrative Genomics and Department of Molecular and Cell Biology, University of California, Berkeley CA 94720

[3] Genetic Information Research Institute, 1925 Landings Drive, Mountain View, CA 94043

[4] Sars International Centre for Marine Molecular Biology, University of Bergen, Thormoeøhlensgt 55; 5008, Bergen, Norway

[5] Department of Biological Chemistry and the Developmental Biology Center, University of California, Irvine, CA 92697

[6] Department of Biology, Boston University, Boston, MA 02215

[7] Kewalo Marine Laboratory, University of Hawaii, Honolulu, HI 96813

Abstract

Sea anemones are seemingly primitive animals that, along with corals, jellyfish, and hydras, constitute the Cnidaria, the oldest eumetazoan phylum. Here we report a comparative analysis of the draft genome of an emerging cnidarian model, the starlet anemone *Nematostella vectensis*. The anemone genome is surprisingly complex, with a gene repertoire, exon-intron structure, and large-scale gene linkage more similar to vertebrates than to flies or nematodes. These results imply that the genome of the eumetazoan ancestor was similarly complex, and that fly and nematode genomes have been modified via sequence divergence, gene and intron loss, and genomic rearrangement. Nearly one-fifth of the genes of the ancestor are eumetazoan novelties in the sense that they have no recognizable homologs outside of animals, or contain new protein domains and/or domain combinations that are not found in other eukaryotes. These eumetazoan-specific genes are enriched for animal functions like cell signaling, adhesion, and synaptic transmission, and analysis of diverse pathways suggests that these gene "inventions" along the lineage leading to animals were already likely well integrated with pre-existing eukaryotic genes in the eumetazoan progenitor. Subsequent diversification in the cnidarian and bilaterian lineages was therefore associated with new regulatory linkages and higher-level integration of these pre-existing pathways and networks.

Introduction

All living "tissue-grade" animals, or "eumetazoans," are descended from the last common ancestor of bilaterians (flies, worms, snails, humans), cnidarians (anemones, jellyfish, hydra), and ctenophores (comb jellies)(1, 2). This eumetazoan ancestor lived perhaps seven hundred million years ago, but is not preserved in the fossil record(3). Yet we can infer many of its characteristics -- flagellated sperm, development through a process of gastrulation, multiple germ layers, true epithelia lying upon a basement membrane, a lined gut (enteron), a neuromuscular system, multiple sensory systems, and fixed body axes -- since they are conserved features retained by its modern descendants.

Similarly, we can characterize the genome of this long-dead eumetazoan progenitor by comparing modern DNA and protein sequences and identifying conserved features in different modern lineages. Our ability to recognize ancient genomic features depends on the availability of sequences from diverse living animals, and can only illuminate genomic characteristics that have an intrinsically slow rate of change and/or are preserved by selective pressures. Comparisons (4-6) between fruit fly, nematode, and vertebrate genomes reveal greater genomic complexity in the vertebrates (and other deuterostomes (7, 8)) as measured by gene content and structure, but at the same time show that many genes and networks are shared across bilaterians. To probe the ancestral eumetazoan genome requires sequences from even deeper branches of the animal tree, comparing bilaterian and non-bilaterian phyla.

In comparison with bilaterians, cnidarians appear morphologically simple. The phylum is defined (see., e.g., (2)) by a sac-like body plan with a single "oral" opening, two-epithelial tissue layers, the presence of numerous tentacles, a nerve net, and the characteristic stinging cells (cnidocytes, literally, "nettle cells") that give the phylum its name (Figure 1g). The class Anthozoa ("flower animals") includes diverse anemones, corals, and sea pens, all of which lack a medusa stage. The other Cnidarian classes are united by their pelagic medusae and uniquely linear mitochondrial genomes (9) into the Medusozoa, including *Hydra* and related hydroids, jellyfish, and box jellies. Some of the oldest animal body fossils (e.g., the Ediacaran *Charnodiscus* (10) but see also (11, 12)) and fossil embryos (13) are plausibly relics of stem cnidarians, suggesting a Precambrian origin for the phylum.

Among Anthozoan cnidarians, the starlet sea anemone *Nematostella vectensis* is an emerging model system (14, 15). This estuarine burrowing anemone is found on the Atlantic and Pacific coasts of North America, as well as the coast of southeast England (16) (Figure 1).

Nematostella cultures are easily maintained in the laboratory. With separate sexes, inducible spawning, and external fertilization (14, 17), embryos are available throughout the year.

Fertilization is followed by cell divisions resulting in a hollow blastula, which gastrulates by invagination and ingression to produce a ciliated, tear-drop-shaped planula larva that swims with an apical tuft of sensory cilia at the front and the blastopore at the rear (Figure 1a-e, h, i). On the seventh day after fertilization, the planula develops into a juvenile polyp, with the blastopore becoming the mouth (14, 18, 19) (Figure 1f). Like many cnidarians, adult *Nematostella* are

apparently immortal, with prodigious powers of regeneration: animals cut in half heal into two complete individuals, mimicking the natural process of asexual reproduction that occurs by transverse pinching. Recent studies with *Nematostella* have addressed the evolutionary origins of mesoderm, germ cell specification, and axial patterning in metazoans (Figure 1j, k) (15, 20-25)

While cnidarians are often characterized as "simple" or "primitive," closer study of *Nematostella* and its relatives is revealing considerable molecular and morphological complexity (15).

Signaling pathways and transcription factors involved in the early patterning and development of bilaterians are present in cnidarians and active in development, indicating that these pathways and regulatory mechanisms predate the eumetazoan radiation. Perhaps most strikingly, genes that establish the main body axes in bilaterian embryos are also expressed asymmetrically in *Nematostella* development, even though cnidarians are conventionally viewed as "radial" animals [for a critical discussion, see (26)]. The expression domains occur with apparent bilateral symmetry, *i.e.*, reflecting distinct directed axes both along and perpendicular to the main body axis, and with a left-right plane of symmetry (27-29). Although anemones show only subtle external morphological manifestations of bilateral symmetry (Figure 1k) (*i.e.*, asymmetry in the structure of the adult pharynx and associated mesenteries (30)), these results suggest the antiquity of "bilaterian" patterning mechanisms.

Here we report the draft genome of the starlet sea anemone, and use its gene repertoire and genome organization to reconstruct features of the ancestral eumetazoan genome. Analysis of the *Nematostella* genome in the context of sequences from other eukaryotes reveals the genomic

complexity of this last common cnidarian-bilaterian ancestor, and begins to illuminate the rich history of genes and gene networks already present at the base of the animal tree of life. The emerging picture is one of surprising conservation in gene content, structure, and organization between *Nematostella* and vertebrates, even to the point of retaining chromosome-scale gene blocks whose linkage in modern genomes has been preserved from the genome of their common ancestor. These are the most ancient conserved linkages known outside of prokaryotic operons. In contrast, the fruit fly and nematode model systems have experienced significant gene loss, intron loss, and genome rearrangement. Thus from a genomic perspective, the eumetazoan ancestor more closely resembled modern vertebrates and anemones.

Genome Sequencing and Assembly

The draft sequence of the *Nematostella* was produced using a random shotgun strategy (31) from approximately 6.5X paired-end sequence coverage from several shotgun libraries of a range of insert sizes (32). The total assembly spans ~357 Mb, with half of this sequence in 181 scaffolds longer than ~470 Kb. Metaphase spreads indicate a diploid chromosome number of $2N=30$ (Fig S2.4). Currently there are no physical or genetic maps of *Nematostella*, so we could not reconstruct the genome as chromosomes. Nevertheless, since half of the predicted genes are in scaffolds containing 48 or more genes, the present draft assembly is sufficiently long-range to permit useful analysis of synteny with other species, as shown below. The typical locus in the draft genome is in a contiguous gap-free stretch of nearly 20 Kb. Comparison of the assembled sequence with open reading frames derived from expressed sequence tags (ESTs, see below) shows that the assembly captures ~95% of the known protein coding content (32). While approximately one-third of the shotgun sequences were not assembled, they could typically be

characterized as derived from long (>100 Kb) tandem-repetitive minisatellite arrays suggestive of heterochromatin, implying a total genome size of ~450 Mb (32).

To avoid contamination from commensal microbes common to adult anemones and minimize the impact of haplotypic variation, we prepared genomic DNA from the larvae of a single mating pair originally isolated from the same lagoon (32). Our dataset thus nominally contains up to four haplotypes at each locus. From the shotgun assembly and the analysis of alignments between shotgun reads, we measured a rate of single nucleotide polymorphism among the four haplotypes as 0.8%, or ~1/125 bp, approximately ten times the SNP rate in the human population. (Some 16,000 SNPs may be searched at the SNP browser available at StellaBase (<http://stellabase.org>; (33)). After correcting for sampling, we estimated that each pair of haplotypes differ at 0.65% of nucleotide positions (32). Thus the parental anemones whose genomes we sampled have somewhat less allelic variation than broadcast spawning invertebrates such as sea squirts (~2%)(7) and sea urchins (5-10%) (8), or outbreeding plants like *Populus* (~2%) (34), but a comparable amount to the pufferfish (0.5%) (35).

Nematostella, however, is not a true broadcast spawner, since while males release sperm into the water, females lay tens to hundreds of eggs encased in a jelly mass that becomes fixed to a benthic substrate. The egg mass may be a derived feature of *Nematostella* that is related to its colonization of the estuarine environment. The relatively low level of intra-specific genetic variation in *Nematostella* vs. marine broadcast spawners might be explained if its estuarine habitat limited gamete dispersal and led to a smaller effective population size. Genetic

fingerprinting of wild *Nematostella* populations indicates a high degree of genetic structuring at fine spatial scales, implying extremely low levels of gene flow between neighboring estuaries (36). The source population for the genome sequence (Rhode River, Maryland) appears typical in this regard (37).

Nematostella gene set

We estimate that the *Nematostella* genome contains ~18,000 *bona fide* protein-coding genes, comparable to gene counts in other animals. Combining homology-based and *ab initio* methods with sequences from over 146,000 expressed sequence tags, we predicted ~27,000 complete or partial protein-coding transcripts in the genome (32). More than 12,000 of these are found in robust eumetazoan gene families, and are therefore supported as orthologs of genes in other animals (see below). While ~22,000 of all predicted genes have a significant alignment (BLAST e-value < 1e-10) to known proteins in SwissProt/Trembl and therefore have some homology support, analysis of a random sampling of genes suggest that some of these appear to be gene fragments, possible pseudogenes, or relics of transposable elements, leading to a discounting of the true gene count to ~18,000 (32). Slightly more than 10% of the EST contigs have significant (95% identify, 75% length) alignments to multiple scaffolds (32), providing an estimate of the redundancy of the assembly, which appears to arise from the occasional separate assembly of divergent haplotypes. More than 25% of the genome is made of repetitive elements that are fossilized copies of transposable elements. Over 500 families of them were discovered in the genome, including DNA transposons and both LTR and non-LTR retrotransposons (Table S2.3).

The ancestral eumetazoan gene set

By comparing the gene complement of *Nematostella* with other metazoans, we attempted to reconstruct the gene repertoire of the eumetazoan (*i.e.*, cnidarian-bilaterian) ancestor and to infer the gains, losses, and duplications that occurred both before and after the eumetazoan radiation. A simple way to identify putative orthologs (genes descended from the same gene in the common ancestor) between genomes is through reciprocal best-scoring BLAST hits (38). Surprisingly, the human genome has many more such orthologous pairs with *Nematostella* (6,989) than with non-vertebrate bilaterians, including *Drosophila* (5,772), *C. elegans* (4,846), and even the invertebrate chordate *Ciona intestinalis* (6,313). These results strongly suggest that many genes and gene families previously assumed to be chordate or vertebrate innovations are actually much more ancient, and conversely that the fruit fly, soil nematode, and sea squirt lineages have experienced higher levels of divergence and gene loss than *Nematostella*, consistent with phylogenetic the analysis described below.

To approximate the gene repertoire of the eumetazoan ancestor we constructed 7,766 putatively orthologous gene families that are anchored by reciprocal best-scoring BLAST alignments between genes from anemone and one or more of fly, nematode, human, frog, or fish [S]. Each family thus represents a single gene in the eumetazoan ancestor whose descendents survive in recognizable form as modern genes in both cnidarians and bilaterians. These families account for a significant fraction of genes in modern animals: we estimate that nearly two thirds of human genes (13,830) are descended from these progenitors through subsequent gene family expansions along the human lineage, and a comparable number (12,319) of predicted *Nematostella* genes arose by independent diversifications along the cnidarian branch, with 7,309 (~50%) and 7,261 (~40%) found in *Drosophila* and *C. elegans*, respectively. Our reconstructed ancestral gene set is

necessarily incomplete since we cannot capture genes that were present in the eumetazoan progenitor but became highly diverged or lost in one or more descendants, nevertheless it provides a starting point for further analysis.

Of the 7,766 ancestral eumetazoan gene families, only 72% (5,626) are represented in the complete genomes of all three major modern eumetazoan lineages: cnidarians (*i.e.*, *Nematostella*), protostomes (*i.e.*, *Drosophila* and/or *C. elegans*), and deuterostomes (requiring presence of at least two of pufferfish, frog, and human). 1,292 eumetazoan gene families have detectable descendants in anemone and at least two of the three vertebrates, but appear to be absent in both fruit fly and soil nematode, and were therefore either lost (or were highly diverged) in both of these model protostomes. Before the *Nematostella* genome sequence, it was more parsimonious to assume that most of these genes were vertebrate or deuterostome innovations (with the exception of individual genes whose phylogenetic distribution has been more widely studied). The forthcoming genome sequences of crustaceans, annelids, and molluscs will help address which of these genes may have survived in the protostome lineage but were lost in flies and nematodes. In contrast, only 33 genes are found in *Nematostella* and both *Drosophila* and *C. elegans* but not in any vertebrate, representing putative deuterostome or vertebrate loss, indicating a much lower degree of gene loss in the vertebrates than in the ecdysozoan model systems. We found 673 gene families represented in model protostomes and vertebrates, but not in *Nematostella*. These are candidates for bilaterian novelties.

Molecular evolution of the Eumetazoa

To address evolutionary relationships between animals, we inferred the phylogeny of Metazoa by

combining *Nematostella* data with available genomic sequences from diverse animals, using a subset of 337 single copy genes suitable for deep phylogenetic analysis (32). In Figure 2, relative branch lengths represent the accumulation of amino acid substitutions in each lineage across this set of proteins. As expected, the two cnidarians *Nematostella* and *Hydra* form a monophyletic group that branched off the metazoan stem prior to the radiation of bilaterians. The depth of the *Nematostella-Hydra* split (comparable to the protostome-deuterostome divergence) emphasizes the distant relationship between anthozoans and hydrozoans. This supports the paleontological evidence that the radiation of the cnidarian phylum is quite ancient, and suggests that significant variation in gene content and gene family diversity may be found when the anemone genome is compared with that of the hydrozoan *Hydra*.

Our whole genome analysis groups the fruit fly with the soil nematode, in support of the superphylum Ecdysozoa, a major element of the "new animal phylogeny" (39). This contrasts with other whole-genome-based studies that support an early branching acoelomate clade that includes *C. elegans* (40, 41). The apparent basal position of the nematode lineage in these studies is widely believed to be a long branch artifact. In other studies (e.g., (42)), the effect of long branch attraction is minimized by including additional taxa that break up long branches, generating a phylogeny that agrees with our more limited taxon sampling but larger gene set. We also generated ~15,000 ESTs from the ctenophore (comb jelly) *Mnemiopsis leidyi* to attempt to place this enigmatic phylum on the tree, but could not resolve its precise phylogenetic position with significant support (32). For convenience, here we refer to the last common ancestor of cnidarians and bilaterians as the "eumetazoan ancestor," although the precise phylogenetic placement of ctenophores may revise this designation.

Long branch lengths, indicating increased levels of sequence divergence, were found along the fly, nematode, and sea squirt lineages. The sea anemone sequences, however, appear to be evolving at a rate comparable to, or even somewhat lower than, vertebrates. The relatively slow rate of protein sequence evolution in *Nematostella* compared to fly and nematode can be seen more directly by considering the amino-acid percent identity between reciprocal-best-hits of selected proteomes vs. human. Despite the fact that flies and nematodes share a more recent common ancestor with human than sea anemones do, we find that the anemone peptides are more similar to human than to either of the model protostomes (32). This surprising similarity between *Nematostella* and vertebrates is a recurring theme of our analysis, indicating that both the anemone and vertebrate genomes retain more ancestral eumetazoan features than sequences from flies and nematodes.

While accelerated rates of molecular evolution have been documented in flies and echinoderms (43) relative to vertebrates, our analysis does not support the extrapolation of these higher rates to all invertebrates. Using our branch lengths, a very crude molecular clock interpolation based on the eukaryotic time scales of Douzery *et al.* (42) suggests that the eumetazoan ancestor lived ~670-820 Mya (32). This is of course only a very rough estimate with numerous caveats, most notably that there is no guarantee that the rate of protein evolution was constant on the eumetazoan stem, but provides a rough time scale for the eumetazoan radiation.

Conservation of ancient eumetazoan introns

Comparison of *Nematostella* genes to those of other animals reveals that the ancestral eumetazoan genome must have been intron-rich, with gene structures closely resembling those of modern vertebrate and anemone genes. Intron-containing genes that are descended from the ancestral eumetazoan gene set in humans and anemones have a median of ~8 and ~6 introns per gene respectively, while those from fruit fly have only ~3. (32). Not only are the number of exons per gene similar between *Nematostella* and vertebrates, but the precise location and phase (*i.e.*, the positioning of the splice sites relative to codon boundaries) of introns are also highly conserved between anemone and human. Intron conservation can be unambiguously assessed by identifying well-aligned regions of orthologous proteins that are interrupted by introns in one or more species (Figure 3a). Note that this analysis is protected from the effects of gene modeling artifacts, since erroneous predictions in the vicinity of splice sites would disrupt alignment, thereby removing such sequences from consideration.

Introns that are shared between *Nematostella* and vertebrates and/or other bilaterians are most parsimoniously interpreted as conserved ancient eumetazoan introns (44). Within alignable regions, nearly 81% of human introns are found in the same position and phase in *Nematostella*, and conversely 82% of the anemone introns are also found in orthologous positions in human genes. The results from *Nematostella* subsume the report of introns conserved between vertebrates and the polychaete *Platynereis dumerlii* (45), since these can now be recognized as ancient eumetazoan introns, rather than "vertebrate-like" gene structures.

Using whole genome data sets we can measure the tempo of intron evolution across metazoan

genomes (32). Figure 3b shows intron gain (left) and loss (right) events inferred by weighted parsimony analysis of 2,645 intron positions that lie within highly conserved protein sequence in two or more animals, the flowering plant *Arabidopsis*, and the relatively intron-rich fungus *Cryptococcus neoformans* (32). Note that although fungi and animals are phylogenetically closer to each other than either group is to plants, fungi are not by themselves a sufficient outgroup for characterizing the history of eumetazoan introns, since there are putative ancient eukaryotic introns shared by modern animals and plants that have evidently been lost in fungi (46).

Although many eumetazoan introns are evidently of ancient eukaryotic origin (46) -- for example, nearly 26% of human and *Nematostella* introns are conserved with *Arabidopsis*, and 24% with *Cryptococcus* -- the remainder appear to be shared only by animals. These animal introns are most parsimoniously accounted for as gains on the eumetazoan stem, as shown by the long "gain" branch in Figure 3b. We cannot rule out the possibility, however, that such apparently animal-specific introns were in fact present in the last common ancestor of plants, fungi, and animals, but were convergently lost in both plants and fungi. Within animals, intron gains range from 8-22% relative to the content of the eumetazoan ancestor. Thus assuming ~8 introns per ancestral gene, ~1 novel intron has been introduced in a typical modern animal gene since the eumetazoan radiation, a rate of approximately $\sim 10^{-9}$ introns/gene/year, which is comparable to the rate of nucleotide substitution and gene duplication (47).

In contrast to intron gains, which seem to occur more or less uniformly across animal phyla,

some lineages appear to have experienced significant intron loss, notably fly, nematode, and sea squirt, which have each discarded 50-90% of inferred ancestral eumetazoan introns. We see again that these model systems are "derived" in the sense of having lost ancestral eumetazoan features (in this case, introns). It remains to be seen if the introns absent in both fly and nematode are the result of ancient loss in the ecdysozoan stem lineage (the most parsimonious explanation, shown in Fig 3b), or are convergent (independent) losses in flies and nematodes. We can rule out ancient loss in the protostome lineage based on the results of Raible *et al.* (2005) for *Platynereis*, which in combination with our analysis shows that the ancestral protostome genome was also intron-rich.

Conservation of ancient eumetazoan linkage groups

Conserved linkage groups representing ancestral vertebrate chromosomes can be defined by comparing fish and mammalian genomes and genetic maps, despite the presence of only modest segments of conserved gene order (48, 49). Similarly, limited conservation of synteny is recognizable within insects (*e.g.*, between flies and bees (50)). Between animal phyla, however, no significant large-scale conserved synteny has been identified, suggesting that signals of the ancestral eumetazoan genome organization were erased by subsequent chromosomal breaks and translocations along the various lineages. Surprisingly, despite extensive local scrambling of gene order, we find extensive conservation of synteny between the *Nematostella* and vertebrate genomes, allowing the identification of ancient eumetazoan linkage groups.

We first searched for regions of approximately conserved gene order between *Nematostella* and human, allowing for local rearrangements as well as independent differential gene loss and/or

duplication in each genome (51). We found 33 conserved syntenic segments, each containing 9 or more orthologous gene pairs, under conditions for which no such segments are expected when gene order is completely randomized in the two genomes (Figure S7.1). Within each segment, however, local gene order is considerably scrambled. Further relaxing gene order constraints dramatically increases the number of such segments expected by chance, reducing the power of this approach to detect even more ancient conserved genome organization in the face of intra-chromosomal rearrangements. To overcome this limitation we developed a new method to search for statistically significant conserved linkage groups that does not rely on gene order.

Reasoning that the prevalence of intra-chromosomal inversions and rearrangements (52) might scramble local gene order yet preserve linkage, we searched for large-scale conserved synteny, that is, sets of orthologous genes on the same chromosomal segment in their respective genomes, regardless of gene order. To remove confounding signals from recent rearrangements, we used comparisons with the genomes of other chordates to identify 98 human segments large enough that they each contain descendants of 40 or more ancestral eumetazoan genes, that do not appear to have undergone recent breaks or fusions (Figures 4a, S7.1) (32). These segments span 89% of the base pairs of the human genome. The human genome was selected as a reference since it is known to have a slow rate of chromosome evolution relative to other mammals (52), and has preserved chromosomal segments relative to teleost fish (48). To search for ancient conserved linkages across eumetazoa, we then compared these human genome segments to the assembled *Nematostella* scaffolds, using a statistical test for distinguishing significant enrichment for genes linked in both species.

For every scaffold-segment pair, we tabulated the number of predicted ancestral eumetazoan genes with descendants found in both the *Nematostella* scaffold and human segment. This number of shared orthologous genes was compared to a null model in which the scaffolds and segments have gene content independently drawn from the ancestral set. The "Oxford grid" shown in Figure 4b illustrates not only that there are many scaffold-segment pairs with a highly significant excess of shared ancestral genes, but that the anemone scaffolds and human chromosome segments can be grouped into classes, such that scaffold-segment pairs drawn from the same class are likely to have a significant excess of shared ancestral genes (32). Each class of scaffolds and chromosome segments is most easily interpreted as collecting together segments of the present day *Nematostella* and human genomes that descend from the same chromosome of the eumetazoan ancestor, and therefore defines a putative ancestral eumetazoan linkage group (PAL). The complete Oxford grid showing all 13 PALs is shown in Table S7.2.

The conserved linkage is extensive, and accounts for a significant fraction of the ancestral eumetazoan set. Of the 4,402 ancestral eumetazoan gene families represented in the largest anemone scaffolds and human segments (*i.e.*, in the genomic regions large enough to permit statistically significant analysis, and therefore eligible for consideration in our analysis), more than 30% (1,336) participate in a conserved linkage group. This is a lower bound on the true extent of the remnant ancient linkage groups, since our analysis is limited by the length of the *Nematostella* scaffolds and the use of conservative statistical criteria. A more sensitive approach can assign more than twice as many ancestral genes to a PAL (32). The 40 human segments that show conserved synteny with *Nematostella* cover half of the human genome; within such human segments, typically 40-50% of eumetazoan-derived genes have counterparts in syntenic

Nematostella segments, and *vice versa*. This is a remarkable total, since any chromosomal fusions and subsequent gene order scrambling on either the human or *Nematostella* lineage during their ~750 million years of independent evolution would attenuate the signal for linkage as seen, for example, in the reconstruction of the teleost chromosomes by comparing fish and mammals (49).

The observation of conserved linkage groups is most easily explained as the remnants of large ancestral chromosomal segments containing hundreds of genes that have evolved without obvious constraint on gene order within each block. Seven of the PALs link anemone scaffolds to multiple regions of the human genome in a manner consistent with multiple large-scale duplication events along the vertebrate lineage (reviewed, for example, in (53)). These seven PALs represent the ancestral (preduplication) linkage of these regions. Five PALs link *Nematostella* scaffolds to single human chromosome regions, which suggests that the vertebrates specific duplicates of these segments have been lost or fused and dispersed among other chromosomes (32). The surprising extent of this conserved linkage suggests that either the neutral rate of inter-chromosomal translocations is low (on the order of a few breaks/fusions per chromosome since the eumetazoan ancestor, excluding intra-chromosomal rearrangements), or that selection has acted to maintain linkage of large groups of genes for unknown reasons.

An ancestral linkage group of particular interest includes the eumetazoan Hox cluster of homeobox transcription factors that regulate anterior-posterior identity in bilaterians. Hox genes in *Nematostella* and other cnidarians are also expressed in spatial patterns consistent with an ancient role in embryonic development (54-56). Tetrapods have four Hox clusters that arose by duplication on the vertebrate stem -- HoxA (human chromosome 7p15.2), HoxB (17q21.32),

HoxC (12q13.13), and HoxD (2q31.1) -- which all appear in the same eumetazoan PAL, linked to eight *Nematostella* scaffolds (Figure 4d). *Nematostella* has several clusters of homeobox genes (56-58), but only those on scaffolds 3 and 61 are embedded within the ancestral eumetazoan Hox context, providing independent support for the assignment of these homeobox genes as *bona fide* *Nematostella* Hox genes (54, 56, 59). Remarkably, we find that not only is the organization of the Hox cluster itself preserved, but that there is an extensive block of 225 ancestral genes (Table S7.3) that were linked to Hox in the eumetazoan ancestor and have (independently) retained that linkage in both the modern human and anemone genomes.

Origins of eumetazoan genes

Where did the eumetazoan gene repertoire come from? Nearly 80% (6,182/7,766) of the ancestral eumetazoan genes have clearly identifiable relatives (*i.e.*, proteins with significant sequence homology and conserved domain architecture) outside of the animals, including fungi, plants, slime molds, ciliates, or other species available from public datasets (32). These are evidently members of ancient eukaryotic gene families that were already established in the unicellular ancestors of the metazoa, and are involved in core eukaryotic cellular functions including amino acid, carbohydrate, and lipid metabolism; small molecule and ion transport; DNA replication, core transcriptional machinery, RNA processing, and translation; intracellular vesicular trafficking and secretion; and structural and regulatory components of the eukaryotic cytoskeleton. Although these eumetazoan gene families are conserved with other eukaryotes, animals have a unique complement due to family expansion/contraction on the eumetazoan stem. The eumetazoan genes of ancient eukaryotic ancestry are themselves descended from approximately ~5,148 eukaryotic progenitors by nearly one thousand gene duplications along the

eumetazoan stem, that is, after the early radiation of eukaryotes ~1100-1500 Mya (60) but prior to the divergence of cnidarians and bilaterians (32).

The remaining 20% (1,584) of the ancestral eumetazoan gene set comprises animal novelties that were apparently "invented" along the eumetazoan stem. The mechanism for the creation of "new" genes is obscure (*e.g.*, (61)), but may involve gene duplication followed by bursts of rapid sequence divergence (thus masking the similarity with related sister sequences) and/or *de novo* recruitment of gene and/or non-coding fragments into functional transcription units - we classified these eumetazoan novelties into three categories based on their origin (Figure 5a).

The first and largest group ("type I" novelty) comprises animal genes that have no identifiable relatives (with BLAST) outside of animals in the available sequence datasets, and accounts for 15% (1,186) of ancestral eumetazoan genes. These include important signaling factors, like the secreted wingless (Wnt) and fibroblast growth factor (FGF) families, and transcription factors, including the T-box and mothers-against-decapentaplegic (SMAD) families (Table 5b).

Interestingly, not only were these genes present in the eumetazoan ancestor, but they had already duplicated and diversified on the eumetazoan stem to establish the subfamilies that, nearly 750 million years later, are still maintained in modern vertebrates. (See for example the wnt family (62).) The diversification of these critical gene families occurred on the stem.

"Type II" novelties (2% of the eumetazoan complement, or 158 genes) incorporate "animal-only" domains in combination with ancient eukaryotic sequence. The ancestry of these genes can be traced back to the eukaryotic radiation through their ancient domains, but the novel domains they contain were evidently "invented" (or evolved into their recognizable animal form) and coupled

to more ancient domains on the eumetazoan stem. For example, Notch proteins have two Notch domains found only in metazoans in addition to ancient eukaryotic ankyrin and EGF domains; focal adhesion kinase (FAK) is targeted to focal adhesions in eumetazoans because of the addition of an animal specific focal adhesion targeting domain to the ancient kinase domain.

Finally, "type III" novelties (3%, or 240 gene families) consist of animal genes whose domains are all ancient (*i.e.*, each found in other eukaryotes) but which occur in apparently unique combination in eumetazoa relative to known non-animal genes (32) due to gene fusions and/or domain shuffling events on the eumetazoan stem. For example, the LIM-homeobox transcription factors are the result of a fusion of the ancient LIM protein-protein interaction and homeobox DNA-binding domains on the eumetazoan stem. While such "domain shuffling" (Patthy 1999) events are relatively rare, they are disproportionately involved in characterized biochemical pathways, perhaps by bringing together existing catalytic capabilities, localization and regulatory domains into the same protein (Table S8.1).

Eumetazoan networks and pathways

How are the genes that were invented along the eumetazoan stem related to the organismal novelties associated with Eumetazoa? Satisfyingly, but perhaps not surprisingly, we find the novel genes to be significantly enriched for signal transduction, cell communication and adhesion, and developmental processes (32). The eumetazoan ancestor was the progenitor of all extant animals with nervous systems, and genes with neuronal activities are abundant among its novelties. Given that present-day cnidarians lack a clear mesoderm, it is at first glance surprising that genes known to be involved in mesoderm development in bilaterians are also enriched among eumetazoan novelties. Yet we know that many of these genes are associated either with

basic patterning functions and/or the regulation of cell migration and fate. The precise deployment and interaction of these genes in the ancestral eumetazoan is therefore still a matter of debate ((24), for reviews see (19, 23)). Experiments in *Nematostella*, however, in comparison with information about mesodermal networks in bilaterians, could in principle constrain the ancestral genetic network and address whether or not the ancestor deployed these genes to generate this key germ layer.

Individual "new" genes are by themselves unlikely to bring about the suite of features needed to evolve animal characteristics from unicellular organisms. Rather, we expect that to generate organismal novelty such new genes must be integrated with other novel and existing genes to evolve expanded or modified biochemical pathways and/or regulatory networks. Given the reconstructed eumetazoan genome and its various types of novel genes, we conclude by briefly considering selected eumetazoan pathways and processes to see how novel animal genes were incorporated into cellular and organismal functions.

Cell Adhesion

In Bilateria, the integrin pathway mediates signaling from the extracellular matrix (ECM) that elicits various responses to modulate cell adhesion, motility, and the cell cycle (Giancotti and Ruoslahti 1999). A detailed look at integrin signaling (Figure 5d) reveals that most of the core components of the FAK and Fyn/Shc pathways were present in the eumetazoan ancestor. Various ancient cytosolic proteins (talin, paxillin, Grb2, Sos and Crk) have been brought under the control of two novel receptors, integrin a and integrin b (the former being a Type I novelty and the latter a Type II novelty). Focal adhesion kinase (FAK) is a cytosolic component that appears as a Type II novelty in eumetazoans and Calpain, a protease that regulates the aggregation of Talin, Paxillin

and FAK around the receptor appears as a novel domain combination of ancient domains.

Caveolin, a membrane adapter that couples the integrin α subunit to Fyn is present in the *Nematostella* genome and is a Type I novel protein. Fyn itself is a more recent invention derived on the tetrapod stem by gene duplication.

Cell-cell adhesion mediated by cell-ECM interactions is a hallmark of animal multicellularity (63). Basement membrane proteins such as collagen and laminin arose as Type II novelties along the stem leading to the Eumetazoa, while others such as nidogen are novel pairings of ancient domains (Figure 5c). Matrix metalloproteases also were invented as Type II novelties, whereas guidance cues such as netrin and semaphorin that mediate adhesion are novelties with no clear homology to ancient eukaryotic proteins.

Signaling Pathways

Animals rely on cell-cell signaling for cellular coordination during and after development (64).

Various components of the Wnt and TGF- β signaling pathways in the genome of *Nematostella* have been reported ((24, 27, 28, 62, 65, 66)). We find that in both pathways, the secreted ligands and their antagonists (wnt, SFRP, BMP, chordin etc.) are novelties (Figure 5b). Some, such as Wnt, SFRP, dpp/BMP, activin and chordin are Type I novelties with no homology to proteins from outgroups; some are Type II novelties (dickkopf) and some, such as tolloid are novel pairings of ancient domains (Type III). The receptor in the Wnt pathway, frizzled, also arose as a Type I eumetazoan novelty. Transcription factors that are activated downstream of Wnt signaling are ancient, but the ones involved in TGF- β signaling are novel. Type I receptors of the TGF- β pathway arose as a pairing of novel animal domains with ancient domains (Type II novelties) and type II receptors turn out to be ancient eukaryotic kinase genes that were co-opted

for this function.

The presence of essentially complete signal transduction pathways in the common gene set of cnidarians and bilaterians strongly suggests that the integration of novel eumetazoan genes into these systems was largely complete in the eumetazoan ancestor. A general trend in the evolution of signaling pathways may have been the co-option of cytosolic signaling components into pathways that could be regulated by newly invented ligands and receptors. For example, in the case of FGF signaling, the interactions of ancient cytosolic components (*e.g.* Grb2, Sos, MAPK) could be elaborated with the addition of novel proteins (*e.g.* FGF and Shc), or of novel domains added to old proteins (*e.g.* Raf homolog) or novel pairings of old domains (*e.g.* FGFR and PLC-gamma).

Emergence of the neuromuscular system

Cnidarians and ctenophores are the earliest branching metazoan phyla that have a nervous system, though they lack overt centralization of the kind observed in bilaterians. Numerous genes known to be involved in neurogenesis, such as members of the homeobox and basic helix-loop helix transcription factor families (Emx, Otp, Otx; achaete-scute), can be traced to ancient eukaryotic genes with these signature domains. Some are novel pairings of ancient domains (such as neuropilin and Lim-homeobox genes), some are pairings of old domains with novel animal-specific domains (such as Dsh, Arx, neuralized) and others are novel animal genes (*e.g.*, Hes, Gcm, netrin, semaphorins, dachshund). Certain enzymes important in synaptic transmission (*e.g.* DOPA-beta monooxygenase) and some vesicular trafficking proteins (*e.g.* synaptophysin) appear as completely novel (Type I) eumetazoan proteins. Regulatory subunits for ion channels important in nerve conduction and muscular function can be Type I novelties (*e.g.* voltage

dependent calcium channel beta subunit, potassium large conductance calcium-activated channel) or Type III novelties (*e.g.* voltage dependent calcium channel alpha2/delta subunit). Various components of the dystrophin-associated protein complex (DPC) in the sarcolemma such as dystrophin, syntrophin, beta-dystrobrevin and beta-sarcoglycan are Type I novelties. Other sarcomere proteins are Type II novelties (*e.g.* nebulin and tropomodulin). This diversity of origins of genes with different roles in the neuromuscular system suggests that tracing the evolution of nerves and muscle will require detailed studies of the functions of these genes in organisms at the base of the metazoan tree.

Concluding remarks

Modern animal genomes retain features inherited from the eumetazoan ancestor that have been elaborated on, and sometimes overwritten by, subsequent evolutionary elaborations and simplifications. By comparing genomes, we can infer conserved ancestral features and characterize the gene- and genome-level changes that occurred during the evolution of different lineages. Here we have compared the genomes of the sea anemone and diverse bilaterians, both to infer the content and organization of the genome of the eumetazoan ancestor, and to trace the origins of uniquely animal features. In many ways, the ancestral genome was not so different from ours; it was intron rich, and contained nearly complete "toolkits" for animal biochemistry and development, which can now be recognized as pan-eumetazoan, as well as the core gene set required to execute sophisticated neural and muscular function. Remarkably, the ancestor had blocks of linked genes that remain together in the modern human and anemone genomes -- the oldest known conserved synteny outside of prokaryotic operons. While fruit flies and soil nematodes have proven to be exquisite model systems for dissecting the genetic underpinnings of

metazoan development and physiology, their genomes are relatively poor models for the ancestral eumetazoan genome, having lost introns, genes, and gene linkages.

The eumetazoan ancestor possessed over fifteen hundred genes that are apparently novel relative to other eukaryotic kingdoms. Where did these genes come from? Some are the result of domain shuffling, bringing together on the animal stem new combinations of domains that are shared with other eukaryotes. But a significant number of animal-specific genes contain sequences with no readily recognizable counterparts outside of animals; these may have arisen by sequence divergence from ancient eukaryotic genes, but the trail is obscured by deep time. While we can crudely assign the origins of these genes to the eumetazoan stem, this remains somewhat unsatisfying. The forthcoming genomes of sponges, placozoans, and choanoflagellates will allow more precise dating of the origins and diversification of modern eumetazoan gene families, but this will not directly reveal the mechanisms for new gene creation. Presumably many of these novelties will ultimately be traced back, through deep sequence or structural comparisons, to ancient genes that underwent extreme "tinkering."

The eumetazoan progenitor was more than just a collection of genes. How did these genes function together within the ancestor? Unfortunately, we cannot read from the genome the nature of its gene- and protein-regulatory interactions and networks. This is particularly vexing as it is becoming clear -- especially given the apparent universality of the eumetazoan toolkit -- that gene regulatory changes can also play a central role in generating novelties, allowing co-option of ancestral genes and networks to new functions (67). *Nematostella* and its genome, however, provide a platform for testing hypotheses about the nature of ancestral eumetazoan pathways and

interactions, using the basic principle of evolutionary developmental biology: processes that are conserved between living species were likely functional in their common ancestor. Of particular interest are the processes that give rise to body axes, germ layers, and differentiated cell types like nerve and muscle, as well as the mechanisms that maintain these cells and their interactions through the growth and repair of the organism.

Although we have focused our initial analysis of the *Nematostella* genome on deciphering the eumetazoan ancestor, and therefore on the similarities between anemone and bilaterian genomes, their differences are also of interest, and the sequence will of course be valuable as a reference for molecular studies of cnidarian biology, especially when combined with the soon-to-be-available genome of *Hydra* to bracket the phylum. An enduring mystery is the development of the unique stinging cells that define the Cnidaria. Of particular interest is an improved understanding of the biology of modern corals that are, like *Nematostella*, anthozoan cnidarians. The relationship of these stony corals with their photosynthetic symbionts is instrumental in the health of coral reefs around the world -- and the continuing maintenance of the rich animal diversity that descended from the eumetazoan ancestor.

FIGURE CAPTIONS

Figure 1. *Nematostella* development and anatomy. a. unfertilized egg (~200 micron diameter) with sperm head; b. early cleavage stage; c. blastula; d. gastrula; e. planula; f. juvenile polyp; g. adult stained with DAPI to show nematocysts with a zoom in on the tentacle in the inset; h, i. confocal images of a tentacle bud stage and a gastrula respectively showing nuclei (red) and actin (green); j. a gastrula showing snail mRNA (purple) in the endoderm and forkhead mRNA (red) in the pharynx and endoderm; k. a gastrula showing Anthox8 mRNA expression; l. an adult *Nematostella*.

Figure 2. Bayesian phylogeny of metazoa. 2a. Bayesian analysis infers metazoan phylogeny and rate of amino acid substitution from sequenced genomes based on 337 single-copy genes in *Ciona intestinalis* (Sea squirt), *Takifugu rubripes* (Fish), *Xenopus tropicalis* (Frog), Human, *Lottia gigantea* (Snail), *Drosophila melanogaster* (Fly), *Caenorhabditis elegans* (Nematode), *Hydra magnipapillata* (Hydra), *Nematostella*, *Reniera sp. JGI-2005* (Sponge), *Monosiga brevicollis* (Choanoflagellate), and *Saccharomyces cerevisiae* (Yeast). All nodes were resolved as shown in 100% of sampled topologies in Bayesian analysis. "E", the eumetazoan (cnidarian-bilaterian) ancestor; "B" the bilaterian (protostome-deuterostome) ancestor. S1 and S2 are the eumetazoan and bilaterian stems respectively (32). 2b. Numbers of inferred gene gains and gene family expansions on the eumetazoan and bilaterian stems.

Figure 3. Patterns of intron evolution in eukaryotes. 3a. Branch lengths proportional to the number of inferred intron gains (left), and intron losses (right) under the weighted parsimony assumption that introns with conserved position and phase were gained only once in evolution. The bottom scale indicates the change in intron number for gains (left) and losses (right), relative to the inferred introns of the eumetazoan ancestor. Based on a sample of 5175 introns at highly conserved protein sequence positions from *Arabidopsis thaliana* (Plant), *Cryptococcus neoformans* (Fungus), *C. elegans* (Nematode), *D. melanogaster* (Fly), *Ciona intestinalis* (Sea squirt), *Homo sapiens* (Human), and *Nematostella* (32). 3b. Examples of different patterns of intron gain/loss. Bars of the same color represent conserved regions across all species. Chevrons indicate introns and the number below the chevron shows the phase of the intron.

Figure 4. Conserved synteny between the human and anemone genomes. 4a. The human genome, segmented into 98 regions that have not rearranged during chordate evolution. Colored segments indicate statistically significant conservation of linkage between human and *Nematostella*. Red segments are members of the 12 compact putative ancestral linkage groups (PAL) labeled A-L. Green segments fall into the diffuse 13th PAL (32). White segments do not show significant conservation of linkage. 4b. Detail of the "Oxford grid" which tabulates the number of ancestral gene clusters shared between the 22 *Nematostella* scaffolds (columns) and 14 segments of the human genome (rows) that are assigned to PALs A, B and C. Cell colors indicate Bonferroni-corrected p-value < 0.01 (yellow), < 0.05 (pink), < 0.5 (blue). Detailed methods, and the complete Oxford grid can be found in supporting online material. 4c. A diagram showing conserved linkage between human chromosomal segments and *Nematostella* scaffolds in the first PAL (which includes the Hox cluster). *Nematostella* scaffolds 26, 61, 53,

46, 3, and 5, and human chromosomes 17, 12, 10, 7, and 2 represented by blue arrows, each proportional in length to the number of genes descended from the inferred ancestral set. The positions of orthologous *Nematostella* and human genes are joined by lines, color-coded by *Nematostella* scaffold. The 5 segments of the human genome which are grouped into PAL A are indicated by black boxes. The four human Hox clusters are indicated by red bars, the vertical extent of which corresponds to the extent of each hox cluster on the chromosome.

Figure 5. Origins of eumetazoan genes. 5a. Pie chart showing the percentages of genes in the eumetazoan ancestors according to their origin - Type I novelties with no homology to proteins in non-animal outgroups (blue), Type II novelties with novel animal domains paired with ancient domains (orange), Type III novelties with new pairings of ancient domains (purple) and ancient genes (green). ; 5b. A schematic representation of the FAK and Shc/Fyn pathways in integrin signaling. The proteins are color coded to reflect their ancestry as in 5a. 5c. Evolution of metazoan signaling pathway components. Genes are categorized by their ancestry. 5d. Evolution of selected metazoan processes as in 5c.

References

1. E. Haeckel, *Generelle Morphologie der Organismen* (Georg Reimer, Berlin, 1866), pp.
2. C. Nielsen, *Animal Evolution, 2nd edition* (Oxford University Press, Oxford, 2001), pp.
3. J. W. Valentine, *On the Origin of Phyla* (U. Chicago Press, Chicago, 2004), pp.
4. G. M. Rubin *et al.*, *Science* **287**, 2204 (Mar 24, 2000).
5. G. Ruvkun, O. Hobert, *Science* **282**, 2033 (Dec 11, 1998).
6. C. I. Bargmann, *Science* **282**, 2028 (Dec 11, 1998).
7. P. Dehal *et al.*, *Science* **298**, 2157 (Dec 13, 2002).
8. E. Sodergren *et al.*, *Science* **314**, 941 (Nov 10, 2006).
9. D. Bridge, C. W. Cunningham, B. Schierwater, R. DeSalle, L. W. Buss, *Proc Natl Acad Sci U S A* **89**, 8750 (Sep 15, 1992).
10. S. Conway Morris, *Paleontology* **36**, 593 (1993a).
11. A. Seilacher, *Lethaia* **22**, 229 (1989).
12. S. Conway Morris, *Nature* **361**, 219 (1993b).
13. J. Y. Chen *et al.*, *Dev Biol* **248**, 182 (Aug 1, 2002).
14. C. Hand, K. Uhlinger, *Biological Bulletin* **182**, 169 (1992).
15. J. A. Darling *et al.*, *Bioessays* **27**, 211 (Feb, 2005).
16. C. Hand, K. Uhlinger, *Estuaries* **17**, 501 (1994).
17. J. H. Fritzenwanker, U. Technau, *Dev Genes Evol* **212**, 99 (Mar, 2002).
18. Y. Kraus, U. Technau, *Dev Genes Evol* **216**, 119 (Mar, 2006).
19. C. A. Byrum, M. Q. Martindale, in *Gastrulation: From Cells to Embryos* C. D. Stern, Ed. (Cold Spring Harbor Laboratory Press, Cold Spring Harbor, 2004) pp. 33-50.
20. M. Q. Martindale, K. Pang, J. R. Finnerty, *Development* **131**, 2463 (May, 2004).

21. J. R. Finnerty, D. Paulson, P. Burton, K. Pang, M. Q. Martindale, *Evol Dev* **5**, 331 (Jul-Aug, 2003).
22. J. H. Fritzenwanker, M. Saina, U. Technau, *Dev Biol* **275**, 389 (Nov 15, 2004).
23. C. B. Scholz, U. Technau, *Dev Genes Evol* **212**, 563 (Jan, 2003).
24. A. H. Wikramanayake *et al.*, *Nature* **426**, 446 (Nov 27, 2003).
25. C. G. Extavour, K. Pang, D. Q. Matus, M. Q. Martindale, *Evol Dev* **7**, 201 (May-Jun, 2005).
26. M. Q. Martindale, J. R. Finnerty, J. Q. Henry, *Mol Phylogenet Evol* **24**, 358 (Sep, 2002).
27. D. Q. Matus *et al.*, *Proc Natl Acad Sci U S A* **103**, 11195 (Jul 25, 2006).
28. D. Q. Matus, G. H. Thomsen, M. Q. Martindale, *Curr Biol* **16**, 499 (Mar 7, 2006).
29. F. Rentzsch *et al.*, *Dev Biol* **296**, 375 (Aug 15, 2006).
30. T. A. Stephenson, *London: The Ray Society II* (1935).
31. J. L. Weber, E. W. Myers, *Genome Res* **7**, 401 (May, 1997).
32. Materials and methods are available as supporting material.
33. J. C. Sullivan *et al.*, *Nucleic Acids Res* **34**, D495 (Jan 1, 2006).
34. G. A. Tuskan *et al.*, *Science* **313**, 1596 (Sep 15, 2006).
35. S. Aparicio *et al.*, *Science* **297**, 1301 (Aug 23, 2002).
36. J. A. Darling, A. M. Reitzel, J. R. Finnerty, *Mol Ecol* **13**, 2969 (Oct, 2004).
37. A. M. Reitzel, *submitted* (2007).
38. R. L. Tatusov, E. V. Koonin, D. J. Lipman, *Science* **278**, 631 (Oct 24, 1997).
39. A. Adoutte *et al.*, *Proc Natl Acad Sci U S A* **97**, 4453 (Apr 25, 2000).
40. Y. I. Wolf, I. B. Rogozin, E. V. Koonin, *Genome Res* **14**, 29 (Jan, 2004).
41. F. D. Ciccarelli *et al.*, *Science* **311**, 1283 (Mar 3, 2006).
42. E. J. Douzery, E. A. Snell, E. Bapteste, F. Delsuc, H. Philippe, *Proc Natl Acad Sci U S A*

- 101**, 15386 (Oct 26, 2004).
43. K. J. Peterson *et al.*, *Proc Natl Acad Sci U S A* **101**, 6536 (Apr 27, 2004).
 44. J. C. Sullivan, A. M. Reitzel, J. R. Finnerty, *Genome Informatics* **17**, 219 (2006, 2006).
 45. F. Raible *et al.*, *Science* **310**, 1325 (Nov 25, 2005).
 46. I. B. Rogozin, Y. I. Wolf, A. V. Sorokin, B. G. Mirkin, E. V. Koonin, *Curr Biol* **13**, 1512 (Sep 2, 2003).
 47. J. S. Conery, M. Lynch, *Pac Symp Biocomput*, 167 (2001).
 48. J. H. Postlethwait *et al.*, *Genome Res* **10**, 1890 (Dec, 2000).
 49. O. Jaillon *et al.*, *Nature* **431**, 946 (Oct 21, 2004).
 50. T. H. Sequencing Consortium, *Nature* **444**, 512 (Nov 23, 2006).
 51. A. McLysaght, K. Hokamp, K. H. Wolfe, *Nat Genet* **31**, 200 (Jun, 2002).
 52. G. Bourque, E. M. Zdobnov, P. Bork, P. A. Pevzner, G. Tesler, *Genome Res* **15**, 98 (Jan, 2005).
 53. L. G. Lundin, D. Larhammar, F. Hallbook, *J Struct Funct Genomics* **3**, 53 (2003).
 54. J. R. Finnerty, K. Pang, P. Burton, D. Paulson, M. Q. Martindale, *Science* **304**, 1335 (May 28, 2004).
 55. K. Kamm, B. Schierwater, W. Jakob, S. L. Dellaporta, D. J. Miller, *Curr Biol* **16**, 920 (May 9, 2006).
 56. J. F. Ryan *et al.*, *Genome Biol* **7**, R64 (Jul 24, 2006).
 57. D. Chourrout *et al.*, *Nature* **442**, 684 (Aug 10, 2006).
 58. K. Kamm, B. Schierwater, *J Exp Zool B Mol Dev Evol* (Jul 12, 2006).
 59. J. R. Finnerty, M. Q. Martindale, *Evol Dev* **1**, 16 (Jul-Aug, 1999).
 60. F. Delsuc, S. F. Vizcaino, E. J. Douzery, *BMC Evol Biol* **4**, 11 (Apr 28, 2004).
 61. L. Patthy, *Protein Evolution* (Blackwell Science Ltd., Oxford, 1999), pp.

62. A. Kusserow *et al.*, *Nature* **433**, 156 (Jan 13, 2005).
63. S. Tyler, *Int Comp Biol* **43**, 55 (2003).
64. A. Pires-daSilva, R. J. Sommer, *Nat Rev Genet* **4**, 39 (Jan, 2003).
65. U. Technau *et al.*, *Trends Genet* **21**, 633 (Dec, 2005).
66. P. N. Lee, K. Pang, D. Q. Matus, M. Q. Martindale, *Semin Cell Dev Biol* **17**, 157 (Apr, 2006).
67. M. Levine, R. Tjian, *Nature* **424**, 147 (Jul 10, 2003).

Acknowledgements.

This work was performed under the auspices of the US Department of Energy's Office of Science, Biological and Environmental Research Program, and by the University of California, Lawrence Livermore National Laboratory under Contract No. W-7405-Eng-48, Lawrence Berkeley National Laboratory under contract No. DE-AC02-05CH11231, and Los Alamos National Laboratory under contract No. DE-AC02-06NA25396. Genetic Information Research Institute under the NIH grant 5 P41 LM006252-08. DSR, MS, and WD gratefully acknowledge the support of the Gordon and Betty Moore Foundation. We thank Heather Marlow, Dave Matus, Kevin Pang, Patricia Lee, Craig Magie for contributions to Figure 1, and Emina Begovic, Eric Edsinger-Gonzales, David Goodstein, Meredith Carpenter, Charles David, Mike Levine, and John Gerhart for useful conversations. This work is dedicated to the late Cadet Hammond Hand, Jr. (1920-2006), a pioneer in cnidarian biology who first reported the starlet sea anemone in California over fifty years ago, and who proposed and helped develop *Nematostella* as a model animal for developmental biology. His contributions to invertebrate zoology are summarized at nematostella.org.

Figure 1.

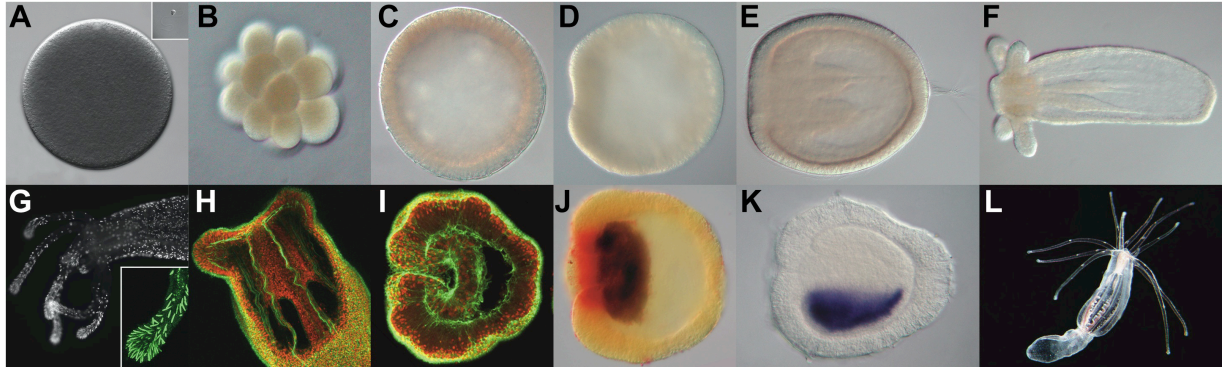


Figure 2a.

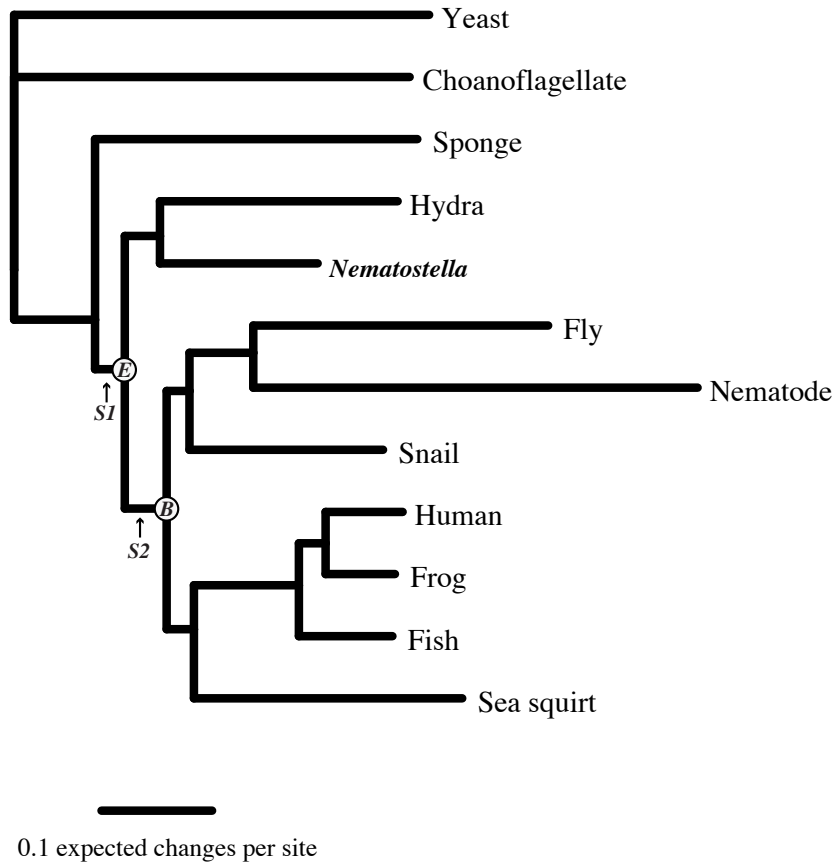


Figure 2b.

	Eumetazoan Stem	Bilaterian Stem
New genes originated	1148	662
New genes created through gene family expansion	1470	320
Reconstructed genes of the recent common ancestor	7766	8748

Figure 3.

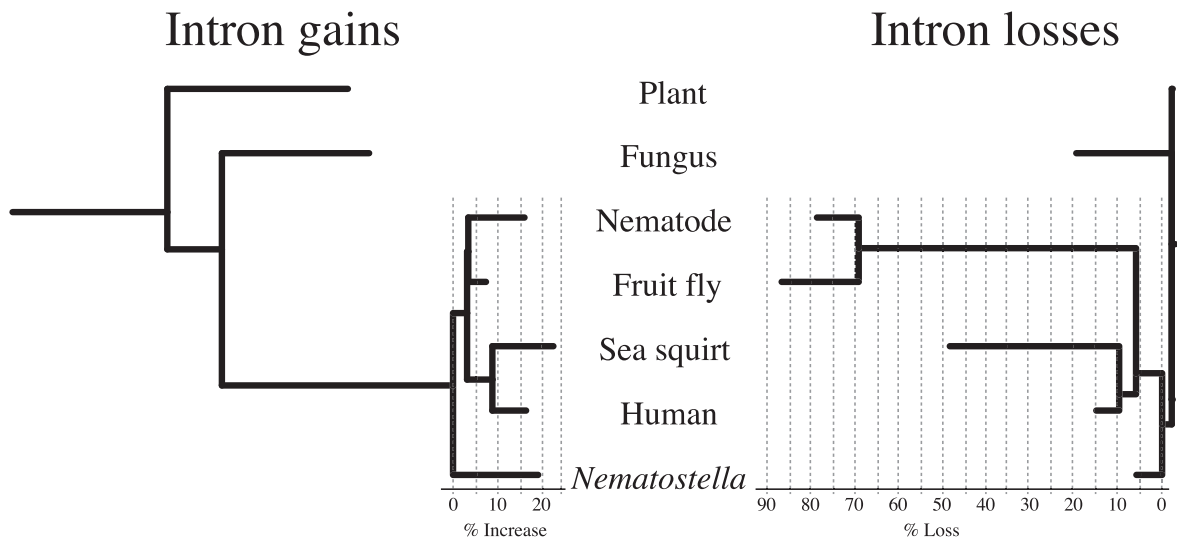


Figure 3b.



Figure 4a.

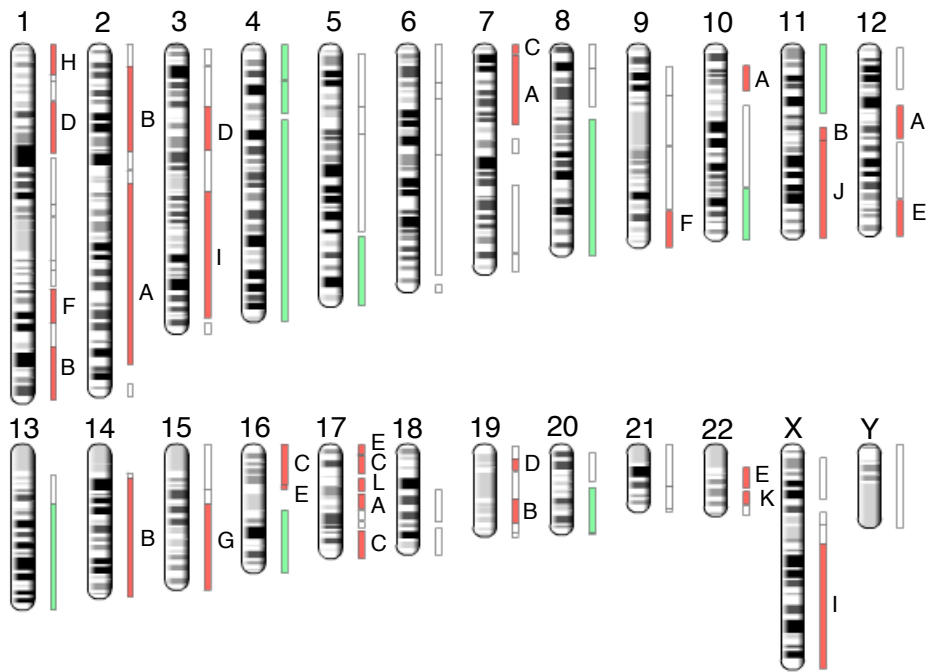


Figure 4b.

		A							B							C							
Nematostella scaffold:		3	5	46	26	53	61	44	144	7	74	18	88	52	42	156	89	10	8	34	118	91	191
Human Chromosome Segment:	2q11.2-35	25	32	17	16	17	9	12	7	1	2			2	1		1	1	1	2			
	12q12-14.3	16	14	9	5	8	3	6	5			1								1	1		
A	17q12-21.32	12	8	4	10	6	4	3	1			1	1		1					1			
	7p11.2-21.3	4	10	3	3	2	7	1	2			1	1					2	1	1	1	1	1
	10p11.22-13	8	6	1	1	2	1	4	1														
B	14q12-32.33	10	3	2	4	5	3	3	2	23	12	13	11	17	11	9	8	1	2				1
	11q12.1-13.1	4					2	2	1	12	7	1	6	6	1	4				2			
	1q32.2-44	6	4		1	1	2		1	11	6	6	3	6	2	2	1						1
	19q13.11-13.33	4	1	2	2	1	2	1		5	8	8	4	6	2	3		2	3		1	1	
C	2p13.2-24.3	5	2	2	1	2	1	2	1	8	5	10	5	3	1	5	3	2		1			
	17q23.3-25.3	1	2						1	2		2	1					19	10	12	8	7	3
	16p11.2-13.3	1			1	1						1	1	1				17	19	9	5	6	6
	7p22.1-22.3											1		1	1			6	3	3	5	2	
	17p11.2-13.1				1							1		1			1	6	2		1	3	

Figure 4c.

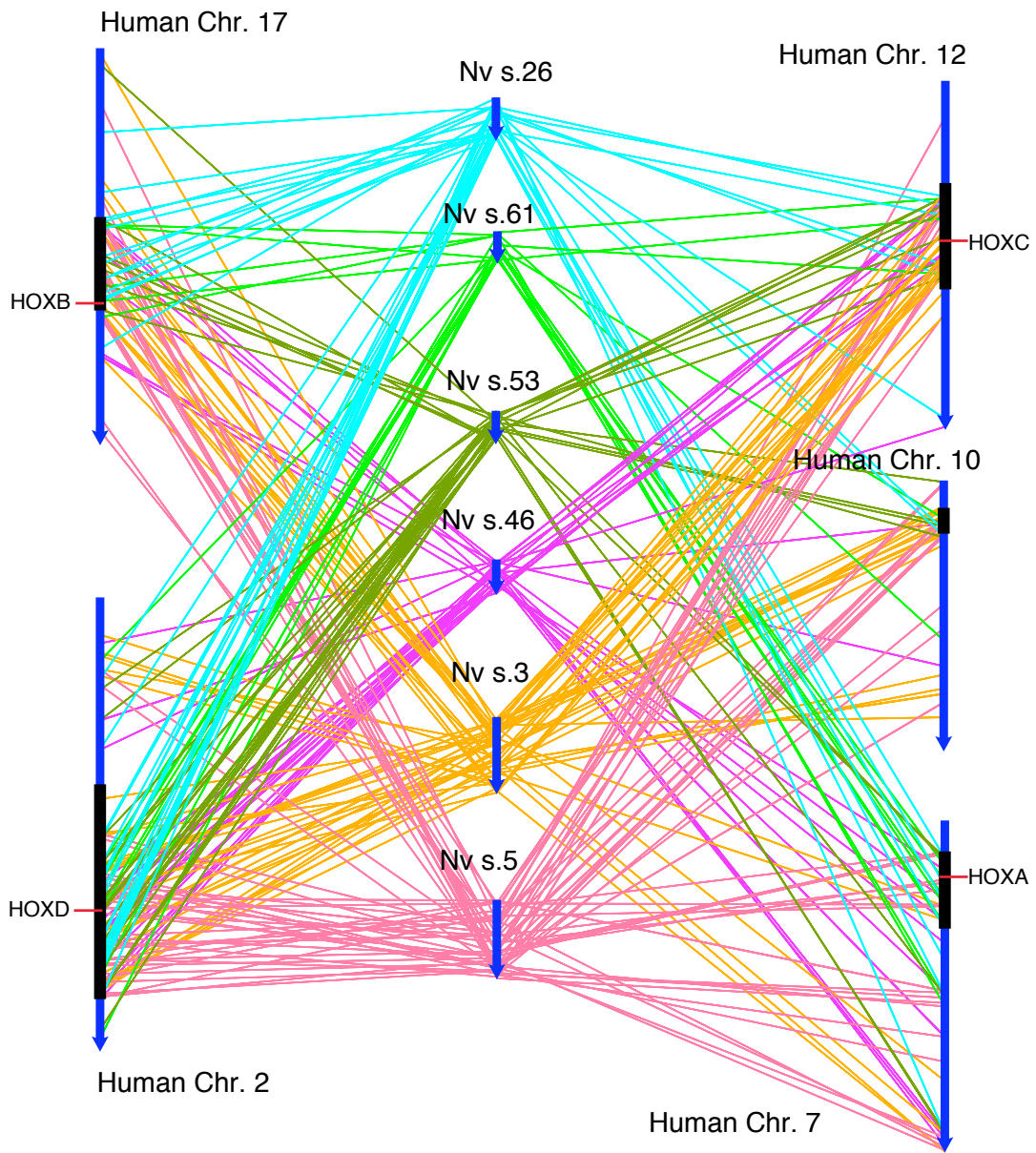
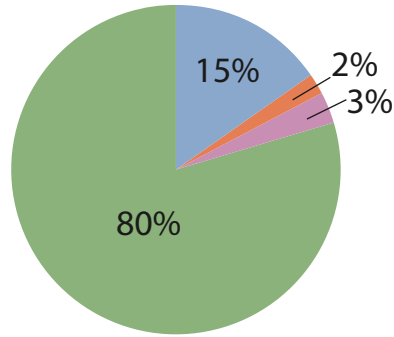
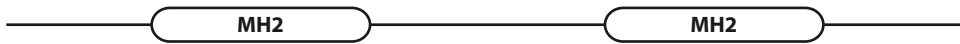


Figure 5a.



- Type I (completely novel)
- Type II (novel domain)
- Type III (novel pairing)
- Ancient

Type I Novelty: SMAD Family Proteins



Type II Novelty: Notch Proteins



Type III Novelty (Lim Homeodomain Proteins)



Figure 5b.

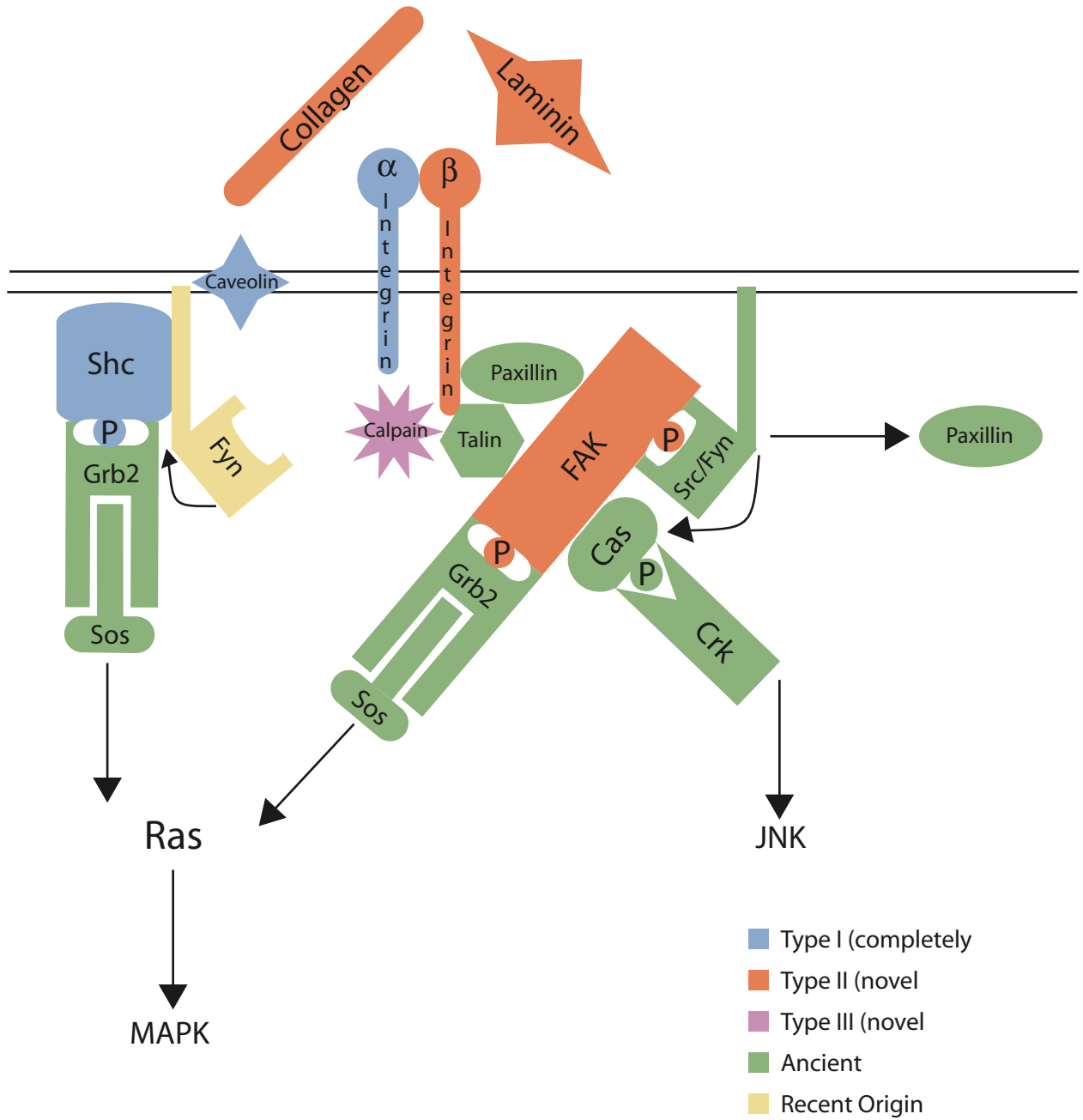


Figure 5c.

Pathway	Type I Novelty	Type II Novelty	Type III Novelty	Ancient Gene
Integrin signaling	Integrin-alpha; caveolin	Collagen; Integrin-beta; Fak; Jun	Calpain	talin; vinculin; Paxillin; Ras; Grb2; So5; Rap; ERK; MEK; Crk
Wnt signaling	Wnt; secreted frizzled related factors; frizzled; strabismus/van gogh	Dickkopf; arrow; dishevelled; axin		Beta-catenin; GSK3; APC; TCF/LEF; groucho
TGF-beta signaling	dpp/BMP; activin (nodal, nodal-related); gremlin; chordin; follistatin; R-SMAD; I-SMAD; co-SMAD	Type I receptors: TGFBR1, BMPRI1A; ATF/JunB; snoN	Tolloid/BMP1	Type II receptors: ACVR2, BMPR2
Notch signaling	Numb; hairy/E(spl)	notch		Jagged; deltex; Fringe; presenilin; ADAM10; nicastrin; furin; Aph1; PEN2; mastermind
Ephrin signaling		Ephrin; Fak	Eph (receptor)	Abl/SYK
Insulin signaling	insulin	insulin receptor substrate; phosphoinositide-3-kinase, catalytic	Insulin receptor/IGFR; phosphoinositide-3-kinase, class 2	phosphoinositide-3-kinase, class 3; phosphoinositide-3-kinase, regulatory subunit; 3-phosphoinositide dependent protein kinase-1; PTEN
FGF signaling	FGF; Shc	Raf homolog serine/threonine-protein kinase; Ras GTPase activating protein	FGFR; RAS protein activator; phospholipase C, gamma; phosphoinositide-3-kinase, class 2; Protein kinase C iota	MAPK; phosphoinositide-3-kinase, class 3; Grb2; Protein kinase C, Sds; Rac
Cytokine signaling	inositol 1,4,5-triphosphate receptor; SOCS; arrestin; guanine nucleotide binding protein (G protein); gamma, regulator of G-protein signalling; REL/NFKB; NFAT	Adenylate cyclase 5/6; STAT5. ATF/Jun	CDC42 binding protein kinase	MAPK; Rho kinase; Rho

Figure 5d.

Process	Type I Novelty	Type II Novelty	Type III Novelty	Ancient Gene
neurogenesis	Hes, Gcm, Ephrin, netrin, semaphorin, dachshund, ski oncogene	notch, NGFR, Dsh, Arx, CREB/ATF, neuralized	neuropilin, Lhx, Eph receptor,	single-minded/HIF, achaete-scute, elav, Emx, Otp, Jagged, Deltex, Irx, Gli, Otx/Phox, stonal/neuroD/neuroG, reticulon
synaptic transmission	nitric oxide synthase (neuronal) adapter protein, DOPA-beta monooxygenase, calcium channel voltage dependent beta, syntrophin, synaptophysin, dystrophin, potassium large conductance calcium-activated channel, subfamily M, beta	cholinergic receptor nicotinic, neurexin	K-voltage gated channel, discs large	glutamate receptor, synaptotagmin, intersectin, synapsin, neuroligin/CES, syntaxin, glutamate transporter
ECM	netrin, dermatopontin, semaphorin, glypican, stereocilin	collagen, spondin, laminin,	nidogen, stabilin, neuropilin, matrix metalloprotease, thrombospondin	leprecan, microfibrillar associated protein
cell junction	par-6	tight junction protein		salvador
muscle contraction	voltage dependent calcium channel beta, beta-sarcoglycan, beta-dystrobrevin	cholinergic receptor nicotinic, nebulin, tropomyosin, calponin/transgelin	voltage dependent calcium channel alpha2/delta subunit, inositol triphosphate receptor, calcium activated potassium channel slowpoke	phosphorylase kinase, myosin light chain cytoplasmic, calcium channel alpha subunit, cGMP dependent protein kinase, calcium/calmodulin dependent kinase II, myosin regulatory light chain
Apoptosis	TNF5/10/11; Bcl2; BOK; GULP; engulfment adaptor PTB domain containing 1; CRADD; caspase 8/10; GULP1; growth arrest and DNA-damage-inducible; DNA fragmentation factor 40 kDa subunit ; Interleukin enhancer-binding factor 3; FMR	BIRC; CARD9/11	NGFR; SLIT-ROBO Rho GTPase activating protein; calpain	TNFRSR; TRAF; scavenger receptor class B; huntingtin interacting protein; programmed cell death 1/5; Bcl2-associated athanogene; Akt; SUMO; defender against cell death 1; apoptosis-inducing factor (AIF)-like mitochondrion-associated inducer of death; death-associated protein kinase
Transcription factors	L3MBT; T-Box; Nuclear hormone receptor; SMAD; dachshund; gcm; NFAT; nuclear respiratory factor; SNO and SKI family: sprouty; AP-2; onecut; MAF-related;	CBP/p300; ETO/MTG8/Nervy; groucho; Jun; Myt1; runt; STAT	hairless; nuclear protein 95; LIM homeobox; CCAAT enhancer binding; aryl hydrocarbon receptor related	zic; Gli; homeobox; bHLH; achaete-scute; sox; retinoblastoma binding protein 5/8; NFKB-related; Krueppel C2H2 type zinc finger; irx; Deltex; ataxin

Supporting Online Material

Supplement S1

Additional background information on *Nematostella vectensis*.

The starlet sea anemone *Nematostella vectensis* (Family: Edwardsiidae) is a burrowing, brackish-water, solitary sea anemone with a worldwide distribution (1, 2). Self-sustaining laboratory cultures can be maintained year-round in artificial seawater, with daily feedings of brine shrimp (3, 4). While sexes are separate, they are not obviously morphologically distinguishable. *Nematostella* is unique among cnidarians in that it can be induced to spawn repeatedly on a regular cycle in the laboratory to produce large numbers of gametes that can be manipulated by simple in vitro fertilization methods (4). Development occurs via planula larvae that emerge from the jelly of the egg mass within two days at 20-25C (5-6 days at 18C) (4). Planulae are formed by gastrulation via invagination, and have an apical tuft at one end of the animal. A single planula larva is about 250 µm in length and consists of over 10,000 cells (Figure 3A-I). Metamorphosis into a four-tentacled juvenile polyp with two mesenteries (partitions that partially divide the gut and increase its surface area, also providing pouches for the production and storage of gametes) takes about a week, with sexual maturity reached in 3-4 months. Mature adults are hollow tubes typically 5-10 cm in length, with an open (oral) end encircled by 10-20 tentacles a few cm long, and a closed (aboral) end (Figure 2). The animals are carnivorous, capturing and consuming plankton, including small animals and their larvae, using tentacles and the characteristic stinging cells of cnidarians, which inject neurotoxin into prey.

Individual animals have been maintained in the laboratory for over fifteen years (C. Hand, private communication). Asexual reproduction can be induced by tying a fine thread around the body tube. Within a few days, the animal will separate into two individuals, producing both a new mouth and basal disc. As with other cnidarians, *Nematostella* possesses considerable regenerative abilities, reconstituting a complete and properly proportioned adult from only a part of the animal. Tentacles can also regrow when cut. It is not known how tentacle number or body tube length is regulated, either in regeneration or embryogenesis.

Table S1.1 contains a partial list of the merits of *Nematostella* as a model organism.

Figure 1 Methods

Nematocyst staining (Figure 1g): (Methods adapted from (5)) Juvenile and small adult *Nematostella* polyps were relaxed in 7.14% MgCl₂ in dH₂O for ten minutes and then washed quickly three times in 1X PBS with 10mM EDTA. They were then fixed in 4% paraformaldehyde in 1X PBS with 10mM EDTA for one hour at 4°C. After washing three times for five minutes each in 1X PBS with 10mM EDTA, the animals were stained in a 200µM DAPI solution in 1X PBS for thirty minutes. Animals were mounted in 70% glycerol in Ptw after washing three times for five minutes each in 1X PBS with 10mM EDTA.

In situ hybridization (Figures 1 j,k): In situ hybridization was carried out as previously described (6).

Supplement S2

Source material for genome sequencing

Genomic DNA was prepared in the laboratory of Ulrich Technau from larval F1 progeny of CH2 males

and CH6 females. These parental strains – clones of which are widely available today in at least four laboratories and can be readily redistributed – are from the original colony established and maintained by Cadet Hand at the Bodega Bay Marine Laboratory in the early 1990's (3). Because commensals or symbionts have been reported for *Nematostella*, gametic or embryonic DNA is preferred to avoid contamination from symbionts and/or undigested food. DNA from the same preparation was used to create a BAC library, described below. Thanks to asexual reproduction, the haplotypes represented in the draft genome sequence and BAC library [see below] can be propagated indefinitely.

CHORI BAC library

A Bacterial Artificial Chromosome (BAC) library was produced by Drs. Baoli Zhu and Pieter de Jong at the Children's Hospital Oakland Research Institute (CHORI). This library provides a ten-fold coverage of the genome. The average size of the inserts in the library is 168 kb. Funding for construction of the library was provided by a grant from the NSF (Robert Steele, PI, Ulrich Technau, Co-PI). The library is available through the CHORI BACPAC resource (deJong et al). More information can be found at <http://bacpac.chori.org/library.php?id=219>.

Whole Genome Shotgun (WGS) Sequencing and Assembly.

The genome of *Nematostella vectensis* was sequenced and assembled by whole genome shotgun (WGS) (7) as previously described (8). Briefly, genomic DNA prepared as described above was used to create shotgun libraries with inserts of approximately 3,000 bp, 6,500 bp and 35,000 bp. The libraries used, their mean insert sizes, and the numbers of reads sequenced are listed in Table S2.1. The shotgun reads were trimmed of low quality and vector-derived sequence, and assembled using JAZZ(8, 9). Approximately one third of the shotgun reads are composed entirely of high copy-number repeat sequences, and are therefore masked at the alignment stage of JAZZ, and therefore remain unassembled. Table S2.2 lists 10 abundant tandemly-repeated sequences in the shotgun dataset which together account for 32% of shotgun reads.

The assembled genome contains a total of 59,124 contiguous reconstructed sequences ("contigs") with a total length of 297 million base pairs (Mbp) and 10,804 "scaffolds", or reconstructed fragments of the genome that include gaps of unknown sequence, with a total length of 356 Mbp. Half of the contig sequence is contained in the largest 3,617 contigs, which are all at least 19,835 bp in length (N50). Half of the total scaffold sequence is contributed by the largest 181 scaffolds, which are each at least 472 Kbp in length.

Approximately 0.8% of positions in the assembly contain a polymorphic site (Figure S2.1), and we estimate that the mean pairwise variation between the four haplotypes represented in the libraries is 0.64 % (Figure S2.2).

Expressed sequence tag (EST) library preparation, sequencing, and assembly

A mixed stage cDNA library for *Nematostella* was prepared in the laboratory of Ulrich Technau, cloning polyA RNA from unfertilized eggs through metamorphosis into pSPORT 6.1. The library contains 56 million colony forming units (cfu) at a concentration of 4.7 million cfu/ml. The average insert size of the library is 1.96 kb, with greater than 99.5% recombinant, and an estimated 75% full length based on pilot sequencing. Of 1,152 sample sequences, 99.9% were passing, and 80% possessed significant BLASTX hits (E-value < 1E-5). 780 contigs were produced, with 680 single clones; the most abundant sequence was EF-1a, found in 3% of the sample, indicating that even without normalization this library

has a relatively low level of redundancy.

To enable the characterization of gene structures and to provide resources for further study, 88,704 cDNA clones from the library were end-sequenced to provide 146,095 expressed sequence tags (ESTs). The ESTs were clustered and assembled into 30,813 contigs via the JGI EST pipeline. Of these, 7,925 contigs were found to have a complete (start codon to stop codon) open reading frame (ORFs) of at least 450 bp. These putatively full-length EST contigs were aligned to the assembled WGS scaffolds using BLAT(10) (-maxIntron=100000 -extendThroughN).

To evaluate the completeness of the WGS assembly with respect to this collection of ESTs, we considered the number of putative full length EST contigs aligned to the genome at varying levels of completeness. For alignments of at least 95% sequence identity, 7,738 (97.6%) had an alignment spanning at least 25% of the length of the EST contig, 7,557 (95.4%) had an alignment spanning at least 75% of the length of the EST contig, and 7,193 (90.8%) had an alignment spanning at least 95% of the length of the EST contig. 138 of the 222 EST contigs that lacked an alignment over at least 50% of their length had an identifiable alignment to human refseq genes by BLASTP(11) (-e 1e-5), indicating that they are likely to represent *bona fide* protein-coding transcripts rather artifactual sequence. Others may be contaminants of the EST library, or novel genes.

839 (11.1%) of the EST contigs had alignments of at least 95% identity spanning at least 75% of their length with multiple locations in the assembly, indicating that up to approximately 10% of the non-repetitive genome may be represented redundantly in the assembly.

For *Mnemiopsis leidyi*, a cDNA library was created from total RNA prepared from gastrula stage embryos and reversed transcribed with oligo dT primers and the ZAP cDNA Synthesis Kit (Stratagene) by Kevin Pang and Mark Martindale. cDNA fragments with sizes ranging from ~500-2000 base pairs were cloned into pBluescript SK, and 15,360 paired clone end sequences were generated at JGI.

Repeat sequences reconstructed from unassembled WGS reads

Repeats were identified by assembling 16-mers (DNA sequences of length 16 bp) that frequently occurred in both ends of a sample of 50,000 fosmid clones from the ASYG library. Any 16-mers that occurred in both ends of at least 20 clones were used in the assemblies. The assemblies were performed using juggernaut.pl, a script developed for this purpose. tRNAScan-SE(12) was used to look for tRNAs and BLASTN(11) against nr and Repbase(13) to identify the 5S,18S,28S,U2,U6 RNAs, and two *Nematostella* transposons (see below). The five elements lacking notes are not identified by either of these methods.

The tandem array sizes are estimated by calculating the probability that a fosmid end matches the repeat given that its sister does. This probability can be used to estimate the expected array size (an average over multiple arrays in some cases) in terms of the mean fosmid length (37kb). These estimates depend on the assumptions of "normal" cloning behavior for these repetitive sequences.

10 families of tandemly repeated sequences were identified which occur in arrays longer than fosmid-length and account for 32% of the WGS data set. The key characteristics of these repeats are described in Table S2.2. See the file juggernaut.fasta for the complete sequences of these 10 elements.

Transposable elements in the sea anemone genome

Transposable elements (TEs) constitute more than 26% of the assembled sea anemone genome (Table S2.3) and belong to >500 families. These families are composed of a small number of copies (from 1 to ~5,000) and they all are relatively young: elements from the oldest families are less than 15% divergent from their consensus sequences and their ORFs coding for transposases, reverse transcriptases, and other transposon-specific proteins are not severely damaged by mutations.

In terms of their bulk contribution to the genome size, DNA transposons are fourfold more abundant than retrotransposons (Table S2.3). However, while different classes of anemone retrotransposons, including Gypsy, DIRS, Penelope, and CR1, are composed of more than 50-100 families each, different classes of autonomous DNA transposons are represented by just a few families. It appears that retrotransposition of retrotransposons, despite their high diversity, has not been as efficient as propagation of DNA transposons in the anemone genome.

The variety of different types of DNA transposons found in the anemone genome is the highest among eukaryotic species studied so far. Representatives of all reported superfamilies and groups of eukaryotic DNA transposons (14-16), excluding the Transib superfamily and the Mariner group of the Mariner superfamily, are present in the anemone genome. Even, En/Spm (also called CACTA) and transposons, which were believed to populate plants genomes only (14), reside in the anemone genome. While the anemone 10,632-bp EnSpm-1_NV and 9,347-bp EnSpm-2_NV transposons encode transposases (TPase) similar to the plant En/Spm TPase and are flanked by 3-bp target site duplications typical for known En/Spm elements, their 5'-CACAG termini differ from the 5'-CACTA termini of the plant transposons.

Over 3% of the anemone genome is made of fossilized copies of self-synthesized Polinton DNA transposons whose transposition depends on the Polinton-encoded DNA polymerase and integrase (17). It makes *Nematostella* the first metazoan with Polintons constituting a substantial portion of the genome (17).

Remarkably, the sea anemone genome is a safe haven for unusual transposons that have never been seen before. For instance, Troyka, a novel type of LTR retrotransposons distantly related to the Gypsy superfamily, is characterized by 3-bp target site duplications (TSDs), while all known LTR retrotransposons, including retroviruses, are defined by 4-6 bp TSDs (14). Among DNA transposons, the hAT superfamily is well-known for TSDs that are always 8 bp long (14). However, the sea anemone genome, in addition to the canonical hAT transposons contains two novel groups, hAT5 and hAT6, characterized by 5- and 6-bp TSDs, respectively. Importantly, using reverse transcriptase/integrase and transposase encoded by the anemone Troyka, hAT5, and hAT6 transposons as queries in TBLASTN searches against GenBank DNA sequences, we found that proteins closest to the queries (>30% protein identity) are encoded by TEs characterized by the same unusual lengths of TSDs. For instance, Troyka retrotransposons are present also in sea urchin, and the hAT5 and hAT6 transposons are wide spread in sea urchin, sea squirts and lancelet.

The anemone genome is also populated by a novel superfamily of eukaryotic "cut and paste" DNA

transposons, called IS4EU, characterized by their TPase distantly related to the bacterial IS4 TPase. Following identification of the IS4EU TEs in the anemone genome, members of this superfamily have been also found in other species, including lancelet.

Analyzing anemone TEs, we have also advanced in our understanding of evolution of non-LTR retrotransposons (Fig. S2.1). For instance, the anemone genome harbors two families of Tx1-like non-LTR retrotransposons, Tx1-1_NV and Tx1-2_NV, inserted in 5S rRNA and U2 smRNA, respectively, at target sites identical to those of different Tx1 elements in fish (18), frog and lancelet. We suggest that Tx1-like elements form a novel clade of non-LTR retrotransposons differing from the L1 clade elements by the strong target-site specificity.

RTE is another clade of non-LTR retrotransposons first described a few years ago (14, 19). All known RTE elements, including those in plants, insects, nematodes, and vertebrates, contain only one ORF and are characterized by extremely frequent 5' truncations of the RTE elements during their retrotransposition. Here, we show that the anemone genome contains several families of RTE-like elements, RTE_X in Fig. S2.1, which are longer than canonical RTE elements and contain an additional ORF at their 5' terminal portion that codes for the esterase domain, analogously to elements from the CR1/L2 clade (20).

Transposable Element Analysis Methods

Transposable elements were identified using WU-BLAST (<http://blast.wustl.edu>) and its implementation in CENSOR (<http://girinst.org/censor/>). First, we detected all fragments of the anemone genome coding for proteins similar to transposases, reverse transcriptases, and DNA polymerases representing all known classes of TEs. The detected DNA sequences have been clustered based on their pairwise identities by using BLASTclust (standalone NCBI BLAST(11)). Each cluster has been treated as a potential family of TEs described by its consensus sequence. The consensus sequences were built automatically based on multiple alignments of the cluster sequences expanded in both directions and manually modified based on structural characteristics of known TEs. Using WU-BLAST/CENSOR we identified fragments of the anemone genome similar to the consensus sequences that were considered as copies of TEs. Second, given the identified consensus sequences, we detected automatically insertions longer than 50-bp present in the identified copies of the protein-coding TEs. The insertions have been treated as potential TEs, clustered based on their pairwise DNA identities and replaced by their consensus sequences built for each cluster. After manual refinements of the consensus sequences, the identified families of TEs were classified based on their structural hallmarks, including target site duplications, terminal repeats, encoded proteins and similarities to TEs classified previously. Identified TEs are deposited in Repbase (13).

Supplement S3

Gene prediction and quality control

The genome of *Nematostella vectensis* includes 27,273 predicted gene models built using the JGI Annotation Pipeline, described below. The genomic sequence, predicted genes and annotations of *Nematostella*, together with available evidence, are available at the JGI Genome Portal (www.jgi.doe.gov/Nematostella)

The JGI Annotation Pipeline was used for annotation of the v1.0 *Nematostella* assembly described here. The pipeline includes the following annotation steps: (1) repeat masking, (2) mapping ESTs, full length cDNAs, and putative full length genes, (3) gene prediction using several methods, (4) protein

annotation using several methods, and (5) combining gene predictions into a non redundant representative set of gene models, which are subject to genome-scale analysis.

Transposons were masked in the *Nematostella* assembly using RepeatMasker (21) tools and a custom library of manually curated repeats (available upon request from V. Kapitonov). 146,095 ESTs were clustered into 30,813 consensus sequences and both individual ESTs and consensus sequences were mapped onto genome assembly using BLAT(10).

Gene predictors used for annotation of *Nematostella* v1.0 included *ab initio* FGENESH (22), homology-based FGENESH+ (22), homology-based GENEWISE (23), and EST-based ESTEXT (Grigoriev, unpublished).

A set of 1,678 genes derived from EST clusters with a putative full length ORF was directly mapped to the genomic sequence to build gene models. FGENESH was trained on this set to achieve sensitivity and specificity of 81% and 80%, respectively. To generate homology-based gene models, proteins from the NCBI NR database were aligned against genomic sequence using BlastX(11). High quality seed proteins were then used to build models using FGENESH+ and GENEWISE. GENEWISE gene models were then filtered to remove models with frameshifts and internal stop-codons and extended to include start and stop codons where possible. FGENESH, FGENESH+ and GENEWISE gene models were then processed using ESTEXT to correct them according to splicing patterns observed in available ESTs and to extend 3' and 5' UTR of the genes.

All gene models were annotated by homology to other proteins from NCBI NR, SwissProt and KEGG databases. Using InterproScan (24) we predicted proteins domains. Using both these sources of information, annotation of each protein was mapped to the terms of Gene Ontology (25), KOG clusters of orthologs (26), and mapped to KEGG pathways (27).

The large set of all predicted models was reduced to a non-redundant set of 27,273 representative models (Filtered Models), where every locus is described by a single best gene model according to the criteria of homology and EST support. For this set of representative gene models we assigned GO (25) terms to 12,786 proteins, 16,625 (78%) proteins to KOG clusters (26), and 695 distinct EC numbers were assigned to 2,822 proteins mapped to KEGG pathways (27). Table S3.1 summarizes the set of predicted genes.

The data are available from JGI Genome Portal (www.jgi.doe.gov/Nematostella) and from the GenBank under accession numbers XXXXXXXXXXXXXXX

Gene Content

Human Genes Sharing Ancestry with *Nematostella* Genes

To determine the number of genes in the *Nematostella* genome, we estimated how many of the 27,273 predicted gene models represent unique genes in the genome, as opposed to spurious gene predictions, fragmentary gene models, pseudogenes or unrecognized transposable element sequence. First, the *Nematostella* gene models were divided into categories based on the quality of their hits to the human proteome. Specifically we define the "best C-value", for each *Nematostella* gene, to be the ratio of the BLAST score of its best hit to the human genome to the highest BLAST score of the best-hitting human gene to any *Nematostella* gene. The number of genes with best C-value greater than or equal to C_{min} , for C_{min} from 0 to 1, is plotted in Figure S3.1 for two choices of BLAST e-value threshold. This value is by construction equal to 1 for genes with a mutual best, and the human and nematostella curves converge at $C_{min}=1$ for each choice of e-value. At the opposite extreme of $C_{min}=0$, the curves reach the total number of genes with detectable alignment in the other genome.

If a species has undergone extensive "paralog-formation", for example by a genome duplication relative to the other, we will expect the curve for genes of the 'duplicated' species hitting genes of the 'unduplicated' species being above the vice versa, for ranges $0.8 \leq C_{min} < 1$, i.e. the 'co-orthologs' range, as we observe for human in the plot.

If the curve for a species does not flatten as $C_{min} \rightarrow 0$ this means that there are many genes in that species having low best C-values, which is what we expect for pseudogenes and/or transposons where partial gene predictions have been made. For *Nematostella*, this curve shows a large excess, exceeding the human curve for values of $C_{min} > 0.5$, while falling below human at high C_{min} values. This type of reversal does not appear in human-*Drosophila*, human-*Caenorhabditis*, or *Drosophila*-*Caenorhabditis* comparisons (data not shown).

To assess whether the excess of gene models with low best C-value in *Nematostella* reflect the contribution of a large number of small, fragmentary models and pseudogenes, 60 *Nematostella* genes were subjected to a detailed manual review. Twenty genes were selected at random from the JGI *Nematostella* Filtered Models version 1.0 ("FM1.0 set") in each of the following categories:

- 1) BCV (best C-value to human) = 0, meaning no BLAST hit to human. 5486 of the FM1.0 set have BCV = 0.
- 2) $0 < BCV < 0.4$. 4889 of the FM1.0 set.
- 3) $BCV \geq 0.4$. 18274 of the FM1.0 set.

Manual review is by definition somewhat subjective, but using conservative criteria, i.e. avoiding dismissing too many genes, the results of the sampling indicate that about one third of all genes in the FM1.0 set could be expected to be rejected by manual reviews.

Category 1), 8 of the 20 were deemed "real genes", i.e. from the total number of genes with BCV = 0 we would expect $\sim 0.4 * 5489 = 2194$ genes to "pass manual scrutiny". Note that 15 of the 20 in this category have 1 or 2 exons.

Category 2). 10 of 20 were deemed real. 11 of the 20 have 1 or 2 exons. Predicted # genes to pass manual review: $4889 * 0.5 = 2445$

Category 3). These are high BCV genes, 13 of which have $BCV > 0.8$. Here, 15 of the 20 are thought to be real genes. In some cases, it looked like two gene models should be merged, and I tried roughly to call a gene here every other time, to approximately get the right gene count. From the counts here, we would expect $\sim 0.75 * 18274 = 13706$ genes in this category.

Adding up these expected numbers gives us an estimate of 18,345 bona fide *Nematostella* genes. Even this may be an overestimate, since quite a few of the genes with lower c-values are at the edges of short scaffolds, and their other half may be picked up by another scaffold, causing 2 annotations for a single gene.

Additional observations on the *Nematostella* proteome

- The human genome has more genes with a mutual best hit in *Nematostella* than in the proteomes of *Ciona*, fruit flies or nematodes. (Figure S3.2)
- The *Nematostella* genome contains many proteins with domain architectures (combinations of PFAM domains) that are shared exclusively with vertebrate genes. (Figure S3.3)
- Of the PFAM domains present in human, mouse, dog, chicken, frog and fugu, *Nematostella* has

more in common than any of *Ciona*, fruit fly, or nematode. (Figure S3.4)

- There are 5 large clusters of short proteins (around ~100aa), each comprising 55-74 members with weak similarity to hypothetical short ORFs from fungi (28)
- There are 242 clusters of tandemly duplicated genes, comprising 2-13 members, with annotated Pfam domains, which apparently were duplicated after split of bilateria
- There are 9 neurotoxins genes, with an anemone neurotoxin domain (PF0076) previously found only in the Cnidaria, but not previously in *Nematostella*, and 5 copies of green fluorescent protein (PF01353), originally found in jellyfish and predominantly found in Cnidaria.
- 16 Pfam domains previously exclusively found only in vertebrates, but not in other phyla of bilateria (or other eukaryotes), are present in *Nematostella* genome, including:

PF01500 - Keratin, high sulfur B2 protein
PF00040 - Fibronectin type II domain
PF06954 - Resistin
PF06990 - Galactose-3-O-sulfotransferase
PF05038 - Cytochrome b558 alpha-subunit

Lineage Specific Expansions

We identified 809 “recent” tandem expansions in the *Nematostella* genome, comprising 1,854 protein-coding genes. A similar algorithm applied to the ENSEMBL annotation of the human genome detected 504 recent expansions with 1,317 genes. The algorithm is as follows: first, all genes on chromosomes or scaffolds with three or more annotated genes were numbered in occurring order. From an all-against-all Smith-Waterman alignment of these peptides, all hits with greater than 60% identity and with at least 25 conserved four-fold degenerate codons were retained. This filtering step helps eliminate pseudogenes and spurious hits of low-complexity regions, and allows a divergence epoch estimate for the pair based on four-fold degenerate transversion frequency (4DTv)(29). Since our focus is on expansions specific to the nematostella lineage, we only consider hits with 4DTv < 0.2, i.e. 20% or less observed transversions at four-fold degenerate 3rd codon positions. Extrapolating from vertebrate calibrations, this corresponds to gene duplications no older than 150-200 million years. For comparison, human-mouse orthologs have typical 4DTv distances of ~ 0.15, and human-opossum have 4DTv ~ 0.26 (data not shown).

Next, the scaffolds were scanned for pairwise hits under the above criteria with no more than three unrelated genes separating them. This allows for intervening spurious gene models as well as small-scale inversions. Finally, all such pairs with one of the genes being within three genes of a member of another pair were clustered in a single-linkage fashion. To assess the probability of detecting tandem expansions by chance, we repeated this approach on versions of the human and nematostella gene sets in which the gene order had been randomly scrambled. We found a single spurious 2-member cluster in nematostella and four in human. Hence, we expect the false positive rate of this approach to be less than 1%.

In order to assess to what extent these relatively recent expansions have been retained by positive selection, and to compare the types of expansions found in *Nematostella* to those in vertebrates, we performed the following analysis: first, we scanned all of the genes in the human and *Nematostella* gene sets for PFAM-A domains using hmmpfam(30). We were able to assign one or more PFAM domains to 15,102 human genes and 12,202 *Nematostella* genes. We then formulated a neutral-evolution hypothesis that any gene has an equal probability of getting duplicated and fixed in the population. For genes with a certain domain we can then test the validity of this hypothesis by comparing the frequencies of such genes in the recent expansions to the overall frequency. For example, the number of recently created genes in *Nematostella* containing a PF000001 seven transmembrane family (rhodopsin family) domain is 33 (subtracting one “seed” member of each tandem cluster). Since 779 of the 12,202 *Nematostella* genes contain this domain, the expected number in the recently expanded set (with a total of 572 genes with PFAM domains) under the neutral hypothesis is 36.5 +- 5.8, where the binomial approximation has been used since the recent genes constitutes a small fraction of the total

genes in both species. Hence, in *Nematostella*, there is no evidence for recent selection for retention of new genes created by tandem duplication with PF000001. In the human genome, on the other hand, 112 such genes are observed, with an expected value of 29 ± 5.3 , consistent with a strong recent selective retention of such receptors (olfactory and visual) within vertebrates or mammals. Tables S3.3 (*Nematostella*) and S3.4 (human) show all PFAM domains found in at least four genes in recent tandem expansions, and with a frequency of at least 3 sigma above the expected frequency under the neutral hypothesis. In general, the gene families showing strong expansions along the two lineages are different. In addition to olfactory and taste receptors, the human genome shows strong recent preference of C2H2 zinc finger genes with a KRAB domain, keratin, and immune defence proteins. This newly acquired repertoire almost certainly plays a key role in defining vertebrates and mammals. Similarly, the genes listed in Table S3.3 can be hypothesized to play a significant role in distinguishing *Nematostella*. Note that this analysis is biased towards vertebrates, for which more domains have been characterized.

Supplement S4

Construction and characterization of eumetazoan gene families

To understand gene creation and duplication we designed a phylogenetically informed clustering algorithm which produces clusters at the base (most distant in time) and tip (most recent point) of a given internal branch (stem) of the species tree. Each cluster is composed of a group of modern genes that are the offspring of one gene in the common ancestor. Our algorithm takes as input:

- a) The genomes that have arisen as descendants from our stem of interest. These are our in-group genomes.
- b) Other genomes which serve as phylogenetic out-groups.
- c) Pairwise alignment scores for all pairs of genes in the in- and out-groups.
- d) Any previous clusterings made of the in-group genomes we want to preserve.

From this data our algorithm operates as follows:

- i) A graph is made where each node is an in-group gene. Edges are added if two genes are mutual best hits between species. Edges are also added if two genes are in any clusters in input (d).
- ii) A single linkage clustering is done of the graph. This represents the clusters at the tip of our stem. The mutual best hits captures the likely orthologs between the organisms while the clusters passed in as input (d) captures the paralogs from the stems emanating from the tip of the current stem of interest.
- iii) For each cluster made in (ii), the top m hits to the out-groups are found where $m =$ twice the number of out-groups. This collection of out-group genes is called the potential blockers for this cluster.
- iv) Two clusters from (ii) are merged if they share at least one potential blocker and for every potential blocker the genes with which it aligns are closer [by BLAST score] to each other than either is to its potential blocker. This gives us a set of clusters that existed at the base of our stem of interest.

Blastp was run using BLOSUM45, evalue cutoff 0.001, and filtering was turned off. Only the top 1500 hits were considered if more hits passed these criteria. The genomes used are as follows:

Xenopus tropicalis JGI v4.1

Takifugu rubripes JGI v4.0

Nematostella vectensis JGI V1.0 (this work)

Homo sapiens Ensembl build 38

Drosophila melanogaster Ensembl build 38

Caenorhabditis elegans Ensembl build 38

Arabidopsis thaliana From NCBI on 11/2005

Saccharomyces cerevisiae From genome-ftp.stanford.edu, version released on July 7, 2004

Dictyostelium discoideum From dictybase.org, Annotations released on 7/11/2005

Supplement S5

Phylogenetic analysis of metazoa

We compared predicted protein sequences from *Nematostella* to those from other metazoan and out-group genomes, and find that *Nematostella* genes are more similar to vertebrate genes than to fly and nematode genes using bayesian branch length estimation and an analysis of percent sequence identity. ((31) came to the same conclusion using ESTs and BLAST e-value to measure similarity.) Of the 7,766 ancestral metazoan gene clusters, 1,619 are composed of a single gene from each of the six representative metazoan genomes listed in Supplement S4: human, fish, frog, *Nematostella*, fruit fly and nematode. Starting with this set of apparently single-copy genes in these six genomes, we searched six additional complete or partial genome sequence data sets (of a tunicate, a gastropod mollusk, a hydrozoan cnidarian, a choanoflagellate, a sponge, and yeast), and a collection of ESTs from the ctenophore *Mnemiopsis leidyi* (see Table S5.1 for a list of data sources) for orthologous genes, making a total of twelve whole genome data sets, plus the EST-derived sequences from *Mnemiopsis*. For each additional genome, if a mutual-best hit existed to the human gene in the cluster, that gene was identified as an ortholog, and added to the cluster. We compared the results obtained with this set with those obtained using *Nematostella* rather than human as the anchor for identifying orthologs, and found that it did not change the results. By this method, 337 ortholog sets were identified that had one gene representing each of the twelve whole genome datasets. Only nine ortholog sets contained one gene from each of the twelve whole genomes plus a *Mnemiopsis* sequence.

We constructed two concatenated multiple sequence alignments from the identified orthologs: one with and one without the ctenophore sequence. In each case, multiple sequence alignments for each orthologous set were computed with MUSCLE(32), and well-aligned regions extracted with GBLOCKS(33) using conservative settings (all available sequences in an orthologous group were required to be well aligned at the start and the end of each extracted block: $-b1=N$ $-b2=N$, where N is equal to the number of sequences in the alignment.). We constructed two concatenated multiple alignments for investigating metazoan phylogeny and relative rates of protein sequence evolution among the different lineages. The first (Alignment 1) excludes sequence from the *Mnemiopsis* ESTs, and includes only the 337 ortholog sets with representation from each of the other twelve genomes. The second (Alignment 2) was compiled from the multiple alignments including the *Mnemiopsis* data and includes all ortholog sets with twelve or thirteen members, plus all ortholog sets including a *Mnemiopsis* sequence.

Alignment 1 consists of 19,563 columns, with no missing data. This data matrix was analyzed using *mrBayes* version 3.1.2(34, 35), using a the WAG(36) model of protein evolution, a Gamma distribution of rate variation among sites, approximated by four rate categories, and a category for invariant sites. Multiple runs from different starting topologies all converged on the same topology, branch lengths and posterior probabilities for protein evolution model parameters within approximately 10,000 monte carlo iterations. The mean and variance of the posterior probabilities for total tree length, Gamma distribution shape parameter alpha and the fraction of invariable sites were 2.278 +- 0.001, 0.818 +-

0.001, and 0.2291 +- 0.0001, respectively. Figure S5.1 shows the consensus tree topology and branch lengths. All nodes were resolved as shown in 100% of the samples trees. The sequences of the genes used in Alignment 1 are available in FASTA format in S5.fasta.

Alignment 2 consists of 19,977 columns, however only 2272 columns contain *Mnemiopsis* sequence. To test whether this data could be used to shed light additional light on the phylogenetic relationships among cnidarians, ctenophores and bilateria, we submitted this dataset to a maximum likelihood analysis using the PHYLIP package's PROML program(37), and compared the likelihood scores of three topologies: ctenophores sister to cnidarians+bilaterians, ctenophores sister to bilaterians, and ctenophores sister to cnidarians. Of these, the first had the highest likelihood score, but it was not significantly better than the second in a Shimodaira-Hasegawa test. The branch lengths for the tree shown in Figure 2 were estimated using PROML, for the defined topology illustrated, with a trifurcation at the cnidarian/ctenophore/bilaterian divergence.

To make an extremely rough estimate of divergence time between bilaterians and cnidarians, we interpolated following Dawkins (38) between recent molecular clock estimates(39) of the timing of the protostome-deuterostome (95% confidence interval: 640-760 Mya) and choanoflagellate-metazoan (95% CI: 760-960 Mya) divergences. We see from Figure 2b that the cnidarian-bilaterian split lies ~30% of the way between these two nodes (adopting the midpoint rooting as shown), suggesting that the eumetazoan ancestor lived between 670 and 820 Mya.

Figure S5.2 shows a more direct way the greater similarity between human and *Nematostella* proteins than between human and fly/nematode proteins.

Supplement S6

Intron Splice Site Conservation

To study intron loss and gain in orthologous genes in multiple species, we first aligned the *Nematostella* gene set to the set of human ENSEMBL models (release 26.35.1) and to the TIGR release 5 of *Arabidopsis thaliana* genes. In 2,347 cases, a human gene was found to have a mutual best hit to both a *Nematostella* and an *Arabidopsis* gene, forming a tentative cluster of orthologous genes to be studied further.

Gene models are often incomplete in the 5' ends and may have have poorly determined splice sites, so we restrict our analysis to regions of highly conserved peptides in the orthologs of all three species. The independent identification of such regions in multiple species provides strong evidence for the accuracy of the gene models in these regions. Hence, we performed multiple alignments of the orthologous clusters and identified gap-free blocks flanked by fully conserved amino acids. We then identified annotated splice sites of all species within these regions, which the additional requirements that 1) none of the peptides must have a gap in the alignment closer than 3 AA from the splice site and 2) no two different peptides must have splice sites at different positions closer than 4 AA. Empirically, these requirements are necessary to avoid spurious detection of "intron losses" due to ambiguities in either the multiple alignment or the gene model's splice sites. While some of these cases may reflect real sliding of donor or acceptor sites, we restrict ourselves to studying gains and losses of introns here. Finally, we required that at least 5 amino acids out of 10 in the flanking regions of the splice sites be either fully conserved or have strong functional similarity among all four species.

9,947 highly reliable intron splice sites were identified by these requirements. The results are summarized as a Venn diagram in figure S6.1, indicating the number of shared introns between the species.

Remarkably, about 81% of the human introns (4,403 of 5,435) are shared with *nematostella*. Assuming that intron losses have occurred independently in the human and *nematostella* lineages, and that the probability of independent intron insertion events at the same location is negligible we estimate the loss in *Nematostella* since the last common ancestor (LCA) with human as $158 / (158 + 1258) = 11\%$. In a similar fashion, we estimate a loss of almost 22% along the human lineage, twice the amount of introns

lost in the *Nematostella* lineage.

The above results also allow us to place upper limits on intron gains within the human and *Nematostella* lineages: 28.6% of all introns shared by human and *Nematostella* (and hence present in their LCA) are also shared by *Arabidopsis*. If additional introns have been independently gained in each lineage we expect a lower fraction of the total introns in each species to be shared with *Arabidopsis*. In fact, we find 26.5% of all *Nematostella* introns and 26.1% of all human introns are shared with *Arabidopsis*, which translate into maximum intron gains of ~9% in human and ~7% in *Nematostella*. These results are strict upper limits, since the lower conservation with *Arabidopsis* can also be explained if the loss rate vary inherently between introns. In this case we will expect introns that are shared between human and *Nematostella* to be less prone to loss, and hence a larger fraction will also have survived in *Arabidopsis*. This scenario is very conceivable since some introns have been shown to contain regulatory elements and the loss of such introns would presumably be selected against.

To the extent that the introns in highly conserved peptide regions studied here are representative of introns in general, the above analysis suggests that the *Nematostella* genome has only lost 11% of its introns since the LCA with human, and gained at most 7%.

We next identified 2,347 clusters of orthologous genes in all bilaterian orthologous clusters with an unambiguous 1:1:1 member relationship in human, *Drosophila melanogaster* (fly), and *C. elegans*. In 1,523 of these clusters, the human gene had a mutual best hit to a *Nematostella* gene, forming clusters of four orthologous genes. 4,951 highly reliable introns were identified by these requirements. The results are summarized in Table S6.1. *Nematostella* has the most introns at these conserved positions, followed by human with a relative intron frequency of about 0.91, whereas nematode and in particular fly have considerably fewer introns (0.37 and 0.21). From these numbers we estimate the intron losses in fly, nematode, and human since their LCA to be 82% , 77%, and 12% respectively. Note that the nematode, although having retained only ~23% of the introns since the LCA with human have ~37% of the number of human introns. This suggests a considerable gain of introns in the nematodes, as also reported by [Logsdon 2004].

This analysis of aligning conserved sequences to identify conservation of introns was further extended to include seven species - *Nematostella vectensis*, *Homo sapiens*, *Ciona intestinalis*, *Drosophila melanogaster*, *Caenorhabditis elegans*, *Cryptococcus neoformans* and *Arabidopsis thaliana*. 4342 introns from the seven genomes at 2645 aligned positions which contain an intron in at least one of the seven orthologs.

Methods for Intron Gain/Loss tree

Starting from the binary character matrix compiled as described above of 2,645 intron positions across 7 taxa, we found the most parsimonious solution to the intron gain/loss problem by projecting these characters onto the (known) topology. Weighted parsimony as implemented in PAUP 4.0b10(40) was used, with the cost of an intron gain significantly greater (more than 10X) the cost of an intron loss. The parsimony assignment of characters to internal nodes is independent of this gain/loss weight ratio. From the branch lengths produced by PAUP, and the known weights, we solved for the number of losses and gains along each branch as show in the main text figure.

Supplement S7

Local conservation of gene order

To search the human and *Nematostella* genomes for regions of conserved linkage, we performed the following analysis. First, the genes on each genome were assigned unique identifiers according to the

order in which they occur on the chromosomes or scaffolds. We then used the sequence alignments described in the clustering section to scan each genome for tandem expanded gene families, defined here as clusters of genes with a maximum of 4 intervening genes, showing similarity at e-values $< 1 \times 10^{-10}$. All but one member, the longest peptide, were excluded from further analysis at each such region in the genomes.

From the human vs *Nematostella* protein alignments we next excluded all genes with more than 15 hits with e-value $< 1 \times 10^{-10}$ from consideration. Finally, of the remaining pair-wise hits we included only hits with a score of more than 70% of the value of the highest score of either of the two genes to any of the genes in the opposite genome. This approach enriches the set for orthologous gene pairs while removing weak super-family similarities from the analysis. At this stage we were left with 11,351 pair-wise hits, involving 6,986 *Nematostella* genes and 8,426 human genes. We then recalculated the gene order IDs in the two genomes, featuring only the genes involved in these high-quality alignments, and scanned for regions of conserved synteny or linkage in the following manner:

For the first pair-wise alignment of genes in the proteomes of the two species, the gene locations on the chromosomes were recorded and a one-pair segment of conserved synteny was defined. Subsequent gene pairs either defines new segments, or, if the genes in both species are located within a specified maximum distance, N_{max} from a gene pair in an existing segment, the pair is added to that segment. If a pair can be added to two segments, these segments are joined into a larger segment of conserved synteny. Note that this method does not require strict conservation of gene order: inversions on scales smaller than N_{max} are tolerated. After traversing all alignments, we have a set of conserved regions, on which we can impose a minimum member limit (typical 3 pairs) to remove potentially spurious regions.

For human-*Nematostella*, we found no strict significant conservation of gene order, but by choosing a large value of N_{max} we nonetheless detect regions of conserved linkage in which the local gene order has been scrambled. In order to detect the significance of these regions, we randomly scrambled the order of the genes on each chromosome or scaffold and applied, for the same sequence alignment data, the algorithm to the scrambled data set. This allows us to choose parameters to minimize false positive detection. Note the importance of the filtering out weak hits in this method, as the presence of such hits would significantly increase the false positive rate in the detection of segments of conserved linkage. Using $N_{max} = 40$ and considering only segments of 9 or more participating genes, we find 33 such segments of conserved synteny between human and *Nematostella*, with none expected by chance, as seen by running the algorithm on the scrambled set.

Identification of human genome segments free of recent chromosomal fusions and large-scale rearrangements

To facilitate the search for large-scale conservation of gene linkage in the presence of extensive changes in local gene order between humans and *Nematostella*, we identified 98 segments of the human genome which appear to be uninterrupted by inter-chromosomal translocations or fusions when compared to the genomes of other chordates. To identify likely locations of chromosomal fusions along the human genome which separate such segments, we followed the following procedure:

1. Putatively orthologous gene pairs were identified between the ENSEMBL human gene set and the chordate *Branchiostoma floridae* draft gene set [JGI web page] using the mutual best BLAST hit criterion.
2. Scaffolds of the *B. floridae* assembly were clustered as described below for *Nematostella*, based on the similarity of the distribution in the human genome of human genes orthologous the genes on the scaffold.
3. A representation of each human chromosome arm was constructed in which each gene along the chromosome was represented by the identifying number of the cluster of scaffolds in which its *B. floridae* ortholog resides.
4. A Hidden Markov Model, constructed and implemented in software for the purpose, was used to segment the human chromosomes into segments with an approximately uniform distribution of hits to a specific subset of the scaffold clusters.

Figure S7.2 illustrates the results of this procedure for human chromosome arms 14q, 15q, 16p and 16q, and Table S7.1 lists the extent of the 98 identified segments in base pair coordinates on the NCBI Human genome build 36.

Construction and Significance Testing of Putative Ancestral Linkage groups (PALs)

To test for conservation of large-scale synteny in the presence of extensive local rearrangement of gene order, we compared 147 of the largest scaffolds of the *Nematostella* assembly to the segments of the 98 human genome described above. The examined scaffolds were selected because, like the 98 human segments, each contains descendants of 40 or more ancestral eumetazoan genes. For each scaffold-segment pair, we tabulated the number of ancestral gene clusters giving rise to descendants on both members of the pair. This number counts the number of independent orthologs shared by the scaffold and the segment. For each scaffold-segment pair, the number of observed orthologs was compared to a null model in which scaffolds and segments comprise genes descending from genes drawn independently from the set of 7,766 ancestral genes. This method of counting orthologs, and this null model control naturally for independent tandem gene duplicates which could otherwise artifactually inflate the number of observed orthologs in circumstances where there is no remnant of conserved synteny, because tandem duplicates arising independently should be contained in a single reconstructed ancestral gene cluster. The expected number of orthologs under this model is governed by the hypergeometric distribution, allowing us to compute a p-value for consistency for each scaffold-segment comparison with the null model. Since we compared 147 scaffolds with 98 segments, we applied a Bonferroni correction factor of 1/14406. The complete set of these numbers of shared orthologous genes are shown in figure S7.3, for all scaffolds (67/147) and segments (40/98) which participated in a statistically significant shared synteny relationship. Table cell backgrounds are colored yellow when $p < 0.01/14406$, and pink when $p < 0.05 / 14406$. A blue background indicates $p < 0.5/14406$.

Table S7.3 has 112 yellow cells, corresponding to 112 cases of statistically significant conservation of synteny between a *Nematostella* scaffold and a segment of the human genome. The rows and columns of this table have been ordered to reveal 13 sets of scaffolds and chromosome segments, defined by the criterion that none can be subdivided without separating into different sets a scaffold-segment pair with significant evidence ($p < 0.01$) for conserved synteny. We interpret these collections of modern sequences to be descended from the same chromosomes, or chromosomal segments of the common ancestor of eumetazoa, and refer to them therefore as putative ancestral linkage groups, or PALs.

Table S7.X lists the 255 ancestral gene clusters linked with the HOX clusters in PAL-A.

A clustering method allows more extensive reconstruction of putative ancestral linkage groups.

Having demonstrated that there is extensive conservation of linkage relationships among genes using the conservative statistical criteria described above, we developed a more sensitive method to reconstruct ancestral linkage groups based on clustering scaffolds or chromosome segments. In this method, a matrix of ortholog counts similar to that shown in figure S7.3 is constructed. The rows and columns of this table are then clustered hierarchically, using Pearson correlation as a measure of similarity and the average pairwise linkage method with the "cluster" program(41). Figure S7.4 shows the result as a "dot plot" as in figure S7.2. Horizontal and vertical lines divide clusters of scaffolds (vertical lines) and human chromosome segments (horizontal lines), defined by a cut of the hierarchical tree at a correlation coefficient of 0.2. This clustering of scaffolds and chromosome segments defines 15 large PALs, each with descendants of more than one hundred ancestral eumetazoan genes. 3055 ancestral genes, or 40% of the ancestral genes are assigned to one of these PALs.

Supplement S8: Eumetazoan Ancestry of Genes

Construction of "Centroid" sequences.

We define the "centroid" of a cluster of orthologous amino acid sequences to be a synthetic amino acid sequence which maximizes the sum of BLAST alignment scores between the centroid and the members of the cluster. This provides a surrogate for the peptide sequence that is ancestral to each cluster.

Classification of eumetazoan genes by ancestry

Centroids (see above) of the ancestral eumetazoan gene clusters were aligned to non-animal entries in SwissProt/TREMBL [Uniprot release 8 from <http://www.uniprot.org>] with BLAST(11), using the NCBI database to remove metazoan entries. The Pfam(30) annotation of SwissProt/TREMBL from swisspfam [Version of Sept. 6 2006. Current version available from <http://pfam.janelia.org>] was parsed to identify Pfam domains found only in animals, as well as pairs of Pfam domains that occur separately in non-animals but only were found together in animals.

Clusters whose centroid had a BLAST hit to out-group proteins of e-value $<1e-6$, and also clusters containing a member which is a mutual best hit to an *Arabidopsis*, *Dictyostelium* or *Saccharomyces* were annotated as "ancient," unless one of the following conditions was met:

- 1) if both the *Nematostella* peptide and at least one other animal protein had an "animal specific" Pfam domain, the cluster was designated a type II novelty.
- 2) if both the *Nematostella* peptide and at least one other animal protein had an "animal specific" Pfam domain combination, the cluster was designated a type III novelty.

Note that type III (animal-specific eukaryotic domain combinations) are based only on pairwise combinations. Thus animal proteins that shuffle the order of domains found within an ancient eukaryotic family are not designated as novel in this analysis.

Functional annotation of ancestral gene clusters

Panther(42, 43) family annotations on the sequences of extant species were transferred to the inferred ancestral clusters when both *Nematostella* and bilaterian members of the clusters shared the same Panther annotation. These annotations were mapped to various overlapping functional categories using the Panther Pathways(43) and Panther Ontology databases.

To assess whether specific functional categories were over- or underrepresented among the different types of novelties, we adapted the GOstat approach of Beissbarth and Speed (44) for use with the Panther ontologies, and computed p-values for enrichment and dearth relative the hypergeometric distribution. For both Panther Pathways and Panther Ontology, we limited our tests to the 100 ontology terms which had the greatest number of inferred ancestral genes assigned to them, and applied a Bonferroni correction for 100 tests, even though this is somewhat conservative, since the categories have significant overlap. Table S8.1 lists the functional categories enriched for novel genes of the three types.

Captions for Supplemental Tables and Figures

Table S1.1 Partial list of the merits of *Nematostella* as a model organism.

Table S2.1 Summary of WGS libraries

Shotgun libraries are identified by their four-letter name, which is used as a prefix to the identifier of all reads from the library. For each library, the table lists: the mean size of genomic DNA inserts in base pairs; the number of sequencing reads attempted for each library; the number of reads with at least 100 bp of high-quality sequence after removal of vector and low-quality sequence, as described previously [Dehal 2002]; the number of reads which have a detected alignment to other reads in the shotgun data set (see discussion above); the number of reads which are placed in the contigs of the assembly; and the mean read length, after trimming. Column totals are shown in bold for selected columns, and the fraction of reads lost to trimming, lack of alignment, and lack of placement in the assembly is shown as a percentage of the previous total.

Figure S2.1: Observed density of polymorphic sites

The rate of single nucleotide polymorphism observed in the assembled genome sequence is 0.8%. Figure S2.2 shows the observed (orange) and Poisson ascertainment bias-corrected (green) frequency of polymorphic positions as a function of local depth of assembly for a sampling of 14.4 million positions in the assembly [Left hand scale]. Positions are considered polymorphic if two or more WGS reads indicate each of two or more different bases at a given position. The red curve shows the number of positions considered for each depth of coverage, and the dotted curve shows poisson distributed counts with the same mean.

Figure S2.2: Four haplotype polymorphism fit

The number of polymorphic sites (red crosses) as a function of local depth of the assembly is compared with expected values for four independent haplotypes with average pairwise differences of 0.5% (green), 0.64% (blue) and 0.7% (purple).

Table S2.2: Summary of tandem repeat elements from raw WGS reads.

Paired fosmid end reads were screened for highly abundant 16-mer DNA words appearing in both ends of fosmid clones, indicating their presence in the genome in large tandem arrays. Identified 16-mers were assembled with JUGGERNAUT, and their abundance in the whole genome shotgun reads was estimated by alignment to a sample of WGS reads from all libraries using BLAST(11).

Table S2.3. Transposable elements in the sea anemone genome.

Figure. S2.3 Neighbor-joining tree of eukaryotic non-LTR retrotransposons constructed for their reverse transcriptase. Black circles mark novel families of non-LTR retrotransposons identified in this study. Unmarked retrotransposons have been described previously and are collected in Repbase Reports. Abbreviations of host species are as follows: NV, *Nematostella vectensis*; XT, frog *Xenopus*

tropicalis; BF, lancelet *Branchiostoma floridae*; AG, mosquito *Anopheles gambiae*; DM, fruit fly *Drosophila melanogaster*; DR, fish *Danio rerio*; CR, green algae *Chlamydomonas reinhardi*; TP, diatom *Thalassiosira pseudonana*; SP, sea urchin *Strongylocentrotus purpuratus*; PS, turtle *Platemys spixii*; SJ, blood fluke *Schistosoma japonica*; Cis, sea squirt *Ciona savignyi*. Only >40% bootstrap values are shown next to corresponding nodes of the tree (based on MEGA3(45)). Clades and groups of non-LTR retrotransposons are indicated by black and blue rectangles.

Figure S2.4 Number of chromosomes

The number of chromosomes was determined by analysing over 90 metaphase plates in spreads. The conclusion is that $2N = 30$, the same number as in Hydra. A sample metaphase plate is shown, with the histogram of the number of observed chromosomes per plate.

Table S3.1: Summary of gene model statistics For Nematostella Filtered Models 1.0

Figure S3.1: Distribution of C-score

The number of genes with a best C-value (see section S3) greater than C_{min} , or C_{min} from zero to one, with alignment e-value threshold *Nematostella* (red) and human (blue), with BLAST e-value threshold $1e-10$ (solid curves) and $1e-3$ (dashed).

Table S3.2: Compared abundances of PFAM domains for selected domains.

The number of proteins with PFAM(30) hits to 10 abundant PFAM domains, along with the abundance rank of that PFAM domain in each genome, is compared among five metazoan genomes, including *Nematostella*.

Figure S3.2: Number of bidirectional BlastP hits (potential 'orthologs') between 22,218 human genes (from Ensembl) and other organisms with known genomes. Despite early divergence, sea anemone shares more hits with human, than other bilaterians, except vertebrates.

Figure S3.3: Fraction of unique multi (Pfam) domain (2 or more domains) gene models from *Nematostella* (total 983) shared by other metazoans and yeast.

Figure S3.4: 2264 Pfam domains present in all 6 vertebrates with known genomes: human, mouse, dog, chicken, frog and fugu. Below is the histogram of numbers of these domains shared by *ciona*, fly, nematode and sea anemone.

Table S3.3: Preferentially retained PFAM domains within recent tandem expansions in *Nematostella*

Tandem gene expansions were identified based on 4DTv as described in the text. PFAM domains with a significantly greater number of observed examples among tandem expansions in the *Nematostella* genome relative to the predication of a model model of the neutral expectation are shown.

Table S3.4: Preferentially retained PFAM domains within recent tandem expansions in *Homo sapien*

Tandem gene expansions were identified based on 4DTv as described in the text. PFAM domains with a

significantly greater number of observed examples among tandem expansions in the human genome relative to the predication of a model model of the neutral expectation are shown.

Table S5.1: Data sources for phylogenetic analysis

Figure S5.1: Distribution of percent ID Against Human Proteins

The distribution of the percent identity in mutual-best-hit protein alignments between human genes and the genes of the frog, *Xenopus tropicalis*, pufferfish *Takifugu rubripes*, *Nematostella*, fruit fly *Drosophila melanogaster*, and nematode *Caenorhabditis elegans*.

Table S6.1: Distribution of 4,951 introns in conserved regions of orthologs in human, fly, nematode, and *Nematostella*. Numbers in parenthesis refer to the number of introns not shared by any other species.

Figure S6.1: Venn diagram for three-way intron conservation comparison

Venn diagram showing the distribution of 9,947 intron splice sites in *Homo sapiens*, *Nematostella vectensis*, and *Arabidopsis thaliana*.

Table S6.1: Four-way intron conservation comparison

The distribution of 4,951 introns in highly conserved, orthologous peptide sequences from human, *Drosophila melanogaster*, and *C. elegans*, and *Nematostella*. The first four lines list the total number of introns in each species, followed in parentheses by the number which are unique to that species. The remaining table rows list the number of introns shared by selected combinations of genomes.

Figure S7.1: Synteny block search

The size distribution of synteny blocks for human vs. *Nematostella* (blue bars) is compared to that for a synthetic data set in which gene positions have been artificially randomized (maroon bars), where synteny blocks are defined as maximal collections of ortholog pairs where pairs of adjacent orthologous pairs have no more than 40 non-participating genes intervening between them.

Figure S7.2: HMM segmentation example

Each graph plots the rank order of human genes along four human chromosome arms (horizontal coordinate) versus the rank position of the *B. floridae* mutual-best-hit ortholog within five clusters of *B. floridae* scaffolds. Vertical red lines indicate the boundaries between human chromosome arms, and horizontal red lines indicate boundaries between scaffold clusters. Discontinuities in the distribution of orthologous gene positions within chromosome arms identified by a hidden markov model are indicated by the addition of vertical black lines on the right. These discontinuities are most easily explained by chromosomal fusions or large-scale re-arrangements in the human lineage which are recent compared to the time scale of gene order evolution.

Table S7.1: Table of human chromosome segments used in large-scale synteny search

A list of the human genome segments used in that PAL analysis. For each segment, the segment name, the human chromosome, and the start and end points on the chromosome, in base pair coordinates on the NCBI Human genome build 36.

Table S7.2: Complete Oxford Grid for Human-Nematostella comparison

"Oxford grid" which tabulates the number of ancestral gene clusters shared between the 22 *Nematostella* scaffolds (columns) and 14 segments of the human genome (rows) that are assigned to PALs A, B and C. Cell colors indicate Bonferroni-corrected p-value < 0.01 (yellow), < 0.05 (pink), < 0.5

(blue).

Figure S7.3: Clustering method for constructing putative ancestral linkage groups (PALs)

Blue dots mark the position in human chromosome segments (vertical coordinate) and the *Nematostella* scaffolds (horizontal coordinate) of a pair of orthologous genes. *Nematostella* scaffolds and human chromosome segments have been ordered by a hierarchical clustering procedure, and concatenated together. Gene positions are in rank order rather than base pair coordinate, where only genes descended from the set of 7,766 ancestral gene clusters have been numbered. Descendants of ancestral eumetazoan clusters with more than 25 genes from the six representative animal genomes were excluded from the analysis. Horizontal and vertical lines divide clusters of human chromosome segments and *Nematostella* scaffolds defined by having an average pairwise correlation coefficient of their distribution of hits to the other genome greater than 0.2. The trees along the left and top of the plot are graphical representations of the average pairwise correlation scores among the hierarchically clustered human segments (left) and *Nematostella* scaffolds (top). Terminal branches are centered

Figure S7.4: Detail of Human chromosome 12 showing genes contributing to PAL A.

Detail of main text figure 4c, showing the region flanking the HOX C gene cluster on human Chromosome 12. Horizontal tick marks indicate positions of human genes descended from the set of 7,766 inferred ancestral genes. Genes with an ortholog in *Nematostella* on scaffolds 26, 61, 53, 46, 3 and 5 are labeled and connected by a colored line to the position of the *Nematostella* ortholog (See Fig 4c), except where the gene falls into an ancestral metazoan cluster for more than 25 genes from human, frog, fish, fly, nematode and *Nematostella* (Section S4). These large genes families are more likely to have members showing spurious conserved synteny, since they may have members in many regions of the genome. The genes of the HOX C cluster fall into such a large family, but have been labeled to show the position of the HOX cluster.

Table S7.3: The 225 ancestral gene clusters linked with the HOX clusters in PAL-A:

This table is available for download from <http://169.229.10.93/~nputnam/palA.clusters.html>

Table S8.1: Table of functional categories enriched for novel genes of the three types.

Panther ontology annotations of the inferred ancestral gene set have been tested for enrichment in each of the three categories of novelty (novel sequence, novel domain, and novel combination of domains), as described in section S8, and significant over- and under-representations have been tabulated here for (A) Panther Ontology Terms for Biological Process and Molecular Function, and (B) Panther Pathways. For each term with a significant over or under representation, the table shows: the ontology term ID from the Panther system; the natural log of the p-value for the enrichment; a "+" or "-" to indicate over- and under-representation, respectively; the number of inferred ancestral genes which both have the annotation in question, and belong to the category of novelty being considered [N(ont & cat)]; the number of inferred ancestral genes which have the annotation in question [N(ont)]; the number of inferred ancestral genes belonging to the category of novelty being considered [N(cat)]; the total number of inferred ancestral genes [N(total)]; the percentage of novelties of the category being considered which are annotated with the ontology term [N(ont & cat)/N(cat)]; the percentage of all ancestral genes which are annotated with the ontology term [N(ont) / N(cat)]; and a short description of the ontology term.

References:

1. T. A. Stephenson, *London: The Ray Society* **II** (1935).
2. R. B. Williams, *Journal of Natural History* **9**, 51 (1975).
3. C. Hand, K. Uhlinger, *Biological Bulletin* **182**, 169 (1992).
4. J. H. Fritzenwanker, U. Technau, *Dev Genes Evol* **212**, 99 (Mar, 2002).
5. S. Szczepanek, M. Cikala, C. N. David, *J Cell Sci* **115**, 745 (Feb 15, 2002).
6. J. R. Finnerty, D. Paulson, P. Burton, K. Pang, M. Q. Martindale, *Evol Dev* **5**, 331 (Jul-Aug, 2003).
7. E. W. Myers *et al.*, *Science* **287**, 2196 (Mar 24, 2000).
8. P. Dehal *et al.*, *Science* **298**, 2157 (Dec 13, 2002).
9. S. Aparicio *et al.*, *Science* **297**, 1301 (Aug 23, 2002).
10. W. J. Kent, *Genome Res* **12**, 656 (Apr, 2002).
11. S. F. Altschul *et al.*, *Nucleic Acids Res* **25**, 3389 (Sep 1, 1997).
12. T. M. Lowe, S. R. Eddy, *Nucleic Acids Res* **25**, 955 (Mar 1, 1997).
13. J. Jurka *et al.*, *Cytogenet Genome Res* **110**, 462 (2005).
14. N. L. Craig, *Mobile DNA II* (ASM Press, Washington, D.C., 2002), pp. xviii, 1204 p., [1232] p. of plates.
15. V. V. Kapitonov, J. Jurka, *DNA Cell Biol* **23**, 311 (May, 2004).
16. V. V. Kapitonov, J. Jurka, *Proc Natl Acad Sci U S A* **100**, 6569 (May 27, 2003).
17. V. V. Kapitonov, J. Jurka, *Proc Natl Acad Sci U S A* **103**, 4540 (Mar 21, 2006).
18. K. K. Kojima, H. Fujiwara, *Mol Biol Evol* **21**, 207 (Feb, 2004).
19. H. S. Malik, T. H. Eickbush, *Mol Biol Evol* **15**, 1123 (Sep, 1998).
20. V. V. Kapitonov, J. Jurka, *Mol Biol Evol* **20**, 38 (Jan, 2003).
21. A. Smit, P. Green, (2002).
22. A. A. Salamov, V. V. Solovyev, *Genome Res* **10**, 516 (Apr, 2000).
23. E. Birney, R. Durbin, *Genome Res* **10**, 547 (Apr, 2000).
24. E. M. Zdobnov, R. Apweiler, *Bioinformatics* **17**, 847 (Sep, 2001).
25. M. Ashburner *et al.*, *Nat Genet* **25**, 25 (May, 2000).
26. E. V. Koonin *et al.*, *Genome Biol* **5**, R7 (2004).
27. M. Kanehisa, S. Goto, S. Kawashima, Y. Okuno, M. Hattori, *Nucleic Acids Res* **32**, D277 (Jan 1, 2004).
28. J. P. Kastenmayer *et al.*, *Genome Res* **16**, 365 (Mar, 2006).
29. G. A. Tuskan *et al.*, *Science* **313**, 1596 (Sep 15, 2006).
30. R. D. Finn *et al.*, *Nucleic Acids Res* **34**, D247 (Jan 1, 2006).
31. U. Technau *et al.*, *Trends Genet* **21**, 633 (Dec, 2005).
32. R. C. Edgar, *Nucleic Acids Res* **32**, 1792 (2004).
33. J. Castresana, *Mol Biol Evol* **17**, 540 (Apr, 2000).
34. J. P. Huelsenbeck, F. Ronquist, *Bioinformatics* **17**, 754 (Aug, 2001).
35. F. Ronquist, J. P. Huelsenbeck, *Bioinformatics* **19**, 1572 (Aug 12, 2003).
36. S. Whelan, N. Goldman, *Mol Biol Evol* **18**, 691 (May, 2001).
37. J. Felsenstein. (Distributed by the author., 2004).
38. R. Dawkins, *The ancestor's tale : a pilgrimage to the dawn of evolution* (Houghton Mifflin, Boston, 2004), pp. xii, 673 p.
39. E. J. Douzery, E. A. Snell, E. Baptiste, F. Delsuc, H. Philippe, *Proc Natl Acad Sci U S A* **101**, 15386 (Oct 26, 2004).
40. D. L. Swofford. (Sinauer Associates, Sinderland, Massachusetts, 2003).
41. M. J. de Hoon, S. Imoto, J. Nolan, S. Miyano, *Bioinformatics* **20**, 1453 (Jun 12, 2004).
42. P. D. Thomas *et al.*, *Genome Res* **13**, 2129 (Sep, 2003).
43. H. Mi *et al.*, *Nucleic Acids Res* **33**, D284 (Jan 1, 2005).
44. T. Beissbarth, T. P. Speed, *Bioinformatics* **20**, 1464 (Jun 12, 2004).
45. S. Kumar, K. Tamura, M. Nei, *Brief Bioinform* **5**, 150 (Jun, 2004).

December 20, 2006

Supplemental figures and tables.

Table S1.1: Partial list of the merits of *Nematostella* as a model organism

Developmental Biology

- short generation time (8-10 weeks from fertilization to spawning)
- sexes are separate; sex determination is stable
- prolific sexual and asexual reproduction in the lab
- rapid regeneration and ease of generating clonal populations
- in situ hybridization protocols have been optimized

Genomic Approaches

- relatively small genome (450 million base pairs haploid size)
- most primitive living eumetazoan
- outgroup to other animal genomic models (fly, mouse, nematode)
- most developmental gene families known from other animal systems have been found
- gene families generally appear simpler (fewer members) than in bilaterians
- cDNA and BAC libraries available
- EST projects under way, along with those from other Cnidarians

Population Genetics and Ecology

- easily collected over a wide geographic range well documented since the 1950s
- representative of benthic marine invertebrates with sessile adults and planktonic larvae
- collected in both pristine and polluted sites
- native versus invasive populations may be compared
- asexual reproduction & gravid state are easily visualized in transparent animals

Table S2.1: Summary of WGS libraries

ID	Insert (bp)	N Reads	N Trimmed Reads	N reads with alignments	N placed	Mean trimmed read length
AFII	3149	7658	6867	4839	4035	574
AOWB	2840	1764309	1554340	1026838	880357	630
ATSY	2840	993061	881391	573406	494101	624
AFIK	6489	1864687	1549006	1076195	901598	640
ATWA	6489	915891	834861	592875	500265	709
AFIN	35000	163392	111408	66999	58809	525
ASYG	35000	209087	175771	92574	80041	613
AUNF	35000	50688	40845	35617	31468	656
AXOW	35000	19200	16536	14483	12810	666
AZGY	35000	9216	7056	5664	5001	658
		5997189	5178081	3489490	2968485	
			-14%	-33%	-15%	

Figure S2.1: Distribution of observed polymorphism rates

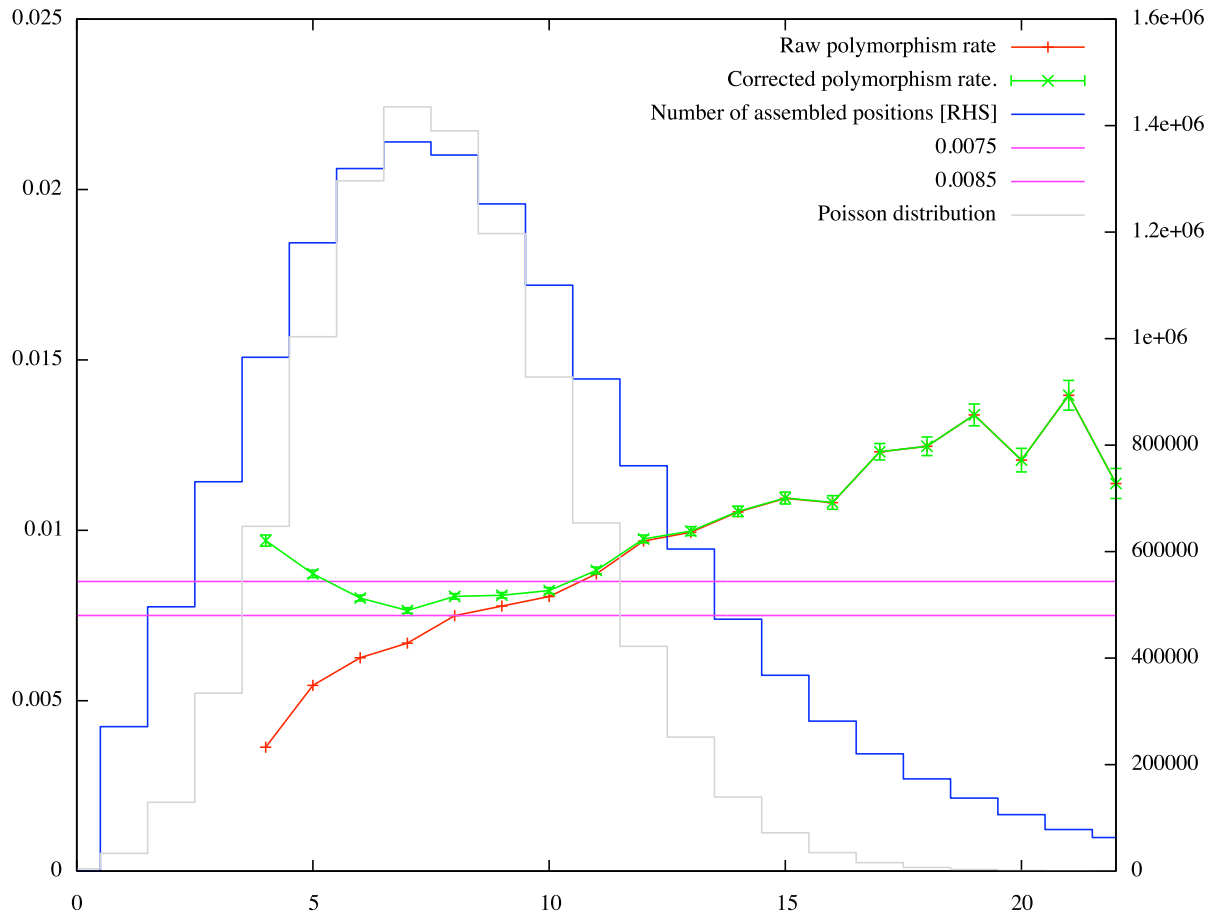


Figure S2.2: Four haplotype polymorphism fit

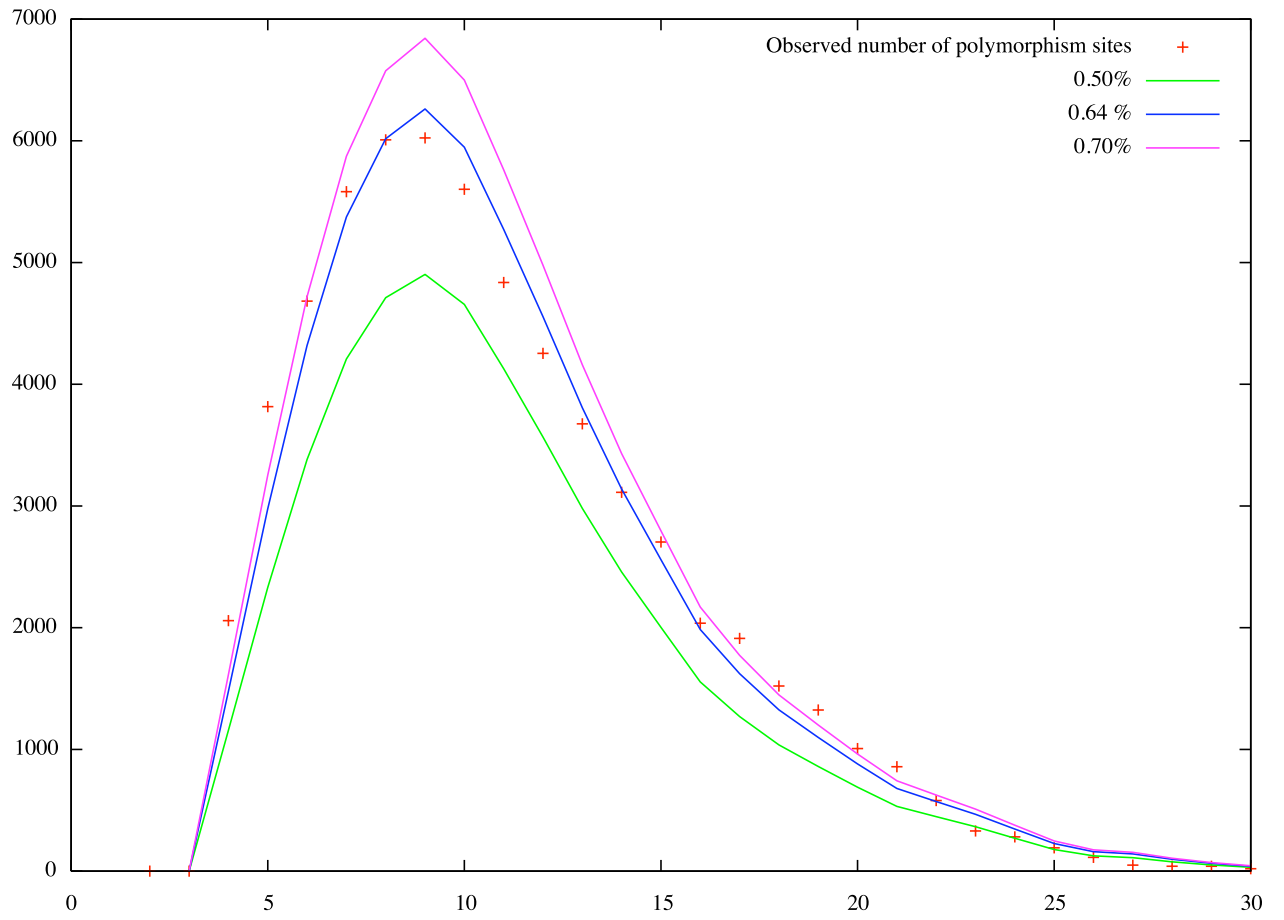


Table S2.2: Summary of tandem repeat elements

Element name	len(bp)	%WGS	Est. Tandem Array size (kb)	Notes
TCTTTGATGTGCTCATjuggernaut	522	10.3%	300	Unclassified cut & paste DNA transposon
AAAAAAAAATCGAACAjuggernaut	7,146	8.8%	2,250	18S, 28S rRNA operon
TTCACGGGTTAATGAAjuggernaut	2,001	7.6%	130	Mariner-3_NVDNA transposon
AAACAAAAGACGCTTTjuggernaut	930	2.3%	360	
GTGTTTGTGGTGTJTTTjuggernaut	175	0.8%	2,130	Met-tRNA
GTGATCGGACGAGAACjuggernaut	186	0.8%	1,040	5S rRNA
CCAATCTTAACGTGCAjuggernaut	622	0.6%	350	
CAAAGTCGGCTTCACGjuggernaut	200	0.4%	710	
TTTTTGATCAAAAAAajuggernaut	770	0.2%	470	U6 snRNA
GTAGACGAAAGATCTCjuggernaut	1,702	0.1%	230	U2 snRNA, 5S rRNA
Total:		31.9%		

Table S2.3: Transposable elements in the sea anemone genome

Classes of TEs	Percent of the genome %
Total DNA transposons	18.5
“cut and paste”:	
<i>Mariner</i> (<i>Tc1</i> , <i>Pogo</i> groups)	2.3
<i>hAT</i>	2.1
<i>Kolobok</i>	1.6
<i>PiggyBac</i>	1.0
<i>Harbinger</i>	1.0
<i>P</i>	0.5
<i>MuDR</i>	0.3
<i>En/Spm</i>	0.05
<i>Merlin</i>	0.01
<i>IS4EU</i>	<0.01
Unclassified	5.2
“self-synthesizing” <i>Polintons</i>	3.0
“rolling circle” <i>Helitrons</i>	1.4
Total retrotransposons	4.6
LTR retrotransposons:	
Gypsy	1.5
BEL	0.2
Copia	0.05
Unclassified	0.2
DIRS	0.4
Non-LTR retrotransposons:	
CR1 (CR1, L2, and REX1 groups)	1.0
RTE (RTE, RTE _X)	0.4
L1 (L1, Tx1)	0.1
R2	<0.01
Penelope	0.7
Unclassified TEs	3.1
Total TEs	26.2

Figure. S2.3: Neighbor-joining tree of eukaryotic non-LTR retrotransposons

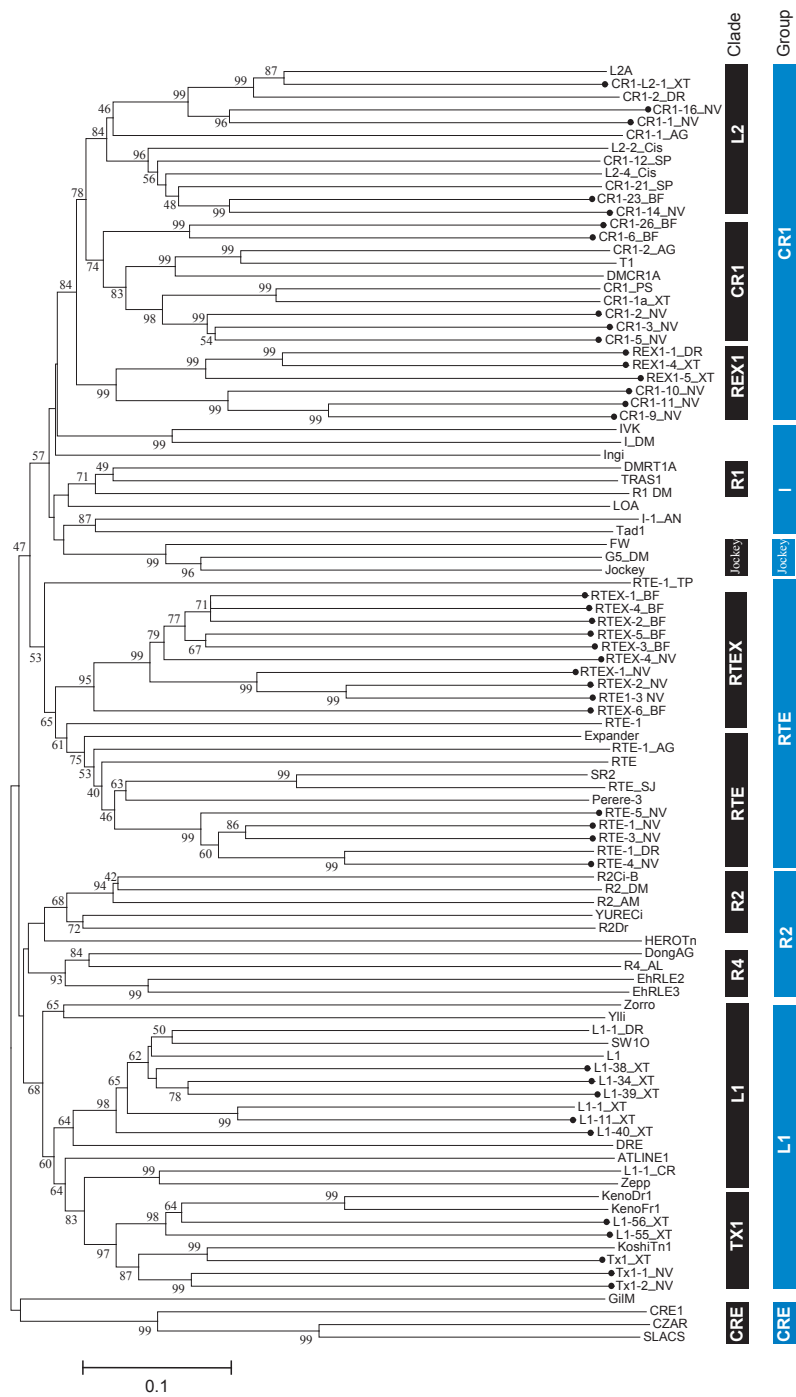


Figure S2.4: Number of chromosomes.

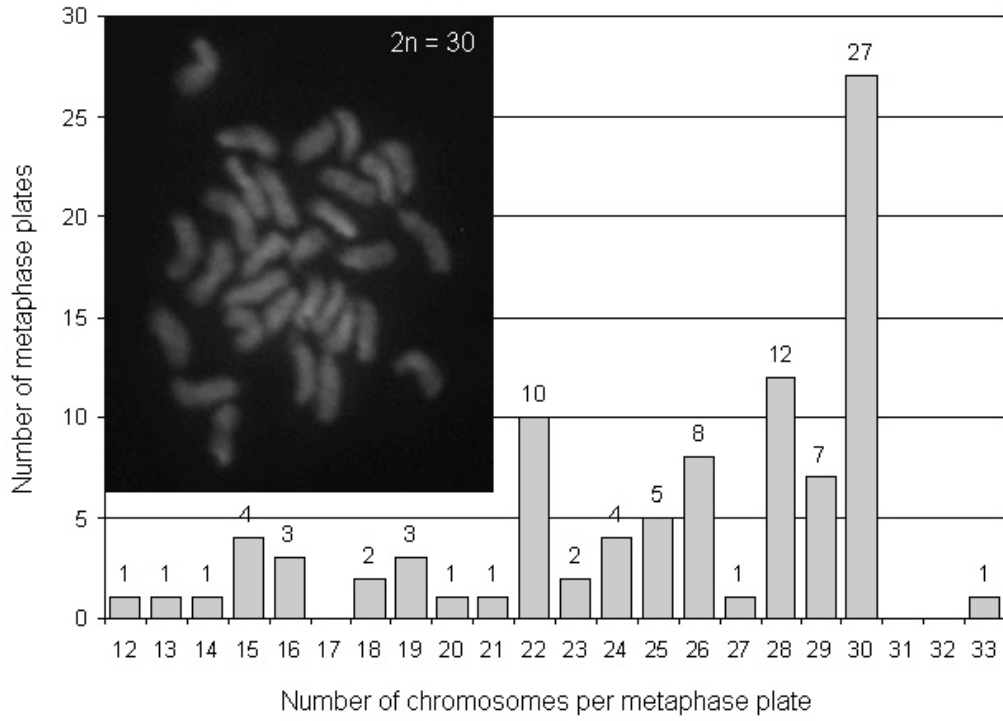


Table S3.1: Summary of gene models

Filtered Models	
Total number of filtered models	27,273
Models without homology to known proteins from NR	896 (3.3%)
Complete models (ATG and Stop codons)	13,343
Half-complete models	6,975
Incomplete models	6,955
Models exactly predicted by fgenesh and genewise	2,182 (8%)
Models extended to UTRs by ESTs	6,144
Number of single-exon genes (some fraction may be pseudo-genes)	8,460 (31%)
Average number of exons per gene	5.3
Average number of exons per gene (excluding single-exon genes)	7.2
Average transcript length	1,092 bp
Average gene length	4.5 kb
Average protein length	331 aa
Average exon length	208 bp
Average intron length	800 bp

Figure S3.1: Distribution of C-scores

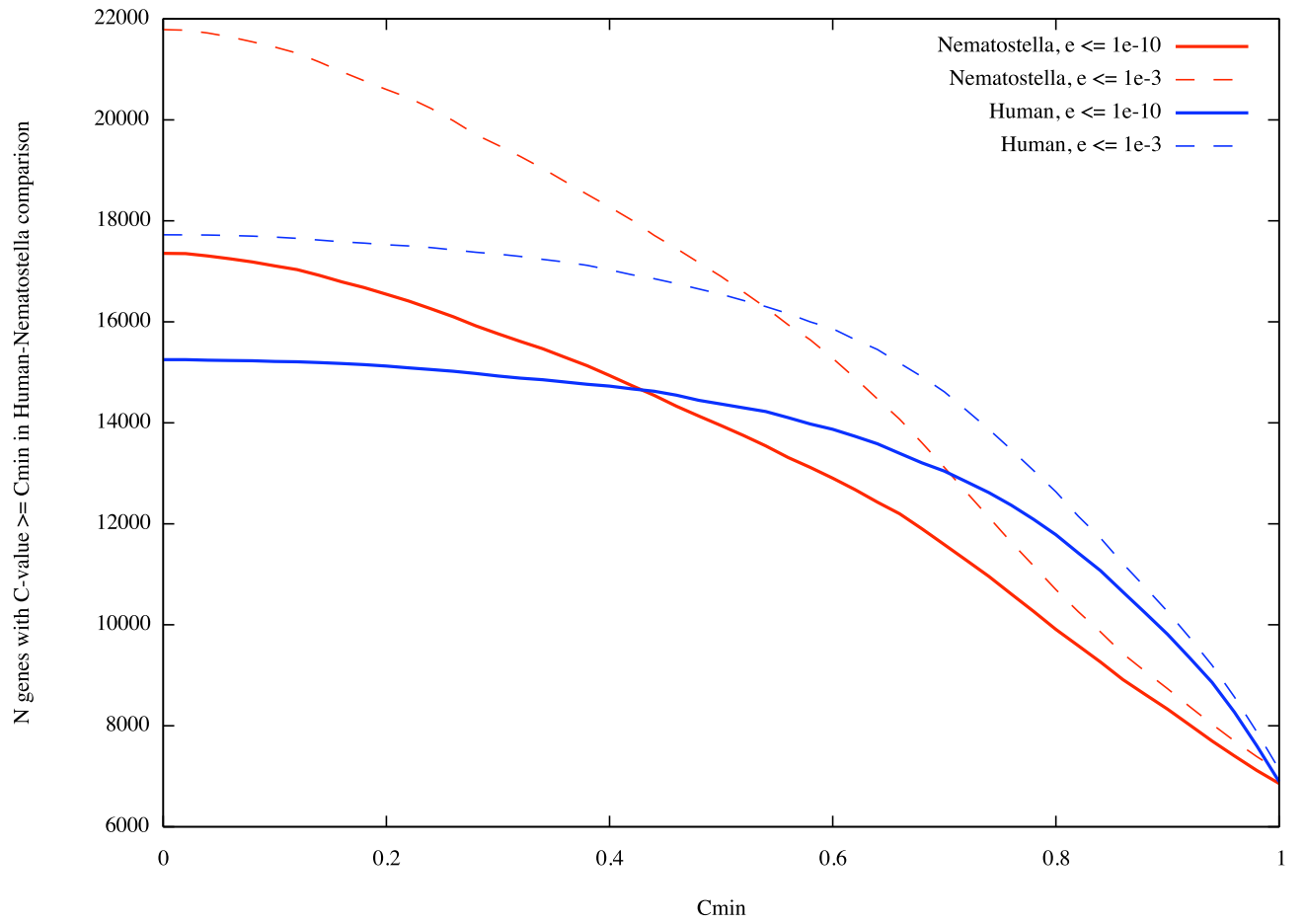


Table S3.2: Compared abundances of PFAM domains for selected domains

	N - number R - rank	<i>N. vectensis</i>		<i>H. sapiens</i>		<i>C. intestinalis</i>		<i>D. melanogaster</i>		<i>C. elegans</i>	
		N	R	N	R	N	R	N	R	N	R
PF00001	7tm_1	617	1	546	2	59	32	53	27	63	31
PF00008	EGF domain	356	2	152	20	162	3	40	39	53	42
PF00069	protein kinase	278	3/4	448	3	251	1	201	3	326	2
PF00754	F5/8 type C	278	3/4	20	179	14	150	5	418	3	687
PF00400	WD domain	262	5	244	7	201	2	156	4	118	11
PF00096	Zinc finger	213	6	711	1	160	4	296	1	117	12
PF00023	Ankyrin repeat	181	7	236	8	117	5	84	13	84	22
PF00097	RING finger	175	8	204	12	71	19	64	19	86	21
PF00036	EF hand	162	9	166	18	110	8	83	15	63	33
PF00046	Homeobox	152	10	221	10	83	14	99	9	19	89

Figure S3.2: Number of bidirectional BlastP hits between 22,218 human genes and other organisms

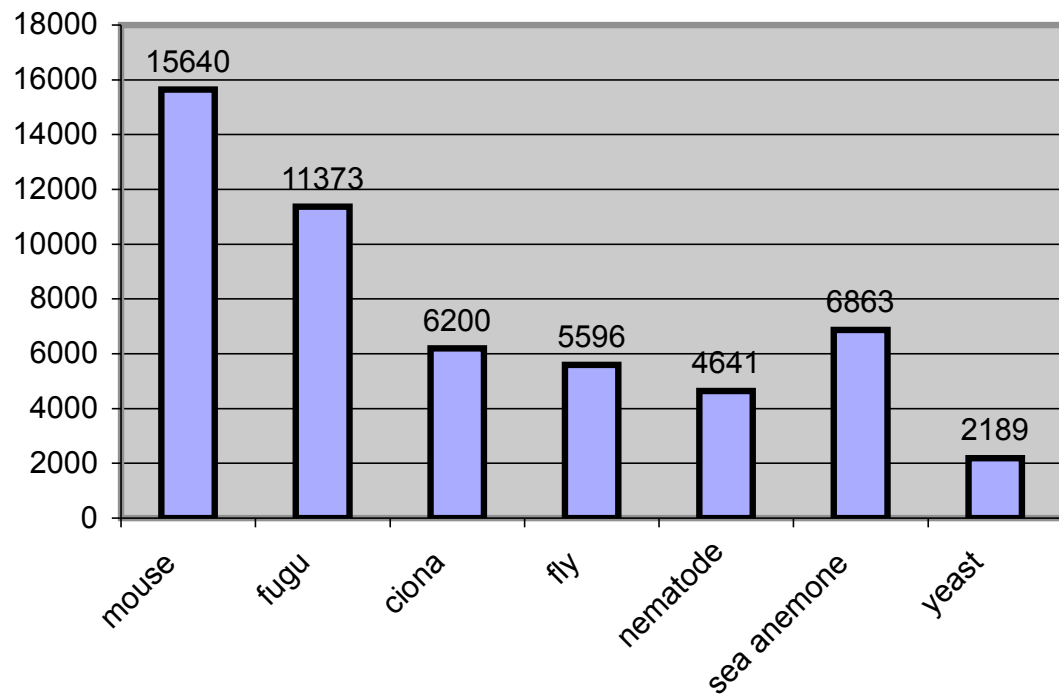


Figure S3.3: Fraction of unique multi (Pfam) domain (2 or more domains) gene models from *Nematostella* (total 983) shared by other metazoans and yeast.

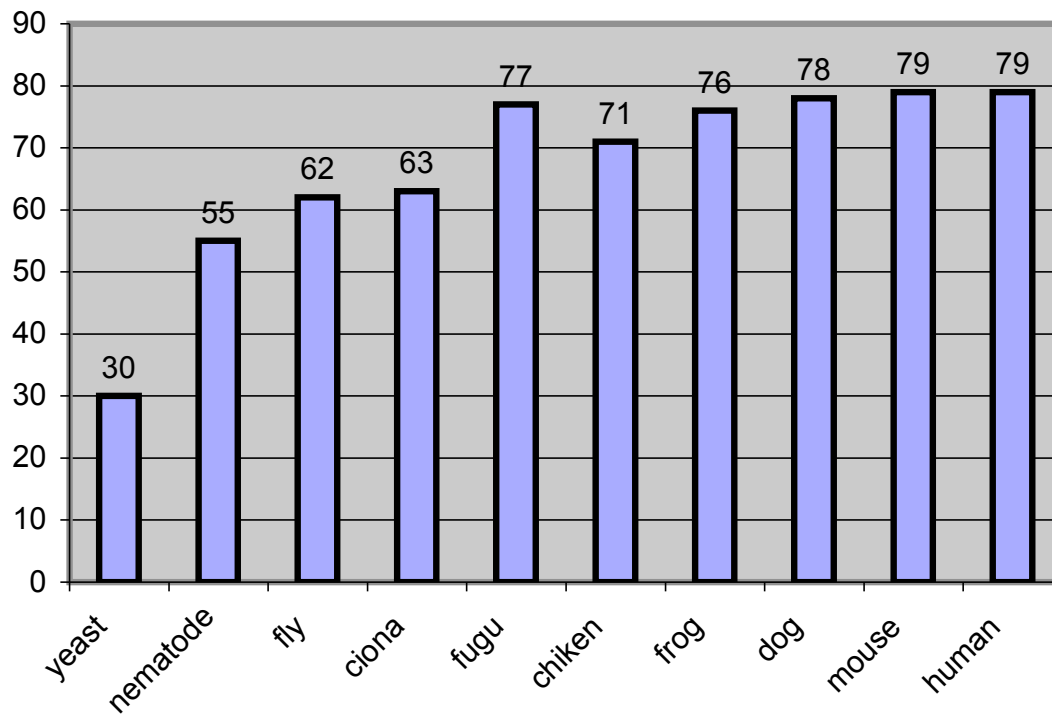


Figure S3.4: 2264 Pfam domains present in all 6 vertebrates

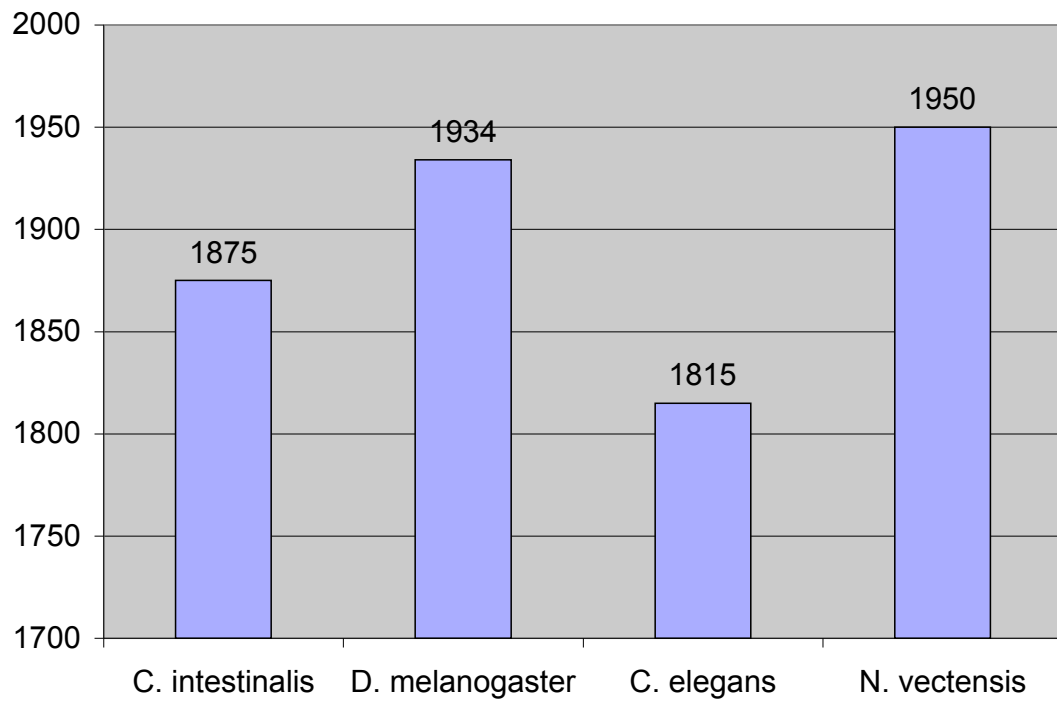


Table S3.3: Preferentially retained PFAM domains within recent tandem expansions in *Nematostella*

PFAM ID	PFAM Description	#recent	sigma
PF00147	Fibrinogen beta and gamma chains, C-terminal globular domain	18	9.4
PF00112	Papain family cysteine protease	11	7.9
PF00067	Cytochrome P450	18	7.8
PF03953	Tubulin/FtsZ family, C-terminal domain	10	7.6
PF00643	B-box zinc finger	16	6.9
PF02140	Galactose binding lectin domain	12	6.8
PF00091	Tubulin/FtsZ family, GTPase domain	9	6.6
PF00515	TPR Domain	22	6.5
PF07719	Tetrapeptide repeat	22	5.5
PF00110	wnt family	5	4.4
PF00125	Core histone H2A/H2B/H3/H4	17	4.3
PF03160	Calx-beta domain	5	4.1
PF00754	F5/8 type C domain	27	3.9
PF00106	short chain dehydrogenase	10	3.7
PF00102	Protein-tyrosine phosphatase	6	3.2

Table S3.4: Preferentially retained PFAM domains within recent tandem expansions in Homo sapien

PFAM ID	PFAM Description	#recent	sigma
PF00001	7 transmembrane receptor (rhodopsin family)	112	15.8
PF01352	KRAB box	62	14.4
PF00143	Interferon alpha/beta domain	12	13.2
PF00201	UDP-glucuronosyl and UDP-glucosyl transferase	9	10.4
PF00038	Intermediate filament protein	21	9.6
PF01500	Keratin high sulfur B2 protein	8	9.5
PF00047	Immunoglobulin domain	60	9.2
PF00048	Small cytokines (intercine/chemokine), interleukin-8 like	13	8.9
PF00028	Cadherin domain	20	8.5
PF02841	Guanylate-binding protein, C-terminal domain	5	8.5
PF00067	Cytochrome P450	16	8.5
PF00248	Aldo/keto reductase family	8	8.2
PF00808	Histone-like transcription factor (CBF/NF-Y) and archaeal histone	16	8.2
PF02806	Alpha amylase, C-terminal all-beta domain	4	8.1
PF00125	Core histone H2A/H2B/H3/H4	19	7.8
PF07686	Immunoglobulin V-set domain	47	7.7
PF00129	Class I Histocompatibility antigen, domains alpha 1 and 2	7	7.6
PF00096	Zinc finger, C2H2 type	70	7.5
PF02798	Glutathione S-transferase, N-terminal domain	9	7.4
PF06623	MHC_I C-terminus	4	7.4
PF00128	Alpha amylase, catalytic domain	4	7.4
PF00043	Glutathione S-transferase, C-terminal domain	9	7.3
PF01454	MAGE family	9	6.8
PF02263	Guanylate-binding protein, N-terminal domain	5	6.6
PF04722	Ssu72-like protein	4	6.2
PF05831	GAGE protein	5	5.9
PF07654	Immunoglobulin C1-set domain	11	5.9
PF05296	Mammalian taste receptor protein (TAS2R)	6	5
PF02736	Myosin N-terminal SH3-like domain	4	4.6
PF06409	Nuclear pore complex interacting protein (NPIP)	4	4.6
PF00007	Cystine-knot domain	4	4.6
PF01576	Myosin tail	4	4.4
PF00622	SPRY domain	10	3.5
PF00059	Lectin C-type domain	8	3.1

Table S5.1: Table of data sources for phylogenetic analysis

Data sources for phylogenetic analysis

Whole or partial genome sequences

Xenopus tropicalis JGI v4.1
Takifugu rubripes JGI v4.0
Homo sapiens Ensembl build 38

Drosophila melanogaster Ensembl build 38
Caenorhabditis elegans Ensembl build 38

Nematostella vectensis JGI V1.0

Ciona intestinalis JGI v2.0

Lottia gigantea [J. Chapman, unpublished]
Hydra magnipapillata [Steele et al, unpublished]
Monosiga brevicollis [JGI unpublished]
Renieria spp. [JGI unpublished]

Saccharomyces cerevisiae From genome-ftp.stanford.edu, version released on July 7, 2004

ESTs:

Mnemiopsis leidyi

Figure S5.1: Distribution of percent ID Against Human Proteins

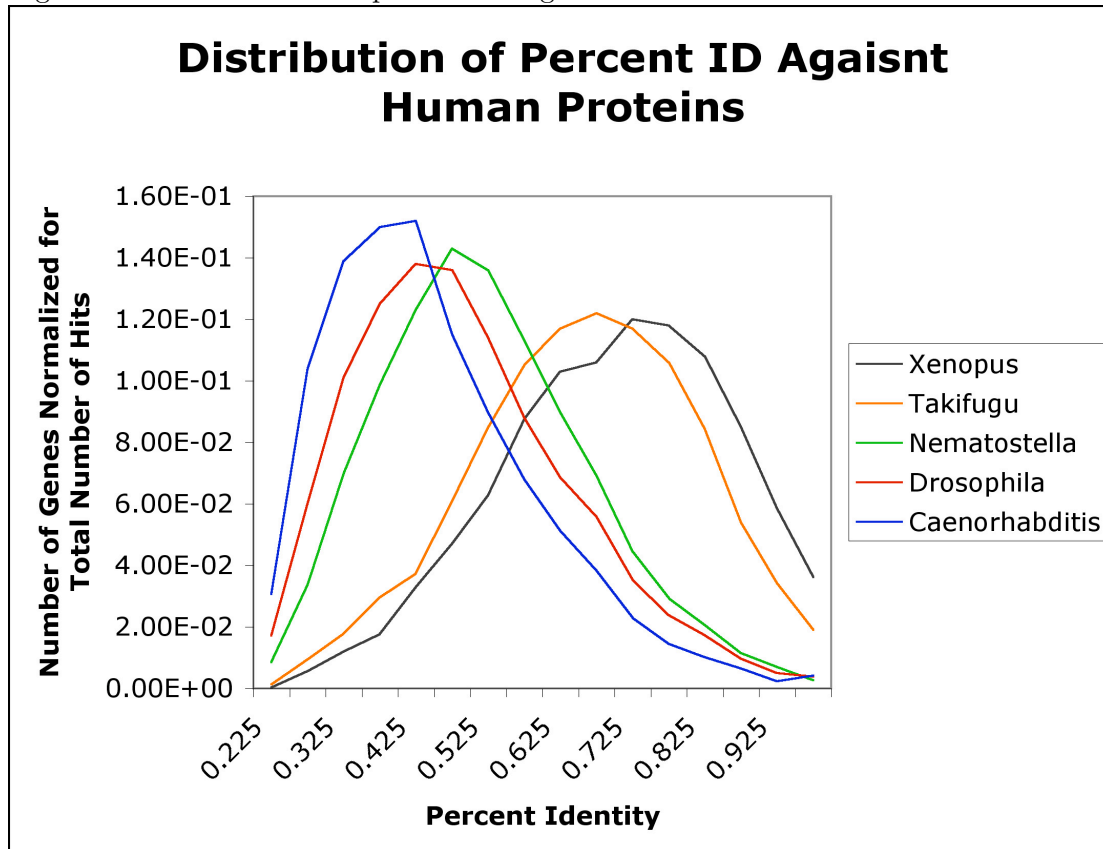
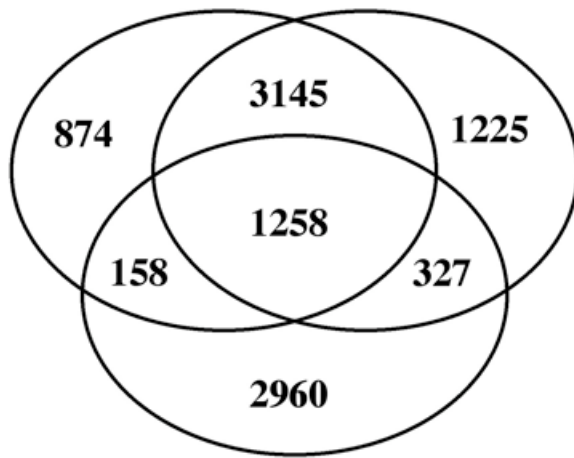


Figure S6.1: Venn diagram for three-way intron conservation comparison

Human *Nematostella*



Arabidopsis

Table S6.1: Four-way intron conservation comparison

Species	Total Introns
<i>H. sapiens</i>	3326 (476)
<i>N. vectensis</i>	3647 (771)
<i>D. melanogaster</i>	761 (171)
<i>C. elegans</i>	1363 (551)
<i>H.sapiens</i> + <i>N. vectensis</i>	2751
<i>H. sapiens</i> + <i>C.elegans</i>	714
<i>H. sapiens</i> + <i>D.melanogaster</i>	536
<i>C.elegans</i> + <i>D.melanogaster</i>	232
<i>H.sapiens</i> + <i>N.vectensis</i> + <i>D. melanogaster</i>	495
<i>H.sapiens</i> + <i>N.vectensis</i> + <i>C.elegans</i>	640
<i>shared by all four species</i>	196

Figure S7.1: Synteny block search

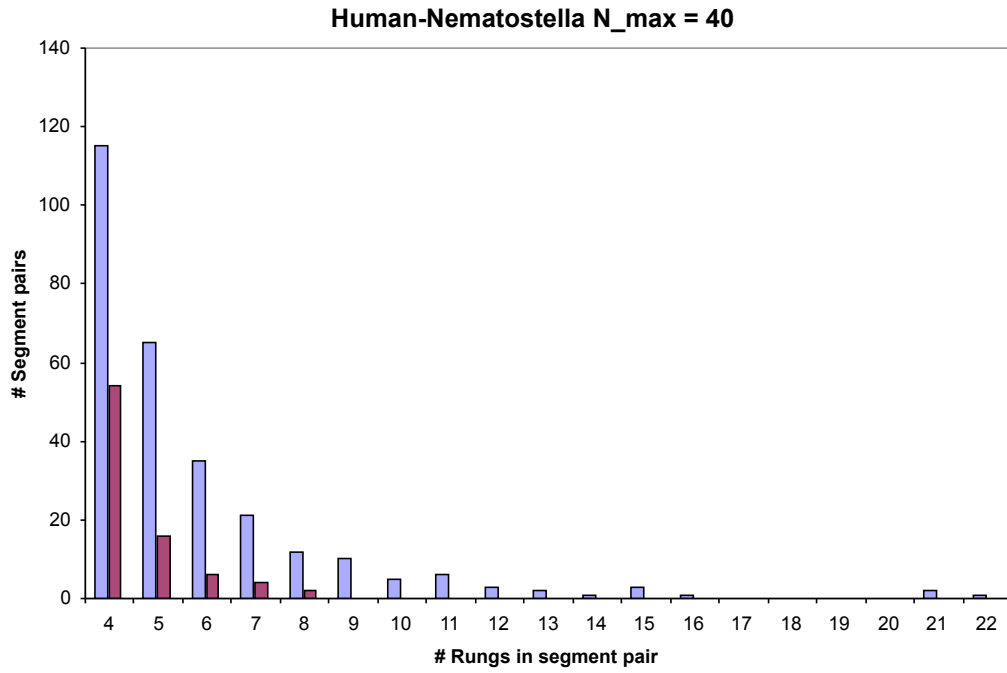


Figure S7.2: HMM segmentation example

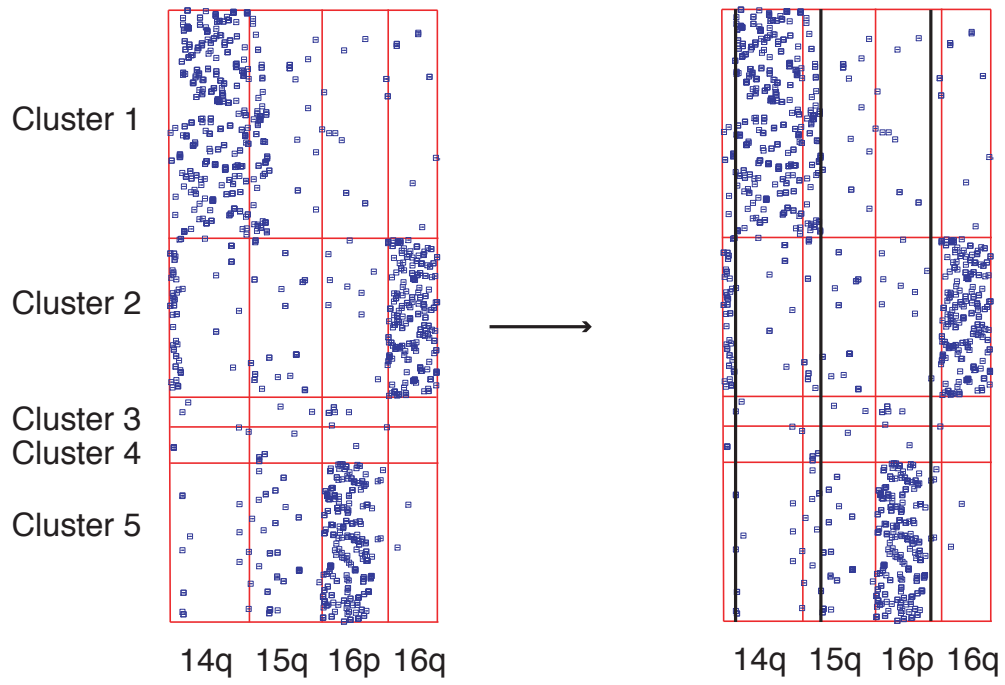


Table S7.1: Table of human chromosome segments used in large-scale synteny search

Name	Chromosome	Start	End
Xp11.4-22.2	X	9673696	37588240
Xp11.21-11.3	X	46887841	55047087
Xp11.21-q13.1	X	55047088	68655440
Xq13.1-28	X	68655440	153978722
Yp11.32-q12	Y	1	57657766
1p36.12-36.33	1	877210	20855970
1p36.11-36.12	1	20855971	25549674
1p34.3-36.11	1	25549674	39269870
1p31.1-34.2	1	40008738	74859196
1p13.3-31.1	1	78330448	110388420
1p12-13.3	1	110388421	118243306
1p12-q21.2	1	119430925	148345068
1q21.2-23.1	1	148345068	155020532
1q23.1-24.2	1	155163302	166097526
1q24.2-31.2	1	168062712	191338566
1q31.2-32.2	1	191336757	208079724
1q32.2-44	1	208079724	244976017
2p24.3-25.3	2	1	15421694
2p13.2-24.3	2	15421694	73578474
2p11.2-13.1	2	74513568	86693774
2p11.2-q11.2	2	86693775	96287750
2q11.2-35	2	96287750	220120257
2q37.1-37.3	2	233900764	242339685
3p24.3-26.3	3	3181960	14740598
3p22.1-24.3	3	15310713	42757316
3p13-22.1	3	43109152	73163221
3p13-q12.2	3	73163222	101930675
3q12.2-27.3	3	101930675	187872602
3q28-29	3	191514553	199135808
4p15.2-16.3	4	929333	25008576
4p12-15.2	4	25278016	48189124
4q12-35.2	4	52592031	190392426
5p12-15.31	5	6704566	43577691
5p12-q12.1	5	43577692	62108653
5q12.1-23.3	5	62108653	128467978
5q21.1-35.3	5	132114396	179586409
6p21.2-25.3	6	1	27327284
6p21.2-22.1	6	27327284	37533628
6p21.2-q14.1	6	37533629	76036806
6q14.1-25.3	6	76036806	158925275
6q27	6	165628122	170899992
7p22.1-22.3	7	762350	6605590
7p11.2-21.3	7	7683932	55720376
7q11.21-11.23	7	65073872	75458076
7q21.3-35	7	96616718	143142128
7q35-36.3	7	143896277	156273990
8p22-23.3	8	1	16976821
8p11.21-22	8	16976821	43145466
8q11.22-24.3	8	51668647	145706329
9p13.3-22.3	9	15431371	35804014
9p13.3-q13	9	35804015	70248716
9q13-31.3	9	70248716	113718168
9q32-34.3	9	114961559	139558315
10p11.22-13	10	15220868	32652190
10q11.21-24.1	10	42623200	98406664
10q24.1-26.3	10	99128910	134856173
11p11.2-15.5	11	188669	47791440
11q12.1-13.1	11	57183558	66019773
11q13.1-25	11	66045396	133689416
12p11.21-13.33	12	2832566	30786824
12q12-14.3	12	42480106	64833745
12q15-23.3	12	67504578	105913314
12q23.3-24.33	12	107435346	131912602
13q12.11-14.11	13	21020596	40815702
13q14.11-34	13	41236742	114076856
14q11.2-12	14	19835780	23731462
14q12-32.33	14	23754046	105032519
15p13-q13.3	15	1	30805828
15q13.3-15.2	15	30805828	41269660
15q15.3-26.3	15	41529412	100004844
16p11.2-13.3	16	72004	27846219
16p11.2	16	28333242	31029424
16q11.2-24.3	16	45265844	88626264
17p13.2-13.3	17	621332	6608690
17p13.1-13.2	17	6608691	8299690
17p11.2-13.1	17	8299690	20458232
17q11.2-12	17	23674170	32434314
17q12-21.32	17	33964971	44369806
17q21.33-22	17	45136933	52026908
17q22-23.2	17	53308380	57331627
17q23.3-25.3	17	59268418	78471871
18q12.2-21.31	18	31310368	53429455
18q21.33-23	18	57933823	75983560
19p13.2-13.3	19	966940	9814179
19p13.11-13.2	19	10080470	18166924
19p13.11-q13.11	19	19470851	37834416
19q13.11-13.33	19	37834416	53822936
19q13.33-13.42	19	54106710	60560743
19q13.42-13.43	19	60560743	63811651
20p11.21-12.3	20	5873116	25355542
20q11.21-13.33	20	29693425	61045004
20q13.33	20	61045004	62435964
21p13-q21.3	21	1	29291902
21q21.3-22.3	21	29291902	44280308
21q22.3	21	44280308	46944323
22q11.1-12.3	22	16056470	30556650
22q12.3-13.2	22	32322586	41325288
22q13.2-13.33	22	41887065	49313184

Figure S7.3: Clustering method for constructing putative ancestral linkage groups (PALs)

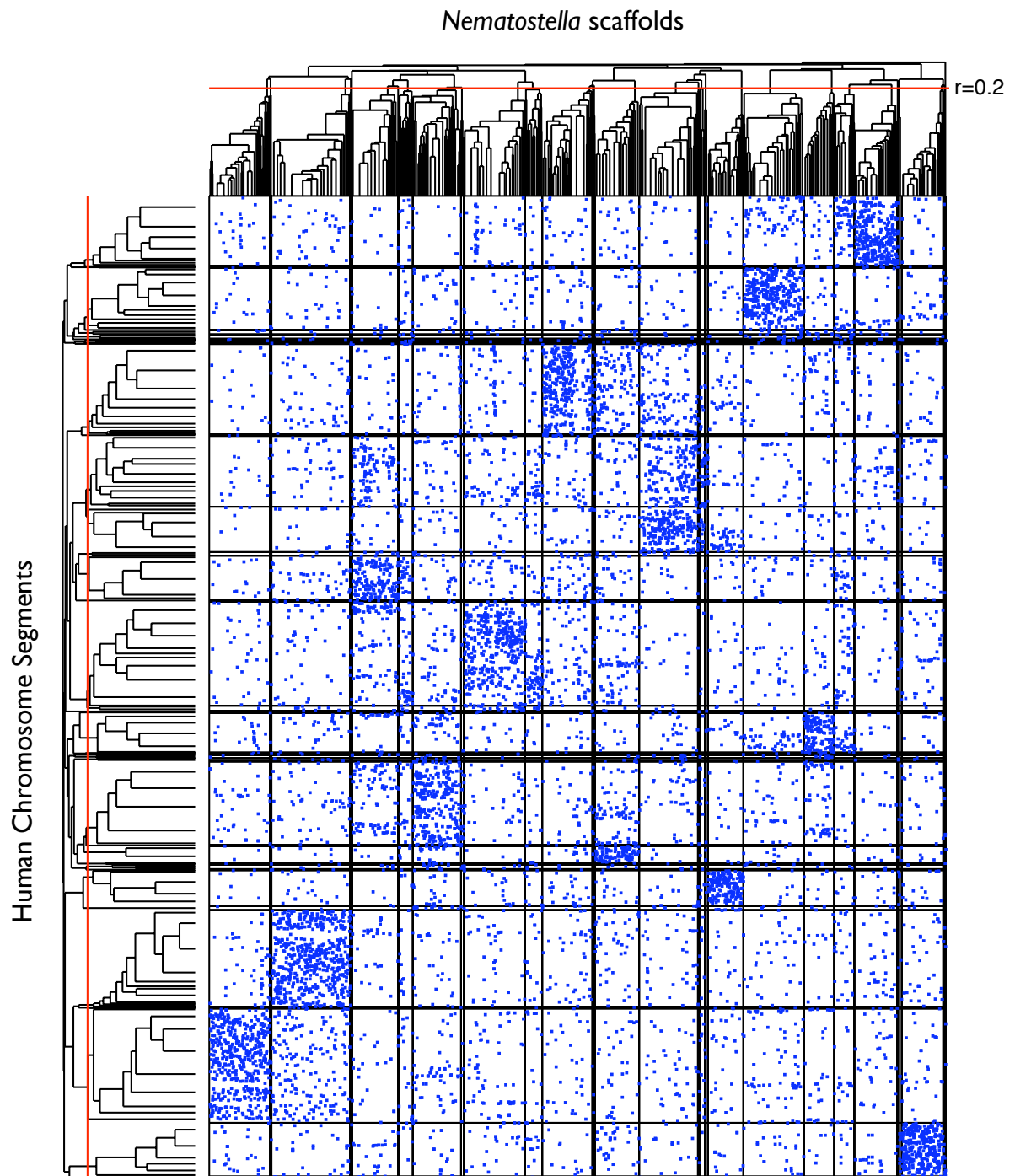


Figure S7.4: Detail of Human chromosome 12 showing genes contributing to PAL A.

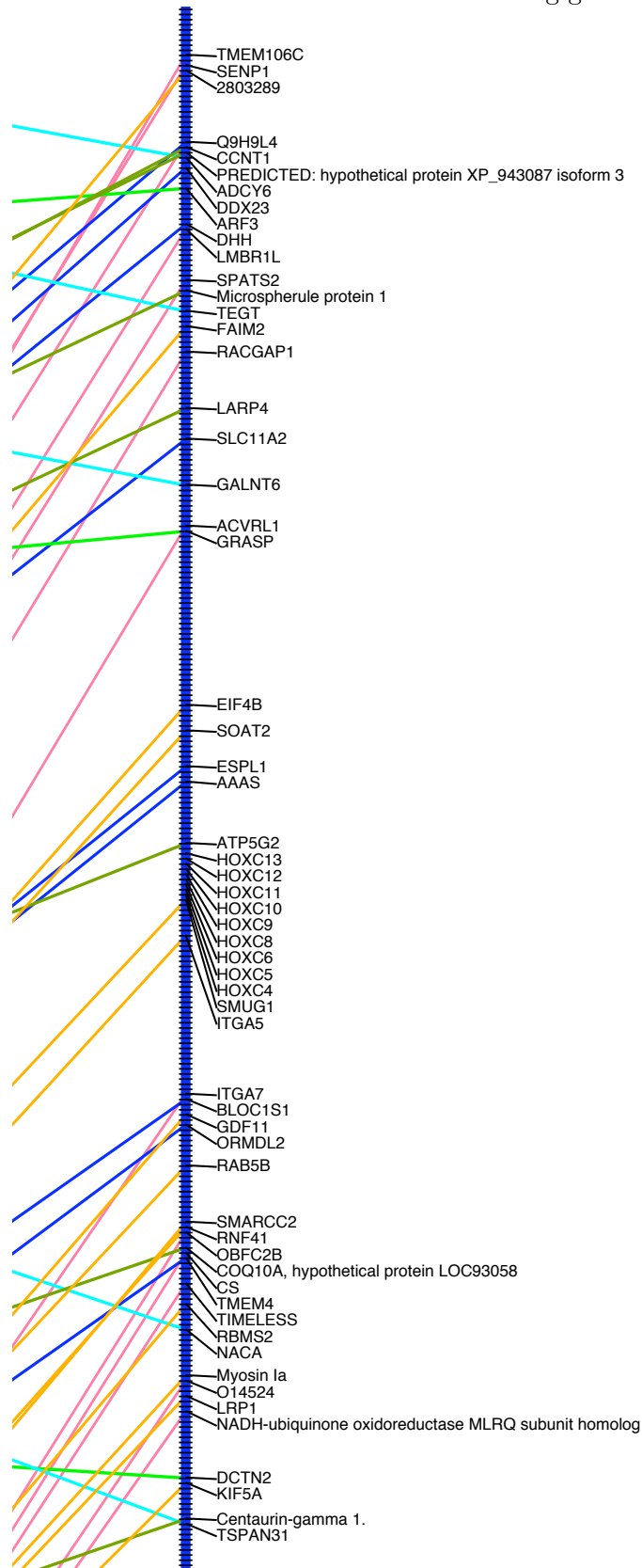


Table S81.a: Panther Ontology Terms for Biological Process and Molecular Function:

Ontology ID	ln(p-value) enrichment /depletion	+/-	N(ont & cat)	N(ont)	N(cat)	N(total)	N(ont& cat) / N(cat)	N(ont)/ N(total)	Ontology Term Desc.
Type III novelty, $p < 0.05/100$ enriched ontology terms:									
BP00102	-52.3	+	68	575	240	7766	28%	7%	Signal transduction
MF00100	-26.5	+	23	125	240	7766	10%	2%	G-protein modulator
BP00285	-21.7	+	29	246	240	7766	12%	3%	Cell structure and motility
BP00111	-20.7	+	29	257	240	7766	12%	3%	Intracellular signaling cascade
MF00093	-20.6	+	36	379	240	7766	15%	5%	Select regulatory molecule
BP00103	-19.3	+	24	192	240	7766	10%	2%	Cell surface receptor mediated signal transduction
MF00212	-18.7	+	14	65	240	7766	6%	1%	Other G-protein modulator
BP00124	-16.7	+	13	64	240	7766	5%	1%	Cell adhesion
MF00261	-16.6	+	16	101	240	7766	7%	1%	Actin binding cytoskeletal protein
BP00166	-16.1	+	16	104	240	7766	7%	1%	Neuronal activities
BP00104	-15.6	+	14	82	240	7766	6%	1%	G-protein mediated signaling
BP00274	-12.5	+	16	135	240	7766	7%	2%	Cell communication
BP00199	-12.3	+	14	107	240	7766	6%	1%	Neurogenesis
BP00064	-11.7	+	21	231	240	7766	9%	3%	Protein phosphorylation
BP00286	-11.6	+	16	145	240	7766	7%	2%	Cell structure
BP00246	-11.3	+	14	116	240	7766	6%	1%	Ectoderm development
MF00107	-11.1	+	22	259	240	7766	9%	3%	Kinase
MF00091	-11.1	+	20	222	240	7766	8%	3%	Cytoskeletal protein
BP00119	-10.0	+	10	69	240	7766	4%	1%	Other intracellular signaling cascade
BP00193	-9.4	+	27	396	240	7766	11%	5%	Developmental processes
Type II novelty, $p < 0.05/100$ enriched ontology terms:									
BP00193	-39.7	+	40	396	158	7766	25%	5%	Developmental processes
BP00102	-38.4	+	47	575	158	7766	30%	7%	Signal transduction
MF00001	-25.2	+	18	115	158	7766	11%	1%	Receptor
BP00274	-24.6	+	19	135	158	7766	12%	2%	Cell communication
BP00246	-20.5	+	16	116	158	7766	10%	1%	Ectoderm development
BP00199	-19.5	+	15	107	158	7766	9%	1%	Neurogenesis
BP00103	-13.4	+	16	192	158	7766	10%	2%	Cell surface receptor mediated signal transduction
BP00287	-11.7	+	9	68	158	7766	6%	1%	Cell motility
BP00044	-11.5	+	18	273	158	7766	11%	4%	mRNA transcription regulation
MF00016	-10.3	+	10	100	158	7766	6%	1%	Signaling molecule
BP00166	-10.0	+	10	104	158	7766	6%	1%	Neuronal activities
BP00111	-9.7	+	16	257	158	7766	10%	3%	Intracellular signaling cascade
MF00036	-9.3	+	19	352	158	7766	12%	5%	Transcription factor
BP00285	-8.9	+	15	246	158	7766	9%	3%	Cell structure and motility
BP00248	-7.8	+	8	89	158	7766	5%	1%	Mesoderm development
BP00040	-7.7	+	19	398	158	7766	12%	5%	mRNA transcription
Type I novelty, $p < 0.05/100$ enriched ontology terms:									
MF00016	-8.0	+	29	100	1186	7766	2%	1%	Signaling molecule
All types of novelty, $p < 0.05/100$ enriched ontology terms:									
BP00102	-24.4	+	182	575	1584	7766	11%	7%	Signal transduction
BP00103	-24.4	+	79	192	1584	7766	5%	2%	Cell surface receptor mediated signal transduction
BP00193	-23.1	+	134	396	1584	7766	8%	5%	Developmental processes
MF00016	-22.8	+	49	100	1584	7766	3%	1%	Signaling molecule
BP00274	-22.5	+	60	135	1584	7766	4%	2%	Cell communication
BP00166	-16.2	+	45	104	1584	7766	3%	1%	Neuronal activities
BP00246	-12.5	+	45	116	1584	7766	3%	1%	Ectoderm development
BP00248	-12.4	+	37	89	1584	7766	2%	1%	Mesoderm development
BP00124	-12.1	+	29	64	1584	7766	2%	1%	Cell adhesion
BP00104	-11.5	+	34	82	1584	7766	2%	1%	G-protein mediated signaling
MF00001	-11.0	+	43	115	1584	7766	3%	1%	Receptor
BP00199	-10.3	+	40	107	1584	7766	3%	1%	Neurogenesis
BP00281	-7.9	+	35	99	1584	7766	2%	1%	Oncogenesis
BP00111	-7.8	+	75	257	1584	7766	5%	3%	Intracellular signaling cascade
Type III novelty, $p < 0.05/100$ depleted ontology terms:									
MF00131	-10.2	-	1	398	240	7766	0%	5%	Transferase
Type II novelty, $p < 0.05/100$ depleted ontology terms:									
Type I novelty, $p < 0.05/100$ depleted ontology terms:									
BP00060	-114.4	-	24	1056	1186	7766	2%	14%	Protein metabolism and modification
MF00042	-55.4	-	46	915	1186	7766	4%	12%	Nucleic acid binding
BP00031	-50.7	-	62	1034	1186	7766	5%	13%	Nucleoside, nucleotide and nucleic acid metabolism

BP00063	-41.2	-	13	447	1186	7766	1%	6% Protein modification
MF00141	-40.1	-	5	330	1186	7766	0%	4% Hydrolase
BP00107	-33.8	-	3	259	1186	7766	0%	3% Kinase
MF00123	-31.4	-	6	289	1186	7766	1%	4% Oxidoreductase
MF00131	-30.9	-	15	398	1186	7766	1%	5% Transferase
BP00019	-30.5	-	4	254	1186	7766	0%	3% Lipid, fatty acid and steroid metabolism
BP00125	-30.3	-	16	405	1186	7766	1%	5% Intracellular protein traffic
BP00141	-29.6	-	14	377	1186	7766	1%	5% Transport
BP00001	-29.4	-	3	231	1186	7766	0%	3% Carbohydrate metabolism
BP00064	-29.4	-	3	231	1186	7766	0%	3% Protein phosphorylation
MF00170	-28.0	-	1	188	1186	7766	0%	2% Ligase
BP00071	-27.0	-	7	273	1186	7766	1%	4% Proteolysis
BP00203	-27.0	-	13	346	1186	7766	1%	4% Cell cycle
MF00082	-23.0	-	5	219	1186	7766	0%	3% Transporter
MF00108	-21.9	-	3	183	1186	7766	0%	2% Protein kinase
MF00126	-21.7	-	0	130	1186	7766	0%	2% Dehydrogenase
BP00282	-21.6	-	0	129	1186	7766	0%	2% Mitosis
BP00013	-21.4	-	0	128	1186	7766	0%	2% Amino acid metabolism
BP00061	-20.8	-	4	190	1186	7766	0%	2% Protein biosynthesis
BP00289	-19.1	-	9	241	1186	7766	1%	3% Other metabolism
MF00153	-18.1	-	3	158	1186	7766	0%	2% Protease
MF00213	-17.6	-	1	124	1186	7766	0%	2% Non-receptor serine/threonine protein kinase
BP00034	-17.4	-	4	167	1186	7766	0%	2% DNA metabolism
BP00036	-17.0	-	0	102	1186	7766	0%	1% DNA repair
MF00051	-16.9	-	0	101	1186	7766	0%	1% Helicase
BP00047	-16.5	-	2	133	1186	7766	0%	2% Pre-mRNA processing
MF00156	-16.4	-	0	98	1186	7766	0%	1% Other hydrolase
MF00264	-16.2	-	0	97	1186	7766	0%	1% Microtubule family cytoskeletal protein
MF00093	-16.1	-	25	379	1186	7766	2%	5% Select regulatory molecule
BP00276	-16.0	-	2	130	1186	7766	0%	2% General vesicle transport
MF00113	-15.2	-	1	109	1186	7766	0%	1% Phosphatase
MF00097	-14.7	-	1	106	1186	7766	0%	1% G-protein
MF00118	-14.6	-	3	135	1186	7766	0%	2% Synthase and synthetase
MF00284	-14.3	-	0	86	1186	7766	0%	1% Other ligase
MF00166	-14.0	-	0	84	1186	7766	0%	1% Isomerase
MF00077	-13.8	-	0	83	1186	7766	0%	1% Chaperone
MF00099	-13.8	-	0	83	1186	7766	0%	1% Small GTPase
MF00075	-13.7	-	2	115	1186	7766	0%	1% Ribosomal protein
BP00062	-13.5	-	0	81	1186	7766	0%	1% Protein folding
BP00048	-13.3	-	1	97	1186	7766	0%	1% mRNA splicing
BP00076	-13.1	-	2	111	1186	7766	0%	1% Electron transport
BP00020	-12.3	-	0	74	1186	7766	0%	1% Fatty acid metabolism
MF00127	-12.3	-	1	91	1186	7766	0%	1% Reductase
MF00086	-12.2	-	3	118	1186	7766	0%	2% Other transporter
BP00285	-12.1	-	15	246	1186	7766	1%	3% Cell structure and motility
MF00157	-11.8	-	1	88	1186	7766	0%	1% Lyase
MF00091	-11.6	-	13	222	1186	7766	1%	3% Cytoskeletal protein
BP00081	-11.2	-	1	84	1186	7766	0%	1% Coenzyme and prosthetic group metabolism
MF00133	-9.5	-	1	73	1186	7766	0%	1% Methyltransferase
BP00273	-8.9	-	1	69	1186	7766	0%	1% Chromatin packaging and remodeling
BP00129	-8.8	-	3	94	1186	7766	0%	1% Endocytosis
MF00100	-8.5	-	6	125	1186	7766	1%	2% G-protein modulator
BP00286	-8.5	-	8	145	1186	7766	1%	2% Cell structure
MF00065	-8.4	-	2	79	1186	7766	0%	1% mRNA processing factor
MF00119	-8.3	-	2	78	1186	7766	0%	1% Synthase
BP00142	-8.2	-	8	143	1186	7766	1%	2% Ion transport
BP00207	-8.0	-	8	141	1186	7766	1%	2% Cell cycle control
MF00087	-7.9	-	4	99	1186	7766	0%	1% Transfer/carrier protein
MF00044	-7.7	-	3	86	1186	7766	0%	1% Nuclease

All types of novelty, $p < 0.05/100$ depleted ontology terms:

BP00060	-64.4	-	91	1056	1584	7766	6%	14% Protein metabolism and modification
MF00042	-42.9	-	91	915	1584	7766	6%	12% Nucleic acid binding
BP00001	-37.8	-	5	231	1584	7766	0%	3% Carbohydrate metabolism
MF00131	-31.0	-	28	398	1584	7766	2%	5% Transferase
BP00031	-28.7	-	128	1034	1584	7766	8%	13% Nucleoside, nucleotide and nucleic acid metabolism
MF00141	-27.4	-	22	330	1584	7766	1%	4% Hydrolase
MF00123	-23.1	-	20	289	1584	7766	1%	4% Oxidoreductase
BP00125	-23.0	-	36	405	1584	7766	2%	5% Intracellular protein traffic
BP00061	-21.5	-	9	190	1584	7766	1%	2% Protein biosynthesis
MF00126	-21.1	-	3	130	1584	7766	0%	2% Dehydrogenase
MF00075	-20.3	-	2	115	1584	7766	0%	1% Ribosomal protein
BP00063	-19.5	-	46	447	1584	7766	3%	6% Protein modification
MF00156	-19.2	-	1	98	1584	7766	0%	1% Other hydrolase
MF00082	-16.7	-	16	219	1584	7766	1%	3% Transporter
BP00289	-16.7	-	19	241	1584	7766	1%	3% Other metabolism
BP00013	-16.6	-	5	128	1584	7766	0%	2% Amino acid metabolism
MF00166	-16.2	-	1	84	1584	7766	0%	1% Isomerase
BP00047	-15.9	-	6	133	1584	7766	0%	2% Pre-mRNA processing
BP00203	-15.9	-	35	346	1584	7766	2%	4% Cell cycle
BP00282	-15.1	-	6	129	1584	7766	0%	2% Mitosis
MF00118	-14.6	-	7	135	1584	7766	0%	2% Synthase and synthetase
BP00036	-13.4	-	4	102	1584	7766	0%	1% DNA repair

BP00034	-13.3	-	12	167	1584	7766	1%	2% DNA metabolism
BP00019	-12.5	-	25	254	1584	7766	2%	3% Lipid, fatty acid and steroid metabolism
MF00097	-12.5	-	5	106	1584	7766	0%	1% G-protein
MF00044	-12.1	-	3	86	1584	7766	0%	1% Nuclease
MF00284	-12.1	-	3	86	1584	7766	0%	1% Other ligase
MF00170	-12.0	-	16	188	1584	7766	1%	2% Ligase
BP00141	-11.9	-	45	377	1584	7766	3%	5% Transport
BP00076	-11.8	-	6	111	1584	7766	0%	1% Electron transport
BP00020	-11.7	-	2	74	1584	7766	0%	1% Fatty acid metabolism
BP00276	-11.0	-	9	130	1584	7766	1%	2% General vesicle transport
BP00048	-10.8	-	5	97	1584	7766	0%	1% mRNA splicing
MF00264	-10.8	-	5	97	1584	7766	0%	1% Microtubule family cytoskeletal protein
MF00065	-10.7	-	3	79	1584	7766	0%	1% mRNA processing factor
MF00051	-10.1	-	6	101	1584	7766	0%	1% Helicase
MF00099	-9.8	-	4	83	1584	7766	0%	1% Small GTPase
MF00127	-9.8	-	5	91	1584	7766	0%	1% Reductase
BP00062	-9.5	-	4	81	1584	7766	0%	1% Protein folding
MF00086	-9.1	-	9	118	1584	7766	1%	2% Other transporter
MF00153	-8.7	-	15	158	1584	7766	1%	2% Protease
BP00071	-8.7	-	33	273	1584	7766	2%	4% Proteolysis
BP00081	-8.5	-	5	84	1584	7766	0%	1% Coenzyme and prosthetic group metabolism
MF00077	-8.4	-	5	83	1584	7766	0%	1% Chaperone
MF00157	-7.9	-	6	88	1584	7766	0%	1% Lyase
BP00129	-7.6	-	7	94	1584	7766	0%	1% Endocytosis

Table S8.1b: Panther Pathways

Ontology ID	ln(p-value) enrichment/depletion	+/-	N(ont& cat)	N(ont)	N(cat)	N(total)	N(ont& cat) / N(cat)	N(ont)/ N(total)	Ontology Term Desc.
Type III novelty, p<0.05/100 enriched ontology categories:									
P00031	-12.91	+	11	62	240	7766	5%	1%	Inflammation mediated by chemokine and cytokine signaling pathway
P00019	-9.85	+	7	33	240	7766	3%	0%	Endothelin signaling pathway
P04385	-7.92	+	4	12	240	7766	2%	0%	Histamine H1 receptor mediated signaling pathway
P00027	-7.91	+	5	21	240	7766	2%	0%	Heterotrimeric G-protein signaling pathway-Gq alpha and Go alpha mediated pathway
Type II novelty, p<0.05/100 enriched ontology categories:									
P00004	-20.96	+	10	34	158	7766	6%	0%	Alzheimer disease-presenilin pathway
P00057	-17.06	+	12	77	158	7766	8%	1%	Wnt signaling pathway
P00005	-14.74	+	10	62	158	7766	6%	1%	Angiogenesis
P00031	-12.47	+	9	62	158	7766	6%	1%	Inflammation mediated by chemokine and cytokine signaling pathway
P00034	-8.03	+	7	65	158	7766	4%	1%	Integrin signalling pathway
P00045	-7.81	+	4	18	158	7766	3%	0%	Notch signaling pathway
Type I novelty, p<0.05/100 enriched ontology categories:									
All types of novelty, p<0.05/100 enriched ontology categories:									
P00031	-10.44	+	27	62	1584	7766	2%	1%	Inflammation mediated by chemokine and cytokine signaling pathway
P00005	-8.28	+	25	62	1584	7766	2%	1%	Angiogenesis
P00057	-7.98	+	29	77	1584	7766	2%	1%	Wnt signaling pathway
Type III novelty, p<0.05/100 depleted ontology categories:									
Type II novelty, p<0.05/100 depleted ontology categories:									
Type I novelty, p<0.05/100 depleted ontology categories:									
P00049	-7.81	-	0	47	1186	7766	0%	1%	Parkinson disease
All types of novelty, p<0.05/100 depleted ontology categories:									